NTNU

Norwegian University of
Science and Technology

Calculations of Resistivity Coefficients and Mass Flux in a Two-Phase Binary Lennard-Jones/spline System Using Non-Equilibrium Thermodynamics and Molecular Dynamics

Laura Edvardsen

Chemical Engineering and Biotechnology
Submission date: June 2018
Supervisor: Bjørn Hafskjold, IKJ
Co-supervisor: Signe Kjelstrup, IKJ

Norwegian University of Science and Technology
Department of Chemistry

Abstract

Fresh water has a vital role in our everyday life. However, it is also increasingly scarce and it is important to obtain better understanding of water purification processes to secure global access to clean water. There exist many processes for water purification. Membrane distillation was investigated in this study. The aim of this study was to use non-equilibrium thermodynamics to create a model to find the resistivity coefficients present due to a thermal and chemical potential driving force. These coefficients can provide accurate information about the mass transport through the membrane. A two-phase system containing two different Lennard-Jones/spline fluids, pure liquid and mixture, separated by a hydrophobic pore was modelled to calculate these coefficients. Lennard-Jones/spline particles were used to simplify the system.

It was first constructed a simple two-component system to find optimal conditions for the mixture in the pore system. For this simple system, a phase diagram was created. Then, four different systems were constructed to find the total and local resistivity coefficients. The total resistivity coefficients were r_{qq}^{tot}= 13±3, $r_{q\mu}^{tot}$= -20±2 and $r_{\mu\mu}^{tot}$= 35±2. The local resistivity coefficients include the coefficients for the surface between mixture and vapor ($r^{s,l}$), the vapor coefficient (r^{vapor}), and for the surface between vapor and pure liquid ($r^{s,r}$). These were found to be $r_{qq}^{s,l}$= 23±2, $r_{q\mu}^{s,l}$= -15±1, $r_{\mu\mu}^{s,l}$= 11±2, r_{qq}^{vapor}= 7±1, $r_{q\mu}^{vapor}$= -0.5±0.7, $r_{\mu\mu}^{vapor}$= 0.05±0.04 and $r_{qq}^{s,r}$= 13.6±0.8, $r_{q\mu}^{s,r}$= -8±2, $r_{\mu\mu}^{s,r}$= 13±1. It was seen that the surfaces had resistivity coefficients that were significantly different from the bulk coefficients. This indicate that surface resistivity coefficients have a crucial role when it comes to providing accurate information regarding the mass flux.

Simulations were also conducted to investigate how mass transport was influenced by temperature and pore diameter. A linear correlation between temperature and mass flux was found, where the mass flux increased with increasing temperature gradient. The greatest mass flux was obtained for the smallest pore investigated (pore diameter equal to $10\sigma_0$). This result implied that a membrane with a greater number of pores with diameter $10\sigma_0$ would provide a greater mass transport compared to a membrane with fewer, larger pores.

Sammendrag

Ferskvann har en sentral rolle i hverdagen vår. Det er derfor viktig å få en bedre forståelse av vannrensingsprosesser for å sikre global tilgang til rent vann. Det finnes mange prosesser for vannutvinning. I denne studien ble det valgt å undersøke membran destillasjon. Målet med denne studien var å bruke ikke-likevekts termodynamikk til å lage en modell for å finne resistivitetskoeffisientene som er tilstede på grunn av en termisk og kjemisk potensiell drivkraft. Disse koeffisientene kan gi nøyaktig informasjon om massetransporten gjennom membranen. Systemet som ble studert var et tofasesystem som inneholdt to forskjellige Lennard-Jones/spline væsker, ren væske og blanding, separert av en hydrofob pore. Lennard-Jones/spline partikler ble brukt til å forenkle systemet.

Det ble først konstruert et enkelt to-komponentsystem for å finne optimale forhold for blandingen i poresystemet. For dette enkle systemet ble et fasediagram laget. Deretter ble fire forskjellige systemer konstruert for å finne de totale og lokale resistivitetskoeffisientene. De totale resistivitetskoeffisientene var r_{qq}^{tot} = 13$\pm$3, $r_{q\mu}^{tot}$ = -20$\pm$2 og $r_{\mu\mu}^{tot}$ = 35$\pm$2. De lokale resistivitetskoeffisientene er koeffisientene for overflaten mellom blanding og gass ($r^{s,l}$), gasskoeffisienten (r^{vapor}) og for overflaten mellom gass og ren væske ($r^{s,r}$). Disse ble funnet å være $r_{qq}^{s,l}$ = 23$\pm$2, $r_{q\mu}^{s,l}$ = -15$\pm$1, $r_{\mu\mu}^{s,l}$ = 11$\pm$2, r_{qq}^{vapor} = 7$\pm$1, $r_{q\mu}^{vapor}$ = -0.5$\pm$0.7, $r_{\mu\mu}^{vapor}$ = 0.05$\pm$0.04 og $r_{qq}^{s,r}$ = 13.6$\pm$0.8, $r_{q\mu}^{s,r}$ = -8$\pm$2, $r_{\mu\mu}^{s,r}$ = 13$\pm$1. Det ble sett at overflatene i systemet hadde resistivitetskoeffisienter som var signifikant forskjellig fra bulk koeffisientene. Dette betyr at overflate resistivitetskoeffisientene har en sentral rolle når det kommer til å oppnå nøyaktig informasjon om massefluksen.

Det ble også utført simuleringer for å undersøke hvordan massetransport ble påvirket av temperatur og porediameter. Det ble funnet en lineær korrelasjon mellom temperatur og massefluks, hvor massefluksen økte med økende temperaturgradient. Den største massefluksen ble oppnådd for den minste poren undersøkt (porediameter lik $10\sigma_0$). Dette resultatet innebærer at en membran med mange porer av diameter $10\sigma_0$ vil gi større massetransport sammenlignet med en membran med færre, større porer.

Acknowledgments

Thanks to my supervisors Signe Kjelstrup and Bjørn Hafskjold for all the help and many great discussions.

Thanks to Dick Bedeaux and Olav Galteland for their many good ideas regarding my master thesis.

To my fellow master students Vilde Bråten and Kristine Veie, thank you for listening to my complaints, offering me advice and for great team spirit throughout this semester.

Finally, thanks to Mats Jønland for proofreading this thesis and for all the encouragement.

Computer resources have been provided by Faculty of Natural Science at NTNU and NOTUR.

List of Figures

List of Tables

List of Symbols

Symbol	Dimension	Description
T	K	Temperature
T_c	K	Temperature of cold thermostat
T_h	K	Temperature of hot thermostat
p	Pa	Pressure
p^*	Pa	Vapor pressure for pure component
p_{tot}	Pa	Total vapor pressure
x_i		Liquid mole fraction of particle i
y_i		Vapor mole fraction of particle i
V	m^3	Volume
V_m	$m^3\ mol^{-1}$	Molar volume
R	$J\ K^{-1}\ mol^{-1}$	Gas constant
a_i		Activity
μ	$J\ mol^{-1}$	Chemical potential
q	J	Heat
r_{qq}	$m^2\ s\ J^{-1}\ K^{-1}$	Resistivity coefficient of transport of heat
$r_{q\mu}$	$m^2\ s\ mol^{-1}\ K^{-1}$	Resistivity coefficient of coupling of heat and mass transport
$r_{\mu\mu}$	$m^2\ s\ J\ mol^{-2}\ K^{-1}$	Resistivity coefficient of transport of mass
J_m	$mol\ m^{-2}\ s^{-1}$	Mass flux
σ	$J\ s^{-1}\ K^{-1}\ m^{-3}$	Entropy production
J_q	$J\ m^{-2}\ s^{-1}$	Heat flux
J_q'	$J\ m^{-2}\ s^{-1}$	Measurable heat flux
q_m^*	$J\ mol^{-1}$	Heat of transfer

S	J K^{-1}	Entropy
H	J	Enthalpy
H_m	J mol^{-1}	Molar enthalpy
U	J	Internal energy
r_{ij}	m	Distance between center of particle i and center of particle j
r_i	m	Positon of center of mass of particle i
N		Number of particles
n	mol	Number of moles
N_A	mol^{-1}	Avogadro's number
L	m	Length
t	s	Time
x	m	Distance
ε_{ij}		Parameter that determines interaction strength.
σ_{ij}	m	Parameter that determines particle size
α_{ij}		Parameter that adjusts the balance between repulsive and attractive forces
σ_0	Molecular diameter	Unit length
U_i		Potential energy of particle i
$u_{ij}^{LJ/s}$		Lennard-Jones/spline potential between particle i and j
u_{ij}		Potential energy between particle i and j
k_B	J K^{-1}	Boltzmann constant
$\boldsymbol{v_i}$	m s^{-1}	Velocity of particle i
$\boldsymbol{a_i}$	m s^{-2}	Acceleration of particle i
m_i	kg	Mass of particle i

$\boldsymbol{f}_i$	N	Force acting on the center of mass of particle i
$\boldsymbol{S}_i$	bar m^3	Stress tensor for particle i
e_i	J	Energy of particle i
E_{kin}	J	Kinetic energy
K_n		Knudsen number
d_p	m	Diameter of pore
d_A	m	Diameter of particle
λ	m	Mean free path
δ	m	Surface thickness
t_s		Test statistic
$\sigma_{SD,m}$		Standard deviation of mean

1 Introduction

Fresh water is an essential resource, not only as drinking water, but fresh water also has a central role in the industry [Keulen, L., et al. (2017)]. Amongst industries that use large amounts of fresh water are food, paper and metal production. The world's population is increasing, meaning there is a greater need for fresh water [Vörösmarty, C. J., et al. (2000)]. Only 1-2% of the process and drinking water produced globally are extracted from sea water and brackish water [Jansen, A. E., et al. (2013)]. A huge opportunity for increasing the global supply of fresh water could lie within the field of water extraction.

There exist many different processes for water extraction. Membrane distillation by thermal osmosis is particularly interesting because it has the possibility to use low-grade heat as its energy source [Keulen, L., et al. (2017)]. In membrane distillation, desalination of seawater is possible due to a phase separation. The hydrophobicity of the pores will provoke a two-phase fluid system, where water vapor will diffuse through the pores. The transport of water is driven by a temperature difference over the membrane, hence the name thermal osmosis.

A two-phase system involves at least one surface barrier. A surface could have a significant resistance to different transport processes and must therefore be accounted for. Non-equilibrium thermodynamics provide a theoretical description of a surface in terms of resistivity coefficients. Molecular dynamics simulation can be used to investigate thermodynamic properties and provide information about the resistivity coefficients. The aim of this study is to find the resistivity coefficients present due to a thermal and chemical potential driving force. These coefficients can provide accurate information about the mass transport and are therefore important in membrane distillation. For simplification, Lennard-Jones/spline particles are used. The system to be studied is a two-phase system containing two different Lennard-Jones/spline fluids, pure liquid and mixture, separated by a hydrophobic pore. Hydrophobicity is here understood as a rejection of Lennard-Jones/spline particles.

As an optimization opportunity for membrane distillation it is interesting to see how the mass flux change with a change in different system variables. The variables chosen to study were size of temperature gradient and pore diameter. Information regarding the mass flux dependency on temperature and pore diameter can be used to find optimal conditions for membrane distillation.

1.1 Outline

This thesis consists of three main parts: theory, methodology, and results and discussion.

The theory offers a literature review of membrane distillation by thermal osmosis and non-equilibrium thermodynamics. The methodology section provides both a theoretical view of the method used for simulating thermodynamic and kinetic properties, and details about the computational methods and the construction of the systems. The results and discussion part present the results obtained during the study, as well as discussions of these results.

2 Theory

This section contains theory that is relevant to describe mass transport trough a hydrophobic pore.

2.1 Membrane distillation

Membrane distillation by thermal osmosis is a thermally driven separation process where separation is obtainable due to a phase change [Khayet, M. (2011)]. For a hydrophobic membrane, the hydrophobicity of the pores will set up a barrier for the liquid phase, preventing the liquid to enter the pore. This provokes a two-phase fluid system where only vapor passes through the pore.

To create a separation of two solutions, the feed and the permeate have different temperatures, respectively hot and cold, see figure 2.1.

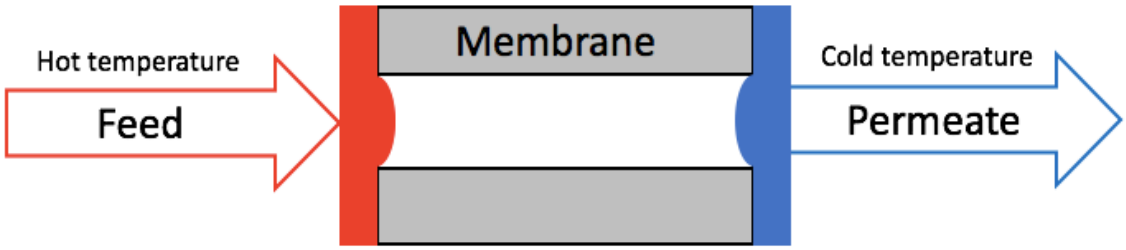

Figure 2. 1 Simple illustration of membrane distillation by thermal osmosis. A hot feed flow is placed on one side of the membrane and a cold permeate flow on the other. The membrane has a hydrophobic character which provokes a phase change.

The temperature gradient results in a vapor pressure difference. The region with the high temperature, the feed, will have the highest vapor pressure [Lawson, K. W., & Lloyd, D. R. (1997)]. This will cause volatile components in the feed to evaporate. The evaporated components will diffuse through the pore towards the area with the lower vapor pressure, which is the permeate. This area has a lower temperature, and the components will condense.

2.2 Non-equilibrium thermodynamics

Non-equilibrium thermodynamics theory describes the transport processes in systems that are not in thermodynamic equilibrium. The theory is based on the local equilibrium assumption.

This assumption states that for a system out of equilibrium, the local and instantaneous relations between thermodynamic quantities will be the same as for a uniform system in equilibrium [Lebon, G. et al. (2008)]. Non-equilibrium thermodynamics provides an accurate description of transport processes, containing their interdependency or coupling [Kjelstrup, S., & Bedeaux, D. (2008)].

Non-equilibrium thermodynamics uses the entropy production as its basis. The entropy production is formulated in the second law of thermodynamics, given by

$$\sigma = \sum_i J_i X_i \geq 0 \tag{2.1}$$

where σ is the entropy production, J_i, are the conjugate fluxes and X_i are the forces. Every flux is assumed to be a linear combination of all the conjugate thermodynamic forces, presented as

$$J_i = \sum_j L_{ij} X_j \tag{2.2}$$

where L_{ij} is the coupling coefficients that couples flux i with driving force j. Coupling in this context means that the presence of a force leads to a flux, and vice versa. These coupling coefficients are characteristic for non-equilibrium thermodynamic and relate through Onsager´s reciprocal by

$$L_{ij} = L_{ji} \ . \tag{2.3}$$

For two pairs of forces and fluxes it follows that $L_{ii}L_{jj} - L_{ij}^2 \geq 0$. Otherwise the entropy production becomes negative and the second law of thermodynamics would not be fulfilled. The main coefficients, which are L_{ii} and L_{jj}, are always positive.

Equations (2.1) -(2.3) contains most of the information regarding the non-equilibrium behavior of a system, in addition comes balance equations.

2.3 Transport of heat and mass in heterogeneous systems

A heterogeneous system consists of two or more homogeneous phases, separated by a surface [Kjelstrup, S., & Bedeaux, D. (2008)]. Figure 2.2 gives a schematic presentation of a system where two homogeneous phases, i and o, are separated by a surface, s, assumed to be in local equilibrium.

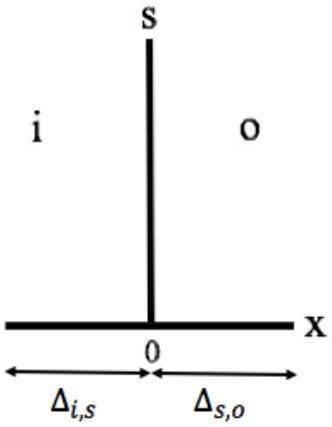

Figure 2. 2 Notation used for transport across a surface, s. The phase at x<0 is denoted with subscript i and the phase at x>0 is denoted with subscript o [Kjelstrup, S., & Bedeaux, D. (2008)].

A surface indicates an interfacial region in which the properties vary from one phase to another [Kjelstrup, S., & Bedeaux, D. (2008)]. This variation occurs because the surface can act as a source or sink of energy. The term interface is described the same way as the term surface; it defines the point where different phases meet and interact [Hiemenz, P.C., & Rajagopalan, R. (1997)]. The term surface and interface will be used interchangeably throughout this thesis.

In the microscopic view, a surface is three-dimensional, but to the human eye it is only two-dimensional. To treat the surface as a plane, Gibbs defined the *dividing surface* [Kjelstrup, S., & Bedeaux, D. (2008)]. The dividing surface is a geometric plane located within the region where the thermodynamic properties vary from the bulk properties. For a two-dimensional surface, the transport processes in the direction normal to the surface will become scalar. This implies that transport of mass and heat in the direction normal to the surface can be coupled with chemical reactions.

2.3.1 Homogeneous phase

For a non-ionic binary mixture subject to a temperature gradient, there are two different transport processes; transport of heat and transport of mass [Kjelstrup, S., & Bedeaux, D. (2008)]. The entropy production for transport of heat and mass of one component in a homogeneous phase is given by

$$\sigma^h = J'_q \left(\frac{\partial}{\partial x}\frac{1}{T}\right) + J_m \left(-\frac{1}{T}\frac{\partial \mu_T}{\partial x}\right) \tag{2.4}$$

where σ^h is the entropy production, q is heat, m is mass, T is the temperature, μ_T is chemical potential at constant temperature T, J'_q is the measurable heat flux and J_m is the mass flux of moving component [Kjelstrup, S., & Bedeaux, D. (2008)].

The transport of heat and mass can be derived from the linear relations of the forces and fluxes. The inverted form of equation (2.2) expresses the forces as linear combinations of the fluxes, where the inverse of the coupling coefficients matrix, L_{ij}, will be the resistivity coefficients matrix, r_{ij}. The Onsager relation holds for the resistivity coefficients, meaning $r_{ij} = r_{ji}$. The force-flux relations are defined as

$$\frac{\partial}{\partial x}\frac{1}{T} = r_{qq}J'_q + r_{q\mu}J_m \tag{2.5}$$

$$-\frac{1}{T}\frac{\partial \mu_T}{\partial x} = r_{\mu q}J'_q + r_{\mu\mu}J_m \tag{2.6}$$

where the coefficients r_{ij} are the resistivity coefficients. The resistivity coefficients can be found by

$$-\left[\frac{J'_q}{\partial T/\partial x}\right]_{J_m=0} = \frac{1}{T^2 r_{qq}} \tag{2.7}$$

$$q^*_m = \left[\frac{J'_q}{J_m}\right]_{\partial T=0} = -\frac{r_{q\mu}}{r_{qq}} \tag{2.8}$$

$$\left[\frac{J'_q}{J_m}\right]_{\partial \mu_T=0} = -\frac{r_{\mu\mu}}{r_{\mu q}} \tag{2.9}$$

where q_m^* is heat of transfer. The r_{qq}, $r_{\mu\mu}$ and $r_{\mu q}$ corresponds to the resistivity coefficient for transport of heat, mass and a coupling between these transport processes, respectively. Knowing them provides information about the force-flux relation of the system.

2.3.2 The surface

A surface is treated as a separate thermodynamic system, meaning the surface has its own thermodynamic properties as temperature and potential energy [Kjelstrup, S., & Bedeaux, D. (2008)]. Transport along the surface is neglected, and therefore, transport is considered as one-dimensional, in the direction normal to the surface [Hafskjold, B. (2017)]. The excess entropy production for transport of heat and mass of one component across a surface barrier is given by

$$\sigma^s = J_q'^i \Delta_{i,s} \frac{1}{T} + J_q'^o \Delta_{s,o} \frac{1}{T} + J_m^i \left(-\frac{1}{T^s} \Delta_{i,s} \mu_{T^s} \right) + J_m^o \left(-\frac{1}{T^s} \Delta_{s,o} \mu_{T^s} \right) \tag{2.10}$$

where σ^s is the excess entropy production, q is heat, m is mass, T is the temperature, T^s is the surface temperature, μ_{T^s} is the chemical potential at constant temperature T^s, J_q' is the measurable heat flux and J_m is the mass flux of moving component. The frame of reference is the surface and the second component in the mixture is at rest with respect to the surface. Notation s represents the surface, and i and o denotes into and out from the surface, respectively, see figure 2.2 for illustration. For a homogeneous phase, the variables are continuous, but for the surface there is a discrete situation regarding the fluxes directed into and out of the surface. This means that the temperature gradient used in equation (2.7) will be replaced by a jump in temperature over the surface.

The transport of heat and mass across the surface at stationary state can be derived from the linear relations of the forces and fluxes [Kjelstrup, S., & Bedeaux, D. (2008)]. For the system illustrated in figure 2.2, the force-flux relations for side i of the surface at stationary state can be expressed as

$$\Delta_{i,s} \left(\frac{1}{T} \right) = r_{qq}^{s,i} J_q'^i + r_{q\mu}^{s,i} J_m^i \tag{2.11}$$

$$-\frac{1}{T^s} \Delta_{i,s} \mu_{T^s} = r_{\mu q}^{s,i} J_q'^i + r_{\mu\mu}^{s,i} J_m^i \tag{2.12}$$

and for side o of the surface

$$\Delta_{s,o}\left(\frac{1}{T}\right) = r_{qq}^{s,o} J_q'^{o} + r_{q\mu}^{s,o} J_m^o \tag{2.13}$$

$$-\frac{1}{T^s}\Delta_{s,o}\mu_{T^s} = r_{\mu q}^{s,o} J_q'^{o} + r_{\mu\mu}^{s,o} J_m^o \tag{2.14}$$

where the coefficients $r_{ij}^{s,i}$ and $r_{ij}^{s,o}$ are the surface resistivity coefficients for the i and o side of the surface, respectively. The surface resistivity coefficients relate the discrete difference in temperature and chemical potential over the surface barrier to the measurable heat and mass flux across the barrier. The measurable heat flux, J_q', is conjugate to the difference in the inverse temperature. The stationary mass flux, J_m, is conjugate to the difference in chemical potential at a constant temperature equal T^s, divided by T^s. The transport processes on the two sides of the surface will occur in series and are therefore expected to be weakly coupled. Consequently, coupling across the surface is neglected.

Combining the force-flux relations in equations (2.11)- (2.14) gives the entropy production for the whole surface with respect to the measurable heat flux on the i side of the surface

$$\sigma^s = J_q'^{i}\Delta_{i,o}\frac{1}{T} - J_m^i\frac{\Delta_{i,o}\mu_{T^o}}{T^o} \tag{2.15}$$

and with respect to the measurable heat flux on the o side of the surface

$$\sigma^s = J_q'^{o}\Delta_{i,o}\frac{1}{T} - J_m^o\frac{\Delta_{i,o}\mu_{T^i}}{T^i} \tag{2.16}$$

The difference in chemical potential across the surface is investigated at the temperature of the adjacent fluid. If the measurable heat flux on the i side of the surface is used, the temperature of the adjacent fluid is T^o, and opposite for side o of the surface. Equation (2.15) and (2.16) provide the same information about the surface.

The surface resistivity coefficients can be defined the same way as for the homogenous phase, except that discrete variables must be used. For the i side of the surface, the equations used for calculating the surface resistivity coefficients are given by

$$\left[\frac{J_q'^i}{\Delta_{i,s}\frac{1}{T}}\right]_{J_{m=0}} = \frac{1}{r_{qq}^{s,i}} \tag{2.17}$$

$$q_m^{*i} = \left[\frac{J_q'^i}{J_m^i}\right]_{\Delta_{i,s}\frac{1}{T}=0} = -\frac{r_{q\mu}^{s,i}}{r_{qq}^{s,i}} \tag{2.18}$$

$$\left[\frac{J_q'^i}{J_m^i}\right]_{\Delta_{i,s}\mu_T=0} = -\frac{r_{\mu\mu}^{s,i}}{r_{\mu q}^{s,i}} \tag{2.19}$$

and for the *o* side of the surface

$$\left[\frac{J_q'^o}{\Delta_{s,o}\frac{1}{T}}\right]_{J_{m=0}} = \frac{1}{r_{qq}^{s,o}} \tag{2.20}$$

$$q_m^{*o} = \left[\frac{J_q'^o}{J_m^o}\right]_{\Delta_{s,o}\frac{1}{T}=0} = -\frac{r_{q\mu}^{s,o}}{r_{qq}^{s,o}} \tag{2.21}$$

$$\left[\frac{J_q'^o}{J_m^o}\right]_{\Delta_{s,o}\mu_T=0} = -\frac{r_{\mu\mu}^{s,o}}{r_{\mu q}^{s,o}} \tag{2.22}$$

Equation (2.17) -(2.22) describe the two sides of the surface. The resistivity coefficient due to transport of heat, r_{qq}, can be expressed for the whole surface, and not just for each side of the surface. At stationary state, $J_m = J_m^o = J_m^i$, and r_{qq} is given by

$$r_{qq}^s = r_{qq}^{s,i} + r_{qq}^{s,o} \tag{2.23}$$

The two other resistivity coefficients cannot be expressed for the entire surface the same way as r_{qq}. They are only defined using the incoming or outgoing fluxes, as expressed in equation (2.17) -(2.22), but they do apply for the whole surface. To obtain surface resistivity coefficients with the same dimension as for the homogeneous phases, they should be divided by the surface thickness.

2.3.3 Heterogeneous system

To describe a heterogeneous system, it is necessary to combine the homogeneous phase and surface to find the total resistivity of the system. A hydrophobic pore is such a heterogeneous system. Hydrophobicity is the property of being repelled from water in its liquid state [Keulen, L., et al. (2017)]. For a hydrophobic membrane, there is a homogeneous vapor phase inside the pore and two homogeneous liquids on each side of the pore. A schematic representation of a hydrophobic pore containing two surfaces is shown in figure 2.3.

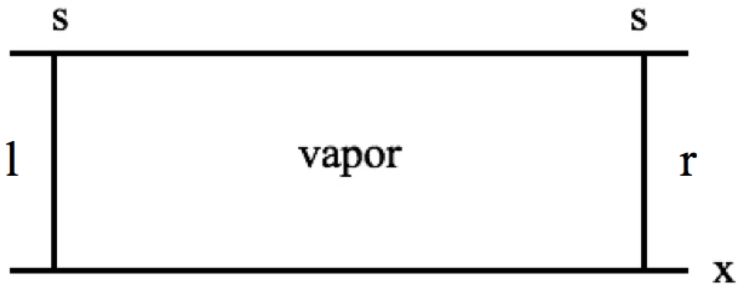

Figure 2. 3 A representation of a hydrophobic pore. The l and r denotes the left and right liquid phases, respectively. The area between phase l and r will be the vapor phase. s represents the different surfaces in the system [Keulen, L., et al. (2017)].

At stationary state the flux-force relations of the heterogeneous system with respect to the measurable heat flux on the outgoing liquid phase r are given as

$$\Delta_{l,r}\left(\frac{1}{T}\right) = r_{qq}^{tot} J_q'^{r} + r_{q\mu}^{tot} J_m \tag{2.24}$$

$$-\frac{1}{T^l}\Delta_{l,r}\mu_{T^l} = r_{\mu q}^{tot} J_q'^{r} + r_{\mu\mu}^{tot} J_m \tag{2.25}$$

where r_{ij}^{tot} are the total resistivity coefficients. These are defined as

$$r_{qq}^{tot} = \left[\frac{\Delta_{l,r}\left(\frac{1}{T}\right)}{J_q'^{r}}\right]_{J_m=0} \tag{2.26}$$

$$r_{q\mu}^{tot} = -\left[\frac{r_{qq}^{tot} J_q'^{r}}{J_m}\right]_{\Delta_{l,r}\frac{1}{T}=0} \tag{2.27}$$

$$r_{\mu\mu}^{tot} = -\left[\frac{r_{q\mu}^{tot} J_q'^r}{J_m}\right]_{\mu_{m,T}=0} \tag{2.28}$$

Since mass is transported mainly in the vapor phase, J_m is understood as the vapor mass flux. For the total resistivity coefficients to be on the same dimensional form as the coefficients in the homogeneous phases, they should be divided by the membrane thickness.

The total resistivity coefficients will arise from the liquid-vapor interface at the left side, l, the vapor inside the pore and the vapor-liquid interface at the right side, r, see figure 2.3. This means that the total resistivity coefficients can be found using the local resistivity coefficients at the surfaces and in the vapor phase. The total resistivity coefficient for transport of heat can easily be found using the local resistivity coefficient only. This is possible because r_{qq}^{tot} is equal to the sum of the local resistivity coefficients for transport of heat [Keulen, L., et al. (2017)]. This simple relationship is not valid for the other two resistivity coefficients, $r_{q\mu}^{tot}$ and $r_{\mu\mu}^{tot}$, as they also depend on enthalpy differences. In this study, the total resistivity coefficients will be calculated directly from equation (2.26), (2.27) and (2.28).

A mass transport though a hydrophobic pore can occur due to a gradient in chemical potential and a gradient in temperature. These two driving forces have the opposite effect on the direction of the mass flux, J_m, if the left-hand side of the pore is impure, and the temperature decrease from left to right. This effect is illustrated in figure 2.4.

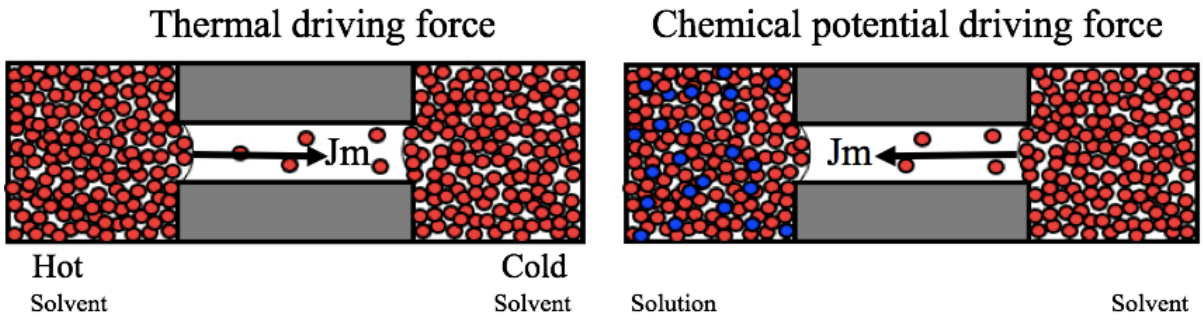

Figure 2. 4 Illustration of how the thermal and chemical potential driving forces affect the direction of the mass flux. The red and blue particles represent solvent and solute, respectively. This is an open system meaning particles can cross the box "walls". This means that even though there is a mass transport, it will never run out of or get filled with particles in the liquids. Also, the concentration in the solution will be constant regardless of the mass transport.

For a one-component system under a temperature gradient, the mass transport will be from hot to cold area [Kjelstrup, S., & Bedeaux, D. (2008)]. This is called thermal osmosis. For a system in thermal equilibrium consisting of a solution and a pure solvent liquid, the mass transport will be towards the region of highest solute concentration. This process is called regular osmosis. A difference in chemical potential results in a difference in pressure. If there exist substantial attractive forces between the solvent and solute in a mixture, the mixture will have the lowest pressure. This is because the vapor pressure decreases due to the strong intermolecular forces between solvent and solute. When chemical potential is the main driving force, as the right illustration shows in figure 2.4, the mass transport will be from the fluid with the highest vapor pressure, to the fluid with the lowest. Eventually, mass transport would lead to increased pressure in the solution, the osmotic pressure, but this will be avoided when the system is open.

To achieve a separation between solvent and solute in the mixture, where solvent component diffuses through the pore towards the pure phase, the thermal driving force must be greater than the chemical potential driving force.

2.4 Particle diffusion through pores- Knudsen diffusion

Knudsen diffusion occurs when particles diffuse in pores that have a diameter smaller than the mean free path of the particle [Hale, W. R., et al. (2001)]. This causes the particles to collide with the pore wall more frequently than with each other. The Knudsen number can be used as a reference point to make sure that a system is within the Knudsen regime. The Knudsen number is a ratio defined by

$$K_n = \frac{\lambda}{d_p} \tag{2.29}$$

where K_n is the Knudsen number, λ is the mean free path of the particle and d_p is the pore diameter [He, W., et al. (2014)]. A Knudsen number much greater than 10 means that the diffusion in the system is significantly explained by the Knudsen diffusion.

The mean free path is given by

$$\lambda = \frac{1}{\sqrt{2}\pi d_A^2 \frac{N}{V}} \tag{2.30}$$

where $\frac{N}{V}$ is the number density and d_A is the diameter of the particle.

2.5 Raoult's law and partial pressure of mixtures

Raoult's law states that for an ideal mixture of liquids, the partial vapor pressure of a component is equal to the product of vapor pressure of the pure component and mole fraction in the liquid mixture [Guggenheim, E. A. (1937)]. In ideal mixtures, the forces between the particles are the same as the forces between particles in pure liquids. In other words, the interaction between a pair of different particles is the same as the interaction between a pair of the same particle.

For component i, the partial vapor pressure is given by

$$p_i = p_i^* x_i \tag{2.31}$$

where p_i is the partial pressure of component i, p_i^* is the vapor pressure of pure component i and x_i is the mole fraction of component i in the liquid mixture. In a mixture of gases, each gas contributes to the total vapor pressure with their partial pressure through the equation

$$p_i = p_{tot} y_i \tag{2.32}$$

where p_{tot} is the total vapor pressure of the mixture and y_i is the mole fraction of component i in the gas.

Raoult's law applies for ideal mixtures. Figure 2.5 illustrates how the vapor pressure of an ideal mixture consisting of component A and B, is changing relative to the mole fraction, according to Raoult's law.

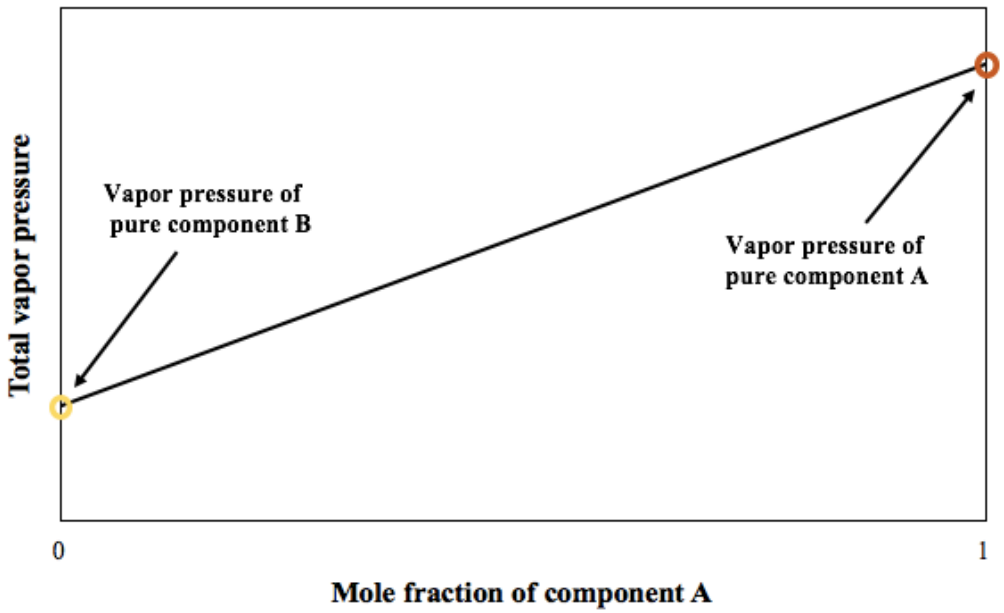

Figure 2. 5 Illustration of Raoult's law for a binary mixture consisting of two components; A and B. The x-axis show the mole fraction of component A, and the y-axis represents the total vapor pressure of the mixture [Guggenheim, E. A. (1937)].

Plotting the vapor pressure of an ideal mixture of two components, A and B, against the composition results in a straight line according to Raoult's law. Figure 2.5 depicts that pure component A has a higher vapor pressure than pure component B. This means that A is the more volatile component.

Real mixtures often deviate from Raoult's law. A negative deviation from Raoult's law means that the mixture has a vapor pressure lower than what would be stated by Raoult's law [Roger W. Kugel (1998)]. If this is the case, the attractive forces between the different types of particles in the mixture are stronger than the forces between particles of same type. A positive deviation from Raoult's law implies that the vapor pressure of the mixture is higher than what expected from an ideal mixture. Here, the attractive forces between the different types of particles in the mixture are weaker than the forces between particles of same type.

3 Methodology

Computer simulation is a valuable tool as it tests theories and models, offers insights to experimental results and provide accurate thermodynamic data [Allen, M. P (2004)]. LAMMPS, which stands for Large-scale Atomic/Molecular Massively Parallel Simulator, is a software from Sandia National Laboratories. This software simulates atoms and molecules using molecular dynamics [Plimpton, S. (1995)]. Molecular dynamics simulations are frequently used in many areas of physical and chemical science. In this study, molecular dynamics was used to simulate mass transport through a hydrophobic pore. The simulations were preformed using the software LAMMPS.

This section provides both a theoretical view of molecular dynamics, presented in section 3.1, computational details, presented in section 3.2, and details about the simulation method specific to this thesis, presented in section 3.3.

3.1 Molecular dynamics simulation

Molecular dynamics simulation is a method for simulating thermodynamic and kinetic properties of a classical many-body system [Frenkel, D., & Smit, B. (2001)]. A classical system is defined as a system that obeys the laws of classical mechanics. Molecular dynamics computes system properties by solving Newton's second law of motion. First, a model system is selected. This system consists of N particles, and the equation of motion is solved for this system until the equilibrium properties no longer change with time. After this equilibration, measurements can be performed.

For a simple atomic system, the equation of motion is defined as

$$\boldsymbol{f}_i = m_i \frac{d^2\boldsymbol{r}_i}{dt^2} \tag{3.1}$$

where $\boldsymbol{f}_i$ is the force acting on the center of mass of particle i, m_i is the mass of particle i, t is time and $\boldsymbol{r}_i$ is a vector expressing the position of the center of mass of particle i. Forces often derive from potential functions, which represents the potential energy of the system. The force acting on a particle is expressed by the change in potential energy with a change in distance, given by

$$\boldsymbol{f}_i = -\sum_{j \neq i} \frac{\partial}{\partial \boldsymbol{r}_{ij}} \mathrm{U}_{ij} \tag{3.2}$$

where U_{ij} is the potential energy of particle i due to particle j, and $\boldsymbol{r}_{ij}$ is a vector defining the difference between position of the center of mass of particle i and particle j.

Integration of the equation of motion produces a time-ordered sequence of solutions that gives a description of the dynamic behavior of the particles over a given simulation time interval [Rice B.M., & Sewell T.D. (2009)]. The velocity Verlet algorithm can be used to integrate the equation of motion, equation (3.1) [Allen, M. P., & Tildesley, D. J. (1987)]. Using this approach, positions, velocities and accelerations of particle i at time $t + \Delta t$ are found the following way:

1. $$\boldsymbol{r_i}(t + \Delta t) = \boldsymbol{r_i}(t) + \boldsymbol{v_i}(t)\Delta t + \frac{1}{2}\boldsymbol{a_i}(t)\Delta t^2 \tag{3.3a}$$
2. $$\boldsymbol{v_i}\left(t + \frac{1}{2}\Delta t\right) = \boldsymbol{v_i}(t) + \frac{1}{2}\boldsymbol{a_i}(t)\Delta t \tag{3.3b}$$
3. $$\boldsymbol{a_i}(t + \Delta t) = \frac{1}{m_i}\boldsymbol{f_i}(t + \Delta t) \tag{3.3c}$$
4. $$\boldsymbol{v_i}(t + \Delta t) = \boldsymbol{v_i}\left(t + \frac{1}{2}\Delta t\right) + \frac{1}{2}\boldsymbol{a_i}(t + \Delta t)\Delta t \tag{3.3d}$$

where $\boldsymbol{r}_i$, $\boldsymbol{v_i}$ and $\boldsymbol{a_i}$ are vectors containing the position of the center of mass of particle i, the velocity of particle i and the acceleration of particle i, respectively. t is time and Δt is the timestep size, which has a huge impact on the accuracy of the simulation. A timestep size too large will provide a large error in the dynamic behavior of the particles. A too small timestep size will provide approximation errors due to an increase in number of calculations and slow evolution of the systems properties. Notice that there is a difference between the expressions timestep size and number of timestep, as the number of timestep gives information about the time perspective of a simulation.

Molecular dynamics can be divided into two main categories; equilibrium molecular dynamics and non-equilibrium molecular dynamics. Equilibrium molecular dynamics (EMD) uses the Green-Kubo formalism and natural occurring fluctuations to derive the transport properties for homogeneous systems [Hafskjold, B. (2002)]. These fluctuations are normally small, which often leads to large signal-to-noise ratios. In EMD there are no external driving forces. It is therefore difficult to directly relate EMD simulations to experimental situations where external

forces drive the transport processes. A decisive advantage of EMD is that the system properties are well defined because the system is uniform.

Non-equilibrium molecular dynamics (NEMD) is another method used to derive transport properties and it provides much better signal-to-noise ratio compared to EMD [Hafskjold, B. (2002)]. For non-equilibrium simulations, driving forces are required to preserve the distance from equilibrium. Boundary-driven NEMD lets the external forces act through the boundaries in the system, which can be related to experimental situations. The external forces need to be compatible with the periodic boundary condition, meaning that "walls" must be introduced to the system. Such "walls" can either be directly interacting walls, or regions set by a local perturbation of the temperature, chemical potential, or other properties. Boundary driven NEMD is an effective method to determine the coupling coefficients in coupled transport processes [Wold, I., & Hafskjold, B. (1999)].

3.1.1 Lennard-Jones/spline potential

To simulate liquid-vapor phase transitions, attractive forces between particles are needed [Xie, Charles]. In real systems, all particles will interact at the same time [Allen, M. P., & Tildesley, D. J. (1987)]. In molecular dynamics simulations, it is common to describe potential energy using a pair potential approximation. This approximation describes potential energy in terms of distinct pairs of particles. This is because computations of higher order interactions are very time consuming.

The Lennard-Jones potential is a popular mathematical model for attractive pair potentials. It models van der Waals interactions between a pair of neutral particles. The Lennard-Jones potential model will generate repulsive forces when two particles get too close to each other, and attractive forces when they are too far apart.

When Lennard-Jones potential models a system, every molecule is approximated by a sphere with a given diameter of σ and a given interaction parameter ε [Kjelstrup, S., & Bedeaux, D. (2008)]. A modified version of the Lennard-Jones (LJ) potential is the Lennard-Jones/spline (LJ/s) potential [Holian, B. L., & Evans, D. J. (1983)]. The advantage of using Lennard-Jones/spline potential compared to standard Lennard-Jones potential is that LJ/s is zero at the cut-off distance, while standard LJ will go asymptotically to zero. This means that for standard

LJ, there will be a little jump in potential energy at the cut-off distance. For a system consisting of many particles, the LJ/s potential is more time efficient since the potential has a shorter range (r_c=1.74σ_0) compared to standard LJ potential (r_c=2.5σ_0-3σ_0).

The LJ/s potential between a pair of particles, with an additional parameter, α_{ij}, is defined as

$$\mathrm{u}_{ij}^{LJ/s}(r_{ij}) = \begin{cases} \mathrm{u}_{ij}^{LJ}(r_{ij}) = 4\varepsilon_{ij}\left[\left(\frac{\sigma_{ij}}{r_{ij}}\right)^{12} - \alpha_{ij}\left(\frac{\sigma_{ij}}{r_{ij}}\right)^{6}\right] & if\ r \le r_s \\ \mathrm{u}_{ij}^{s}(r_{ij}) = a_{ij}(r_{ij} - r_c)^2 + b_{ij}(r_{ij} - r_c)^3 & if\ r_s \le r \le r_c \\ 0 & if\ r \ge r_c \end{cases} \quad (3.4)$$

where $\mathrm{u}_{ij}^{LJ/s}(r_{ij})$ is the Lennard-Jones/spline potential between particle i and j, $\mathrm{u}_{ij}^{LJ}(r_{ij})$ is the Lennard-Jones potential between particle i and j, and $\mathrm{u}_{ij}^{s}(r_{ij})$ is the spline potential between particle i and j. The parameter σ_{ij} is the distance between particle i and j when the intermolecular potential between them is zero. This means that σ_{ij} is the parameter that determines the particle size. r_{ij} is the distance between the center of particle i and the center of particle j.

The parameter ε_{ij} is the minimum of the potential between particle i and j. ε_{ij} also describes the interaction strength. The interactions between a pair of particles increases with increasing ε_{ij}. The parameter can be used to scale the temperature. The relation between ε and the temperature is presented in table 3.1. An increase of ε_{ij} means that the vapor pressure decreases.

The additional α_{ij} parameter makes it possible to adjust the balance between repulsive and attractive forces in the Lennard-Jones potential. The repulsive term is proportional to $\left(1/r_{ij}\right)^{12}$, and the attractive term is proportional to $\left(1/r_{ij}\right)^{6}$. For $\alpha_{ij} > 1$ particle i and j will be more attracted to each other. The increase of the alpha parameter will decrease the Lennard-Jones potential between particle i and j, which means the two particles will be closer together. For $\alpha_{ij} < 1$, the attractive term in equation (3.4) will be reduced. This causes a more repulsive interaction between particle i and j.

The spline distance is defined as r_s and the cut-off distance is r_c. From equation (3.4) it is seen that the LJ and LJ/s are identical until the spline distance is reached. After that the LJ/s potential will continue until the cut-off distance is reached. In Molecular dynamics simulations, the forces are truncated at the cut-off distance. The values for r_s, r_c, and the parameters a_{ij} and b_{ij}, are calculated internally so that the potential energy and its first and second derivative are smooth at r_s, and the potential energy and its first derivative are zero at r_c. The relations between the spline distance and cut-off distance, and the definition of the parameters a_{ij} and b_{ij} are presented in equations (3.5) -(3.7).

$$r_c = \frac{67}{48} r_s \tag{3.5}$$

$$r_s = \left(\frac{26}{7}\right)^{\frac{1}{6}} \sigma_{ij} \tag{3.6}$$

$$a_{ij} = -\frac{387072}{61009} \frac{\varepsilon_{ij}}{r_s^3}, \qquad b_{ij} = -\frac{24192}{3211} \frac{\varepsilon_{ij}}{r_s^2} \tag{3.7}$$

The pair potential in equation (3.4) is additive, meaning the potential energy of a particle can be found by

$$\mathrm{U}_i = \frac{1}{2} \sum_{i \neq j} \mathrm{u}_{ij} \tag{3.8}$$

where U_i is the potential energy of particle i. The summation is taken over all particles. To ensure that no pairs are counted twice the factor $\frac{1}{2}$ is included.

3.1.2 Ensembles

For an ensemble, certain thermodynamic variables are fixed [Allen, M. P., & Tildesley, D. J. (1987)]. In this study, two ensembles are of interest; the canonical ensemble and the microcanonical ensemble.

In the canonical ensemble (*NVT*), the number of particles (N), volume (V) and temperature (T) are constant. To keep the temperature constant a thermostat is needed. For the simulations performed in the *NVT* ensemble, the Nosé-Hoover thermostat was used. This is a deterministic

algorithm for molecular dynamics simulation with constant temperature [Hoover, W. G. (1985)]. The idea behind the Nosé-Hoover thermostat is to add a fictive, dynamic variable to the equation of motion, equation (3.1). This variable will either accelerate or slow down the particles in the system, generating a temperature equal to the desired value and with no drift.

In the microcanonical ensemble (*NVE*), the number of particles (N), volume (V) and the total energy in the system (E) are constant [Allen, M. P., & Tildesley, D. J. (1987)]. This is obtained by solving the equation of motion, equation (3.1), without any pressure and temperature control. When the *NVE* ensemble is generated, the energy is conserved. A fluctuation, and possibly a drift, in the total energy may occur due to truncation and rounding errors during the integration process.

3.1.3 Periodic boundary condition

In molecular simulations, the aim is often to compute macroscopic properties using as few particles as possible. To do that, periodic boundary conditions is extremely useful. This is a set of boundary conditions which approximates an infinite system.

For a simulation cell consisting of N particles, a significant amount of these particles will be positioned on the outer surfaces of the cell [Allen, M. P. (2004)]. This causes a "surface effect" which will have a significant influence on the measured properties of the system. Periodic boundary conditions will ensure that the simulation cell is surrounded by an infinite number of replicates of itself. This means that whenever a particle crosses one of the cell borders, a copy of that exact particle will enter the opposite side of the simulation cell. This way, the number of particles is conserved, and the "surface effect" is eliminated.

3.1.4 Dimensionless units

When working with molecular simulation it is useful to work with dimensionless units. Dimensionless units avoid the very small values that can occur on the atomic scale. Instead, they give the opportunity to work with values that are of the order of unity [Allen, M. P., & Tildesley, D. J. (1987)]. Real quantities are made dimensionless by using distance σ_0, mass m_0, minimum interaction potential ε_0 and the Boltzmann constant k_B, see table 3.1 [Kjelstrup, S., & Bedeaux, D. (2008)]. All units used in the simulations in this thesis are dimensionless.

Table 3. 1 Definitions of physical quantities in Lennard-Jones reduced units [Kjelstrup, S., & Bedeaux, D. (2008)].

Quantity	Reduction formula
Distance	$x^* = \frac{x}{\sigma_0}$
Density	$\rho^* = \frac{\rho\sigma_0^3}{m_0}$
Temperature	$T^* = \frac{k_B T}{\varepsilon_0}$
Number density	$n^* = \frac{N}{V}\sigma_0^3$
Time	$t^* = t\left(\frac{\varepsilon_0}{m_0\sigma_0^2}\right)^{\frac{1}{2}}$
Pressure	$p^* = p\frac{\sigma_0^3}{\varepsilon_0}$

3.2 Computational methods

This section provides a description of computational methods relevant for this study. The molecular dynamics cell, or simulation box, was divided into layers, or control volumes, perpendicular to the x-direction, see figure 3.1. These layers had dimensions $\{L_x, L_y, L_z\} = \{5\sigma_0,\ 30\sigma_0,\ 30\sigma_0\}$. It was assumed that local equilibrium was established in each layer. Different thermodynamic properties were computed for each of these layers.

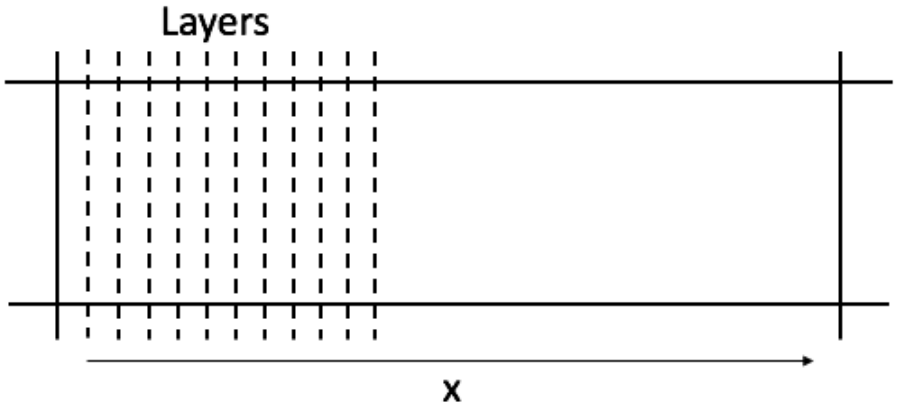

Figure 3. 1 Layout of a molecular dynamics cell.

3.2.1 Mass flux

Mass flux, J_m, is the amount of mass that flows through area, given by

$$J_m = \frac{1}{V_{CV}} \sum_{i \in V_{CV}} m_i (\boldsymbol{v}_i - \boldsymbol{v}_0) \tag{3.9}$$

where V_{CV} is the control volume, m_i is mass of particle i, $\boldsymbol{v}_i$ is a vector consisting of the velocities in all dimensions for particle i and $\boldsymbol{v}_0$ is a vector consisting of the velocities of the reference frame in all dimensions [Hafskjold, B. (2002)].

In molecular dynamics simulations, the simulation box is often used as the reference frame. This is equivalent with setting $\boldsymbol{v}_0$ equal to zero. Equation (3.9) then becomes

$$J_{m,MD} = \frac{1}{V_{CV}} \sum_{i \in V_{CV}} m_i \boldsymbol{v}_i \tag{3.10}$$

which is the equation used to calculate the mass flux in this study. In the simulated systems, mass transport will only occur in the x-direction. Therefore, only this dimension will be accounted for in the mass flux calculations. There will only be transport of one component in the systems, meaning J_m refers to the mass flux of moving component.

3.2.2 Measurable heat flux

Heat is transported by collisions of particles, and it spontaneously flows from hot to cold areas [Ã–zisik, M. N. (1993)]. The higher density of a substance, the easier it will be to transfer heat between particles. This means that conduction of heat increases with increasing density of a substance.

The total heat flux, J_q, in a control volume is the amount of energy that flows through area, given by

$$J_q = \frac{1}{V_{CV}} [\sum_i e_i \boldsymbol{v}_i - \sum_i \boldsymbol{S}_i \boldsymbol{v}_i] \tag{3.11}$$

where V_{CV} is the control volume, e_i is the energy of particle i, $\boldsymbol{v}_i$ is the velocity vector of particle i and $\boldsymbol{S}_i$ is the stress tensor for particle i [Caro, M., et al. (2015)].

The measurable heat flux is used in the calculations regarding the resistivity coefficients. This flux cannot be computed directly in each control volume because it is not a mechanical property [Kjelstrup, S., & Bedeaux, D. (2008)]. The measurable heat flux is related to the total heat flux by

$$J_q' = J_q - \sum_{j=1}^{n} H_{M,j} J_{m,j} \tag{3.12}$$

where J_q' is the measurable heat flux, $H_{M,j}$ is partial molar enthalpy of moving component j and $J_{m,j}$ is molar flux of moving component. Since only one component is moving, n=1. This means that molar enthalpy can be used. The measurable heat flux will not be independent of position because the enthalpy will vary as a function of concentration.

3.2.3 Temperature correction due to mass flow

The temperature in a control volume can be found using the formula for kinetic energy, given as

$$E_{kin} = \frac{dim}{2} N k_B T \tag{3.13}$$

where E_{kin} is the total kinetic energy for particles within a given control volume, dim is the dimensionality of the simulation, N is the number of particles in the control volume, k_B is the Boltzmann constant and T is the kinetic temperature [Hafskjold, B., et al. (1993)]. Another way of expressing the total kinetic energy of a group of particles is

$$E_{kin} = \frac{1}{2} \sum_{i=1}^{N} m_i v_i^2 \tag{3.14}$$

where m_i and v_i is the mass and velocity of particle i in the control volume, respectively. The kinetic energy can be divided into x, y and z contributions as the velocity can be defined for each direction. The temperature can be found by using equation (3.13) and (3.14).

If the simulations contain a transport of mass, there is need for a correction of the temperature because equation (3.14) only accounts for kinetic energy without mass transport. For a three-dimensional system with mass transport in one direction, the kinetic temperature is related to the kinetic energy by

$$\frac{3}{2}Nk_BT = \frac{1}{2}\sum_{i=1}^{N} m_i(v_i - v_{cm})^2 \tag{3.15}$$

where v_{cm} is the center of mass velocity, which refers to the center of mass of the control volume in one dimension. Written out, equation (3.15) becomes

$$\frac{3}{2}Nk_BT = \frac{1}{2}\sum_{i=1}^{N} m_i v_i^2 + v_{cm}\sum_{i=1}^{N} m_i v_i + \frac{1}{2}v_{cm}^2\sum_{i=1}^{N} m_i \tag{3.16}$$

The first term on the right-hand side of equation (3.16) is the kinetic energy for a system without a mass flux. This could also be expressed as $\frac{3}{2}Nk_BT'$, where T' represents the temperature without correction.

For a system with a transport of mass in x-direction, the center of mass velocity is given by

$$v_{cm} = \frac{1}{\sum_{i=1}^{N} m_i}\sum_{i=1}^{N} m_i v_{i,x} \tag{3.17}$$

Using the equation for mass flux, see equation (3.10), equation (3.17) becomes

$$v_{cm} = \frac{1}{\sum_{i=1}^{N} m_i} V_{CV} J_{m,x} \tag{3.18}$$

where V_{CV} is the control volume for the group of particles and J_m is the mass flux within that control volume.

Inserting equation (3.18) into equation (3.16) gives

$$\frac{3}{2}Nk_BT = \frac{3}{2}Nk_BT' - \frac{1}{2\sum_{i=1}^{N} m_i} V_{CV}^2 J_{m,x}^2 \tag{3.19}$$

The temperature in the control volume, with the correction, will be

$$T = T' - \frac{V_{CV}^2 J_m^2}{3Nk_B \sum_{i=1}^{N} m_i} \tag{3.20}$$

3.2.4 Number density and surface thickness

In LAMMPS, [Plimpton, S. (1995)], the density is found by dividing the simulation box into layers and counting the number of particles inside each layer. By dividing the number of particles in each layer by the volume of the layer one achieves the number density.

The number density can provide information regarding the different phases present in the system, where a surface is located and the surface thickness. The surface thickness, δ, is defined as the region in the density profile that is not a part of the bulk liquid nor the bulk vapor, see figure 3.2.

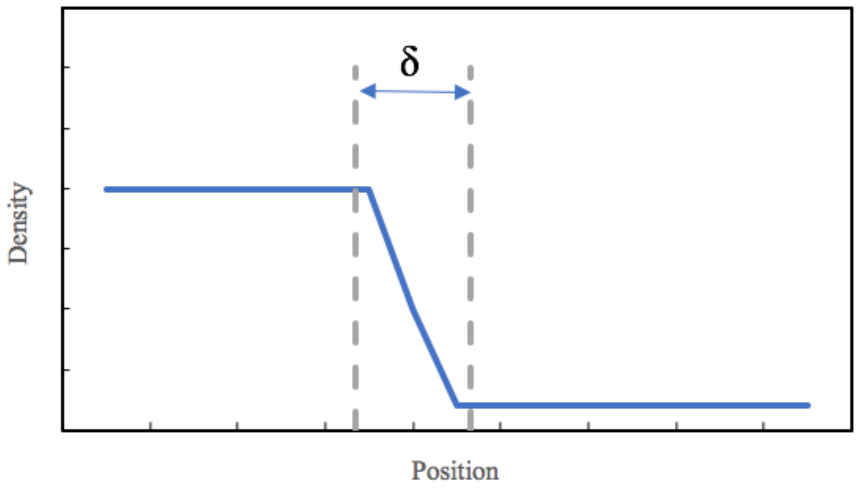

Figure 3. 2 Illustration of how the surface thickness, δ, is found. The vertical lines define the area that it not a part of the bulk phases.

Gibbs dividing surface would be located somewhere between the vertical lines in figure 3.2 [Kjelstrup, S., & Bedeaux, D. (2008)].

3.2.5 Error analysis

The best estimate of a quantity x is generally the average [Taylor, J. R. (1997)]. The average of N separated measurements of quantity x is defined as

$$\bar{x} = \frac{1}{N} \sum_{i}^{N} x_i \tag{3.21}$$

The uncertainty within the average of quantity x is given by the standard deviation of mean, defined as

$$\sigma_{SD,m} = \sqrt{\frac{\sum_i^N (x_i - \bar{x})^2}{N(N-1)}} \tag{3.22}$$

It is usual to use the standard deviation of mean when the reported value is a mean of several independent measurements. When using standard deviation, approximately 68% of the measurements of quantity x will lie within a distance $\pm 1\sigma_{SD,m}$ of the correct value, and 95% within $\pm 2\sigma_{SD,m}$. It is normal practice to use a confidence interval of 95%, meaning that two numbers should be separated by at least two standard deviations if they should be considered significantly different from each other. By calculating the uncertainties in the data points using standard deviation of mean, error bars can be added to the data. In this study, the error bars are defined as $\pm 1\sigma_{SD,m}$ and will give a graphical representation of the uncertainty within the data.

Regression is a method for finding the best model to represent a set of different data points [Taylor, J. R. (1997)]. When using regression, it is important to express a measure of how well the model fits the data points. The coefficient R^2 reflects the portion of the variation in the response variable that is explained by the regression model. In other word, how close the data points are to the regression model. A high value of R^2, close to 1, indicates that the model explains a significant amount of the variability of the response data. The higher the value of R^2, the better the model fits the data. In this study, it was decided that if $R^2 \geq 0.95$, then the model would be considered as a good representation of the data.

To compare different values, a statistical tool is required. A 1-sample t-test is a statistical method to test if there is a significant difference between the average of two datasets [Ross, S. M. (2014)]. The 1-sample t-test uses two different hypotheses; a null hypothesis and an alternative hypothesis. The null hypothesis assumes that there is no significant difference between the two averages, while the alternative hypothesis assumes that there is. A comparison of the average of N separated measurements of a quantity x, which is $\bar{x}$, to a theoretical value, μ_p, can be done using the formula

$$t_s = \frac{\bar{x} - \mu_p}{\sigma_{SD,m}} \tag{3.23}$$

where t_s is the test statistics. The probability value, called p-value, of the test statistic is the probability of observing test results under the null hypothesis. The p-value will help determine the significance of the results. A p-value less or equal to a chosen significance level shows strong evidence against the null hypothesis, and the null hypothesis will be rejected. The significance level is often chosen to be equal to 0.05, which corresponds to a 5% chance that the null hypothesis is rejected even though it was true. To find the p-value for the hypothesis tested in this study, the spreadsheet program Microsoft Excel[1] was used. The program provides a built-in function, T.TEST, that returns the probability associated with the t-test.

3.3 Simulation details

The software LAMMPS, version 11 August 2017 [Plimpton, S. (1995)], was used to create the simulation models used in this study. Lennard-Jones/spline potential was used in all simulations to describe the interparticle interactions. Water is a complicated liquid to simulate, so to simplify the systems, Lennard-Jones/spline particles were used instead. This study should consequently be treated as a model case for other systems that are closer to reality.

Membrane distillation can be used to separate two or several components. In this study, the mixture to be purified contained two components. The difference between the two components was their ε_{ij} and α_{ij} parameter, see section 3.3.6. The molecular diameter, σ_{ij}, and mass, m_i, was equal for all i and j. Besides being a crucial parameter for the mixture fluid, the α-parameter also controls the attraction strength of the pore wall-fluid interaction. Since water was not present in this study, hydrophobicity was understood as rejection of Lennard-Jones/spline particles.

Periodic boundary condition was used in all simulations, meaning that all systems were surrounded by periodic images of itself in all dimensions. For all systems, the system geometry was constructed so that the applied force, the gradient in temperature and chemical potential, was in the x-direction.

[1] Microsoft Excel version 15.31

The systems constructed were a simple two component system to investigate the separation effect, an equilibrium pore system created to determine the number of timesteps needed to reach stationary state (equilibrium system), and three pore systems used to find three resistivity coefficients. These three systems were: a system consisting of two different fluids in thermal equilibrium (system 1), a one-component system under a temperature gradient (system 2), and a system consisting of two different fluids under a temperature gradient with a mass flux equal to zero (system 3). For system 2 it was important that there was no gradient in chemical potential. To ensure that this was the case throughout the simulation time, pure fluid was used. If a two-component mixture had been used on both sides of the pore, and there had been a mass flux of solvent particles, then it would be likely that a gradient in chemical potential had developed over time.

A system containing two different fluids under a temperature gradient with a mass flux different from zero was also created to investigate the effect of temperature gradient and pore diameter on the mass flux (system 4). See section 3.3.6 for information about the different systems.

3.3.1 Separation effect of a two-component mixture

To purify a solution, a separation between solvent and solute is necessary. In this study, purification of a mixture is obtained using a hydrophobic pore, where only vapor will diffuse through the pore. Solvent will be understood as one type of Lennard-Jones/spline particle, type 1, while the solute will be another type of Lennar-Jones particle, type 2. It is desirable that only solvent particles diffuse through the pore in a vapor phase. This was defined as a separation effect. To understand how to obtain a separation effect, a simple, two-component system was constructed.

To create a separation effect in the mixture the Lennard-Jones/spline parameters ε and α were changed in relation to their value for pure solvent. For pure solvent, the ε and α had a value equal to 1. The epsilon parameter affects the strength of the Lennard-Jones potential. If this parameter increased a pair of particles would want to stay closer together. If the parameter decreased, they would want to stay further apart. Epsilon also affects the vapor pressure of a component. An increase of epsilon between a pair of particles of the same type means a lower vapor pressure. This because the vapor pressure decreases due to the stronger intermolecular forces between the particles. The alpha parameter can influence the miscibility of the mixture.

An increase in the alpha parameter between the solvent and solute particles would cause the mixture to behave more miscible.

A simulation box with dimensions $\{L_x, L_y, L_z\} = \{66\sigma_0, 33\sigma_0, 33\sigma_0\}$ was constructed. This volume was assumed to give a good representation of bulk phases. The box was filled with a faced centered cubic crystal consisting of two different types of Lennard-Jones/spline particles, solvent and solute. The two types of particles had different values for ε and α. Various combinations of the alpha and epsilon parameters were simulated to find the combination optimal for the binary mixture in the pore system. An optimal binary mixture would be a mixture that under a separation only allows solvent particles to separate into the vapor phase. Section 3.3.6 shows all the combinations that were simulated, and section 4.1 shows the results.

Solvent and solute particles were placed on the crystal lattice according to the desired mole fraction. The density of the crystal, which was n^*=0.8, was chosen so that the total density of the vapor-liquid system would lie within the two-phase range. The crystal was melted with temperature T^*=10 for 200,000 timesteps using *NVT* ensemble with the Nosé-Hoover thermostat. This approach will fix the temperature by changing the velocities of all fluid particles in the system. This will cause all the particles to have the same temperature. Such a high temperature was chosen because the request was to melt the crystal to obtain a liquid phase with randomly selected positions for the particles.

After the crystal had melted, the temperature was rescaled to 0.7, which was assumed to provide a two-phase system consisting of liquid and vapor. Later, this choice of temperature was confirmed by creating a Lennard-Jones/spline phase diagram for the two-component mixture, see figure 4.5. The temperature was rescaled using *NVT* ensemble with the Nosé-Hoover thermostat. This was done for 500,000 timesteps before any calculations were performed, to ensure that the temperature was 0.7 during the calculations.

A region of x=26σ_0 was defined in the center of the simulation box, from x=20σ_0 to x=46σ_0, and the particles that were outside this region were deleted. This created a two-phase system. The size of this region was chosen so that the liquid-vapor interfaces would not interact with each other or the other interfaces present due to periodic boundary conditions.

The calculations of the density, temperature and pressure were run over 2.0 million timesteps. This number of timesteps was chosen to obtain good statistical results.

3.3.2 Construction of a pore

During this study, several pore systems were made. All pores were constructed the same way, which is described below. A simple illustration of the simulation box is presented in figure 3.3.

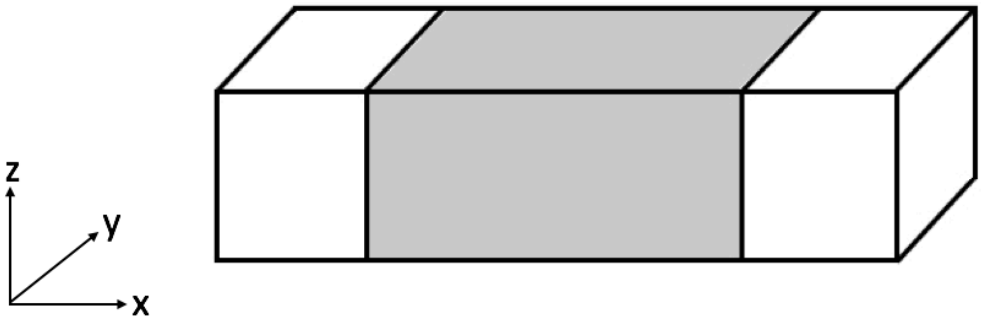

Figure 3. 3 Illustration of the simulation box. The grey area is the pore.

All systems containing a pore had the dimensions $\{L_x, L_y, L_z\} = \{180\sigma_0,\ 30\sigma_0,\ 30\sigma_0\}$. The length of the pore in the x-direction had to be large enough to avoid interaction between the two liquid-vapor interfaces. A pore length five times longer that the pore diameter was considered suitable, which meant that L_x had to be significantly larger than L_y and L_z.

The pore diameter must be of such size that the Knudsen diffusion regime apply, see section 2.4. Equation (2.30) was used to calculate the mean free path of the moving particles. For this calculation, the particle diameter of the vapor particle was set to $1\sigma_0$ and the number density was equal to $0.001\sigma_0^{-3}$. This gave a mean free path value of $225.08\sigma_0$. A Knudsen number greater than 10 indicates that Knudsen diffusion is significant to explain the diffusion in the system. To find a suitable pore diameter, equation (2.29) was used. A pore with a diameter of $20\sigma_0$ should be well within the Knudsen regime and was therefore used for the pores. A pore diameter equal to $20\sigma_0$ means that the pore length should be $100\sigma_0$.

To see how the mass transport depends on the pore diameter, simulations were also run for smaller diameters. A smaller pore diameter means that the length of the pore could be reduced. This was not done because a pore length of $100\sigma_0$ will prevent that the meniscus interacts

regardless of whether the pore diameter is smaller or equal to $20\sigma_0$. The chosen pore diameters were $15\sigma_0$ and $10\sigma_0$. They obey the Knudsen regime constraint and they are significantly different. A pore with a diameter smaller than $10\,\sigma_0$ was considered not credible. The simulations regarding finding the resistivity coefficients were only run with a pore diameter equal to $20\sigma_0$.

A region of length $100\sigma_0$ in the x-direction, and $30\sigma_0$ in the y- and z-direction, was filled with Lennard-Jones/spline particles with a density equal to n^*=1.189. These particles represented the pore wall and with such high density it is possible to avoid particles penetrating the wall. The location of the pore wall was from x =$40\sigma_0$ to x =$140\sigma_0$, in other words in the middle of the simulation box. The pore wall particles were fixed in a crystal faced centered cubic lattice structure. They had no temperature and acted like a Lennard-Jones wall throughout the simulations, meaning this crystal was not melted.

The remaining voids on each side of the pore were filled with a faced centered cubic crystal consisting of Lennard-Jones/spline particles. These particles represented the desired fluid, whether the fluid was pure or a mixture. The mixture contained two types of Lennard-Jones/spline particles. Type 1 was solvent and type 2 solute. These particles had different values for ε and α . The values used was ε_{12} =1.1, ε_{22} =1.2 and α_{12} =1.5. They were found in section 4.1.2. The pure liquid had all Lennard-Jones/spline parameters equal to 1.

The density of the pure crystal was n^*=0.8, and the density of the two-component mixture was n^*=1.0. These densities were chosen so that a liquid-vapor curved interface could form at the start and end of the pore. They were found using figure 4.5 and appendix C. The reason why the density of the mixture was higher than the pure crystal was because the increase in the epsilon and alpha parameters created a more compressed liquid when the temperature was reduced after the melting process. This led to a void between the pore wall and the mixture. A mixture density equal to 1.0 eliminated this void.

The crystals representing the fluids were melted with a temperature T^* =10 for 500,000 timesteps the same way as in section 3.3.1. The intention was to obtain a liquid phase. A high temperature was chosen so that there was no doubt that the crystal would melt. The number of timesteps for the melting process was increased relative to the system in section 3.3.1. This

because the pore system was a larger system and therefore considered necessary to run the melting process for a longer time. After the crystal had melted, the temperature was rescaled for 500,000 timesteps before any calculations were performed. The method used to rescale the temperature is explained in section 3.3.5.

A cylindrical pore was constructed by deleting a cylindrical unit from the pore wall. This unit had a length and diameter of $100\sigma_0$ and $20\sigma_0$, respectively. The pore diameter varied for simulations regarding the mass flux dependency on the pore diameter. To create a hydrophobic pore, the α-parameter between the Lennard-Jones fluid particles and the pore wall particles was set to 0.25. This low value decreased the attractive interaction between the pore wall particles and the fluid particles. A two-phase system with a convex liquid-vapor interface was formed at the start and end of the pore. Figure 3.4 shows an illustration of the pore.

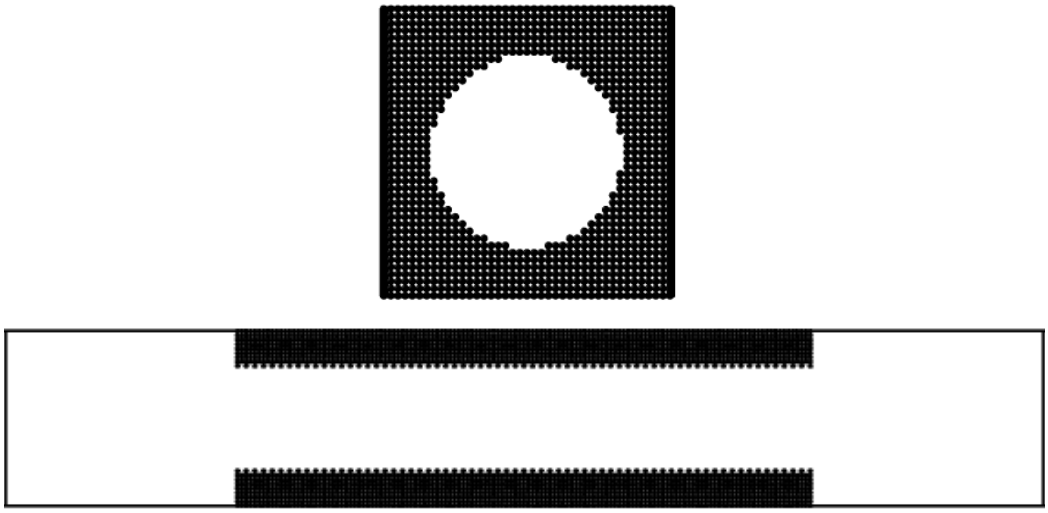

Figure 3. 4 Illustrations of the pore in the y-z plane, upper figure, and in the x-z plane, lower figure. The pore wall particles are shown in black. The pore diameter is $20\sigma_0$ and the length is $100\sigma_0$. The wall atoms have a density equal 1.189 and behave like a soft wall. With α=0.25 the pore has a hydrophobic character.

3.3.3 Reflective Particle Method

To maintain a mass transport over time, a source and sink of particles must be accounted for. The liquid phases in the system are containing a lot of particles, which means that there is little room for new particles to join the liquid phases, see figure 3.5.

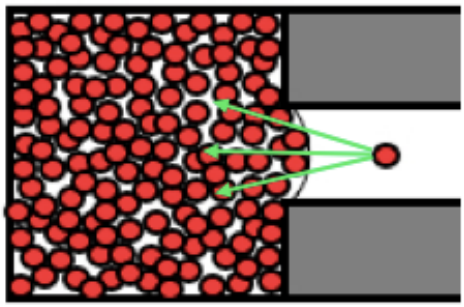

Figure 3. 5 Illustration of how a particle can struggle to find room to join the liquid phase without a source and sink of particles. The illustration shows half a pore.

Little room for new particles will inhibit the mass transport. To maintain a mass transport through a pore system, Reflective Particle Method (RPM) can be used [Li, J., Liao, D., & Yip, S. (1998)]. In this method, a fictitious membrane is introduced to the system. This membrane will allow some particles to pass and deny others. Figure 3.6 illustrates this.

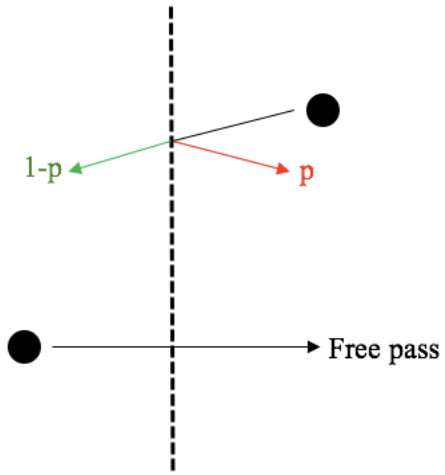

Figure 3. 6 Illustration of the Reflecting Particle Method [Li, J., Liao, D., & Yip, S. (1998)]. If a particle crosses the membrane from left to right it passes through without hindrance. If a particle crosses the membrane from right to left it will be elastically reflected with a probability p.

The membrane in figure 3.6 will allow particles from one side to cross the membrane without any hindrance, while particles from the other side will be elastically reflected with a probability equal to p. The membrane does not reject interactions between particles on the two different sides. Beside affecting the ability to cross the membrane, the membrane has no other effect on the particles in the system.

For a pore system with a binary mixture on one side of the pore, and a pure fluid on the other, there is a need for two RPM membranes. RPM membrane 1 will control particle crossing from right to left, and RPM membrane 2 from left to right. Figure 3.7 illustrates such a system.

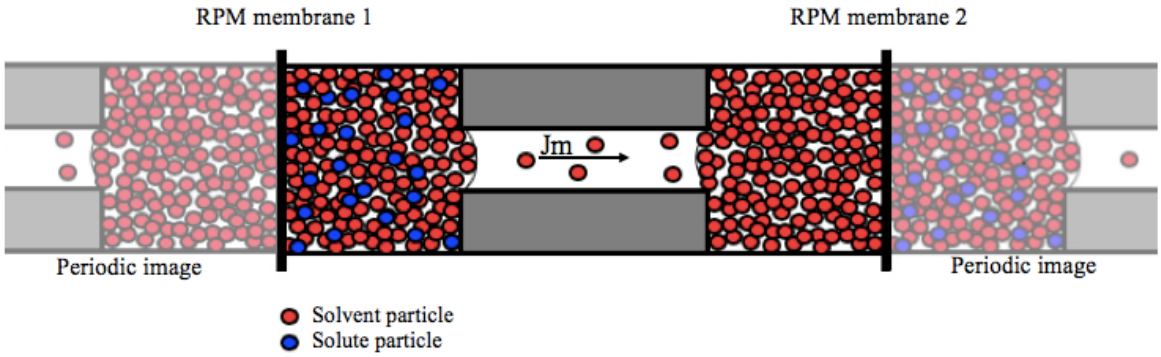

Figure 3. 7 Illustration of a system with two RPM membranes that inhibits particles from crossing the membrane. The illustration shows a system with only one pore and the systems periodic images due to periodic boundary conditions. Solvent and solute particles are shown in red and blue, respectively.

The idea behind the system presented in figure 3.7 is that RPM membrane 1 will prevent solute particles to emigrate to the pure phase, while solvent particles can cross the membrane from right to left. The degree to which they can pass depends on the system. The same applies for RPM membrane 2, which can create a little hindrance when solvent particles want to cross from left to right. The RPM method creates a source and sink of particles. The probabilities, p, for the two membranes are affected by system variables as temperature, composition and pore geometry. Which probability that was chosen for the different simulation cases are presented in section 3.3.6.

3.3.4 Pore system under equilibrium

A pore system with no driving forces, meaning a constant temperature and only one component, was constructed to find the minimum number of timesteps required for the equilibrium system to obtain steady state. This number of timesteps would indicate how many timesteps were needed for the non-equilibrium systems to obtain steady state. Steady state for the equilibrium system means a mass flux equal to zero, but for the non-equilibrium systems it means a mass flux constant through time.

For the equilibrium simulation, the number of timesteps was found by trial and error, see the results in section 4.2.1. If the time average mass flux was equal to zero, or not significantly

different from zero, within a given time interval, this number of timesteps was considered sufficient to achieve stationary state for the equilibrium system. Non-equilibrium systems are expected to use longer time to reach stationary state. The chosen number of timesteps for non-equilibrium systems should consequently be twice the size as what found for the equilibrium system.

The pore was constructed as described in section 3.3.2, but to simplify the equilibrium system, the liquid-vapor interface had no curvature, see figure 3.8.

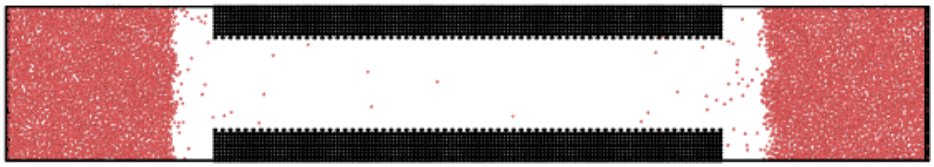

Figure 3. 8 Snapshot of the equilibrium pore system in the x-z plane with $T^* = 0.7$. The fluid particles are shown in red, while the pore wall particles are in black. The pore diameter is $20\sigma_0$.

When the pore wall was introduced to the system, the rest of the simulation box was supposed to be filled with fluid particles. For the equilibrium system, the simulation box was only partially filled with fluid particles. This means parts of the simulation box contained voids. These voids created vapor phases located outside the pore, which acted as a sink and source of particles. Hence, mass could be transported without adding RPM membranes.

The temperature was kept constant equal to T^*=0.7. *NVT* ensemble and Nosé-Hoover thermostat was used to fix the temperature. The temperature chosen here was the same temperature chosen for the separation system. Based on the phase diagram, see appendix C, this temperature will provide a two-phase system.

3.3.5 Thermostatting

Thermostatting is in this study defined as controlling the system temperature by applying a thermostat. Thermostatting was either applied to all particles in the system, as for the melting processes, the separation system in section 3.3.1 and the equilibrium system in section 3.3.4, or only applied to the two outer layers of the simulation box. When the thermostatting was applied to all particles, the system was in the *NVT* ensemble. When only the two outer layers where

thermostatted, the rest of the system was in the *NVE* ensemble. The energy was not preserved in the thermostatted layers.

If a system contained a temperature gradient then only the two outer layers of the simulation box were thermostatted, with one exception; system 1. System 1 was under thermal equilibrium but had a gradient in chemical potential. For this system, only the two outer layers were thermostatted because thermostatting all fluid particles did not maintain a constant temperature. The outer layers were thermostatted the same way as for a temperature gradient, but the layers had the same temperature.

To create a one-dimensional temperature gradient, two layers were defined perpendicular to the x-direction. The layers where located at the two ends of the box, and had dimensions $\{L_x, L_y, L_z\} = \{5\sigma_0, 30\sigma_0, 30\sigma_0\}$. The particles within one of the two layers were thermostatted with a high temperature and the particles within the other layer were thermostatted with a low temperature, see figure 3.9 for visualization. This was done by changing the velocities of the particles within the layers. To maintain a constant temperature gradient, the velocities of the particles within each layer was rescaled every 10^{th} timestep so that they obtained a constant temperature.

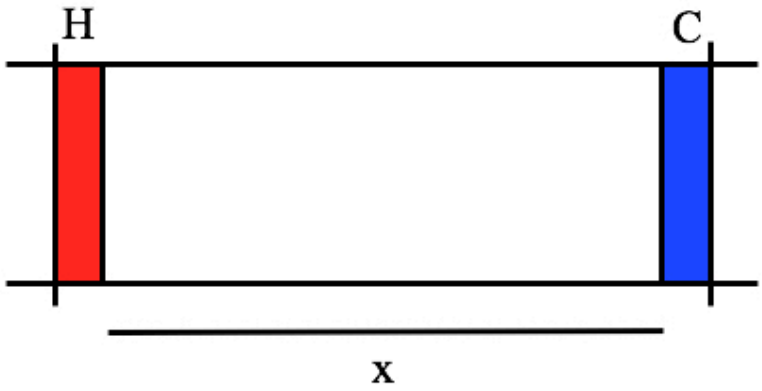

Figure 3. 9 Illustration of a thermostatted molecular dynamics cell. The red region, named H, is the hot region, and the blue region, named C, is the cold region.

For the system shown in figure 3.9, the heat flux will be from hot to cold area, and the linear temperature gradient will be defined as

$$\frac{\Delta T}{\Delta x} = \frac{T_c - T_h}{x_c - x_h} \tag{3.24}$$

where $\Delta T/\Delta x$ is the temperature gradient, T_c and T_h are the temperatures of the cold and hot thermostatted regions, and x_c and x_h are the position of the cold and hot thermostat along the x-direction. Equation (3.24) only holds for linear temperature gradients. For the system in figure 3.9 the temperature gradient will be negative.

The placement of the hot and cold thermostats was so that the mixture had the highest temperature. This was chosen for two reasons; according to figure 2.4, in order to achieve the desired direction of the mass transport, the mixture must have the highest temperature, and by comparing the phase diagrams for the mixture and pure component it was seen that the mixture requires a higher temperature to achieve a phase change.

The systems to be studied consists of two phases; vapor and liquid. It was important to select temperatures to provoke such a two-phase system. For the three systems used to find the resistivity coefficients, the different system temperatures were chosen so that the average temperatures in each system were approximately the same. Phase diagrams for the two-component system, see figure 4.5, and pure liquid, see Appendix C, were used to find suitable choice of temperatures so that both liquids could obtain a phase change.

To obtain a mass flux equal to zero in system 3, the values for the temperature gradient was found by trial and error to be 0.78 and 0.7 for the hot and cold thermostats. A mass flux equal to zero was essential for system 3, and therefore the temperatures found here were further used. With these temperatures, both liquids could achieve a phase change. The two-component system with thermal equilibrium had a constant temperature. This temperature was chosen to be equal the average temperature of the hot and cold thermostats, which was 0.74.

To see how the size of the temperature gradient affected the mass flux, simulations were run of system 4 with several different temperature gradients. There were certain criteria behind the choice of these temperature gradient. It was emphasized that the average temperature in the systems was equal to 0.74. The selected values also had to be within the vapor-liquid region on the phase diagrams. The chosen temperature gradients are presented in table 3.2, from lowest to highest gradient.

Table 3. 2 Table of temperatures for hot thermostat, T_h, and cold thermostat, T_c, used for system 4. All values are in reduced units.

T_h^*	T_c^*
0.76	0.72
0.78	0.70
0.80	0.68
0.82	0.66
0.84	0.64
0.86	0.62
0.88	0.60

3.3.6 Simulated cases

This section gives an overview of the different cases studied, see table 3.3, 3.4 and 3.5. For the study regarding the separation effect, the parameters that were studied was the ε_{22}, to change the vapor pressure of component 2, and α_{12}, to change the attraction between particle 1 and 2. Component 1 and 2 are solvent and solute component, respectively. The different cases studied can be found in table 3.3. The values of the parameters were chosen to be somewhere between 1 and 2, where 2 was viewed as a rather extreme increase in parameter value and 1 was the value used to describe the pure fluid.

A consequence of changing ε_{22} will be a change in ε_{12} due to the Berthelot rule [Delhommelle, J., & Millié, P. (2001)]. Equation (3.25) shows the geometric mean of ε_{12}

$$\varepsilon_{ij} = \sqrt{\varepsilon_{ii}\varepsilon_{jj}} \tag{3.25}$$

Table 3. 3 Table of input values for the different cases studied regarding evaluating the separation effect. 1 indicates solvent particles and 2 the solute particles. $N_{solvent}$ and N_{solute} are number of solute and solvent particles, respectively. T is temperature. Only Lennard-Jones/spline parameters ε_{12}, ε_{22} and α_{12} are represented in this table because all other Lennard-Jones/spline parameters were set to 1. All values are in reduced units.

System	σ_{ij}	ε_{ij}	α_{ij}	T^*	$N_{solvent}$	N_{solute}
Separation case A	σ_{11}=1 σ_{12}=1 σ_{22}=1	ε_{11}=1 ε_{12}=1 ε_{22}=1	α_{11}=1 α_{12}=1 α_{22}=1	0.70	16424	5577
Separation case B	σ_{11}=1 σ_{12}=1 σ_{22}=1	ε_{11}=1 ε_{12}=1.2 ε_{22}=1.5	α_{11}=1 α_{12}=1 α_{22}=1	0.70	16560	5485
Separation case C	σ_{11}=1 σ_{12}=1 σ_{22}=1	ε_{11}=1 ε_{12}=1.4 ε_{22}=2	α_{11}=1 α_{12}=1 α_{22}=1	0.70	16615	5537
Separation case D	σ_{11}=1 σ_{12}=1 σ_{22}=1	ε_{11}=1 ε_{12}=1.2 ε_{22}=1.5	α_{11}=1 α_{12}=1.5 α_{22}=1	0.70	16532	5554
Separation case E	σ_{11}=1 σ_{12}=1 σ_{22}=1	ε_{11}=1 ε_{12}=1.2 ε_{22}=1.5	α_{11}=1 α_{12}=2 α_{22}=1	0.70	16493	5540
Separation case F	σ_{11}=1 σ_{12}=1 σ_{22}=1	ε_{11}=1 ε_{12}=1.4 ε_{22}=2	α_{11}=1 α_{12}=1.5 α_{22}=1	0.70	16461	5567
Separation case G	σ_{11}=1 σ_{12}=1 σ_{22}=1	ε_{11}=1 ε_{12}=1.4 ε_{22}=2	α_{11}=1 α_{12}=2 α_{22}=1	0.70	16496	5542
Separation case H	σ_{11}=1 σ_{12}=1 σ_{22}=1	ε_{11}=1 ε_{12}=1.1 ε_{22}=1.2	α_{11}=1 α_{12}=1.5 α_{22}=1	0.70	16478	5541
Separation case I	σ_{11}=1 σ_{12}=1 σ_{22}=1	ε_{11}=1 ε_{12}=1.1 ε_{22}=1.2	α_{11}=1 α_{12}=2 α_{22}=1	0.70	16484	5566

The volume and density of the Lennard-Jones/spline crystals were the same for all simulation cases presented in table 3.3. Since the number of particles was not constant for all simulated cases, as seen from table 3.3, this implies that the number of particles was affected by the ε and α parameters.

The simulated cases regarding finding the three independent resistivity coefficients, r_{qq}, $r_{q\mu}$ and $r_{\mu\mu}$, are presented in table 3.4. The probability p was found by trial and error, and accepted if no drift were observed in the meniscus for the last millionth timestep.

Table 3. 4 Table of input values for the different cases studied regarding finding the resistivity coefficients. Only Lennard-Jones/spline parameters ε_{12}, ε_{22} and α_{12} are represented in this table because all other Lennard-Jones/spline parameters were set to 1. 1 and 2 represent solvent and solute particles, respectively. If the pore system only contains solvent particles, then there is not presented any value for the parameters. For the probability regarding the RPM membranes, p_1 and p_2 are understood as the probability of solvent and solute particles to cross the membrane, respectively. T is temperature, where T_h and T_c represent the hot and cold temperature, respectively. $N_{solvent}$, N_{solute} and $N_{pore\ wall}$ are number of solute, solvent and pore wall particles, respectively. All values are in reduced units.

System	ε_{12}	ε_{22}	α_{12}	probability RPM 1	probability RPM 2	T^*	$N_{solvent}$	N_{solute}	$N_{pore\ wall}$
Equilibrium system	-	-	-	-	-	0.70	41650	0	74744
System 1	1.1	1.2	1.5	p_1=0.45 p_2=1	p_1=0.9 p_2=0	0.74	53966	7935	74744
System 2	-	-	-	p_1=0	p_1=0.009	T_h^*=0.78 T_c^*=0.70	55737	0	74744
System 3	1.1	1.2	1.5	p_1=1 p_2=1	p_1=1 p_2=1	T_h^*=0.78 T_c^*=0.70	53966	7935	74744

To investigate how the temperature gradient and pore diameter affected the mass flux, several simulations were run with different temperatures. These simulation cases are presented in table 3.5.

Table 3. 5 Table of input values for the different cases studied regarding system 4. Only Lennard-Jones/spline parameters ε_{12}, ε_{22} and α_{12} are represented in this table because all other Lennard-Jones/spline parameters were set to 1. 1 and 2 represent solvent and solute particles. For the probability regarding the RPM membranes, p_1 and p_2 are understood as the probability of solvent and solute particles to cross the membrane, respectively. d_p is the pore diameter. T is temperature, where T_h and T_c represent the hot and cold temperature, respectively. $N_{solvent}$, N_{solute} and $N_{pore\ wall}$ are number of solute, solvent and pore wall particles, respectively. All values are in reduced units.

ε_{12}	ε_{22}	α_{12}	probability RPM 1	probability RPM 2	d_p^*	T^*	$N_{solvent}$	N_{solute}	$N_{pore\ wall}$
1.1	1.2	1.5	p_1=0, p_2=1	p_1=0.08 p_2=0	$20\sigma_0$	T_h^*=0.76 T_c^*=0.72	53966	7935	74744
1.1	1.2	1.5	p_1=0, p_2=1	p_1=0.08 p_2=0	$15\sigma_0$	T_h^*=0.76 T_c^*=0.72	53966	7935	90972
1.1	1.2	1.5	p_1=0, p_2=1	p_1=0.08 p_2=0	$10\sigma_0$	T_h^*=0.76 T_c^*=0.72	53966	7935	102676
1.1	1.2	1.5	p_1=0, p_2=1	p_1=0.08 p_2=0	$20\sigma_0$	T_h^*=0.78 T_c^*=0.70	53966	7935	74744
1.1	1.2	1.5	p_1=0, p_2=1	p_1=0.08 p_2=0	$15\sigma_0$	T_h^*=0.78 T_c^*=0.70	53966	7935	90972
1.1	1.2	1.5	p_1=0, p_2=1	p_1=0.08 p_2=0	$10\sigma_0$	T_h^*=0.78 T_c^*=0.70	53966	7935	102676
1.1	1.2	1.5	p_1=0, p_2=1	p_1=0.08 p_2=0	$20\sigma_0$	T_h^*=0.8 T_c^*=0.68	53966	7935	74744
1.1	1.2	1.5	p_1=0, p_2=1	p_1=0.08 p_2=0	$15\sigma_0$	T_h^*=0.8 T_c^*=0.68	53966	7935	90972
1.1	1.2	1.5	p_1=0, p_2=1	p_1=0.08 p_2=0	$10\sigma_0$	T_h^*=0.8 T_c^*=0.68	53966	7935	102676
1.1	1.2	1.5	p_1=0, p_2=1	p_1=0.08 p_2=0	$20\sigma_0$	T_h^*=0.82 T_c^*=0.66	53966	7935	74744
1.1	1.2	1.5	p_1=0, p_2=1	p_1=0.08 p_2=0	$15\sigma_0$	T_h^*=0.82 T_c^*=0.66	53966	7935	90972
1.1	1.2	1.5	p_1=0, p_2=1	p_1=0.08 p_2=0	$10\sigma_0$	T_h^*=0.82 T_c^*=0.66	53966	7935	102676

1.1	1.2	1.5	p_1=0, p_2=1	p_1=0.08 p_2=0	$20\sigma_0$	T_h^*=0.84 T_c^*=0.64	53966	7935	74744
1.1	1.2	1.5	p_1=0, p_2=1	p_1=0.08 p_2=0	$15\sigma_0$	T_h^*=0.84 T_c^*=0.64	53966	7935	90972
1.1	1.2	1.5	p_1=0, p_2=1	p_1=0.16 p_2=0	$10\sigma_0$	T_h^*=0.84 T_c^*=0.64	53966	7935	102676
1.1	1.2	1.5	p_1=0, p_2=1	p_1=0.08 p_2=0	$20\sigma_0$	T_h^*=0.86 T_c^*=0.62	53966	7935	74744
1.1	1.2	1.5	p_1=0, p_2=1	p_1=0.08 p_2=0	$15\sigma_0$	T_h^*=0.86 T_c^*=0.62	53966	7935	90972
1.1	1.2	1.5	p_1=0, p_2=1	p_1=0.18 p_2=0	$10\sigma_0$	T_h^*=0.86 T_c^*=0.62	53966	7935	102676
1.1	1.2	1.5	p_1=0, p_2=1	p_1=0.08 p_2=0	$20\sigma_0$	T_h^*=0.88 T_c^*=0.60	53966	7935	74744
1.1	1.2	1.5	p_1=0, p_2=1	p_1=0.11 p_2=0	$15\sigma_0$	T_h^*=0.88 T_c^*=0.60	53966	7935	90972
1.1	1.2	1.5	p_1=0, p_2=1	p_1=0.2 p_2=0	$10\sigma_0$	T_h^*=0.88 T_c^*=0.60	53966	7935	102676

4 Results and discussion

In this section, the results obtained during the study, as well as discussions of these results, are presented. The aim of this study was to find the resistivity coefficients present due to a thermal and chemical potential driving force. These coefficients are important for providing accurate information regarding the mass transport and are therefore important in membrane distillation. Also, how the mass flux depended on size of temperature gradient and pore geometry was studied. This information is essential for finding optimal conditions for membrane distillation.

Section 4.1 contains results and discussions regarding the separation effect, which is an important effect when purifying a mixture. Section 4.2 concerns finding the independent resistivity coefficients r_{qq}, $r_{\mu q}$ and $r_{\mu\mu}$. To find the resistivity coefficients the mass and measurable heat flux were important. Plots of the mass and measurable heat flux were presented for all systems involved in the resistivity coefficient calculations. In section 4.3, the mass flux dependence on the temperature gradient and pore diameter was evaluated.

Temperature profiles for all systems are presented to confirm that they have the desired temperature. The number density assists in confirming that a two-phase system is achieved and therefore a density profile is also presented for all systems. All property calculations were performed after the systems reached stationary state. For all mixtures used in the pore systems, the initial composition was a 75/25 solvent-solute mixture. This composition was chosen as a threshold. If a separation effect was observed at this composition, a separation effect would also arise for more realistic compositions, which have a significantly smaller concentration of solute compared to the threshold.

4.1 Separation of a two-component Lennard-Jones/spline mixture

Membrane distillation is a separation process where separation is obtainable due to a phase change. A simple two-component system was constructed to create and verify a separation effect in a two-phase system. In this study, separation effect was defined as no solute particles present in the vapor phase. The system consisted of two different types of Lennard-Jones/spline particles, solvent and solute. These particles had different values for the ε and α parameters. A various of different combinations of the ε and α parameters were simulated to find the optimal

combination for obtaining a separation effect. The different values investigated can be found in section 3.3.6. It is important to understand how these parameters affect the system, so a thorough analysis is performed to find optimal conditions for the pore systems.

A snapshot to illustrate the system is presented in figure 4.1, which corresponds to simulation case F with a solvent mole fraction equal to 0.75.

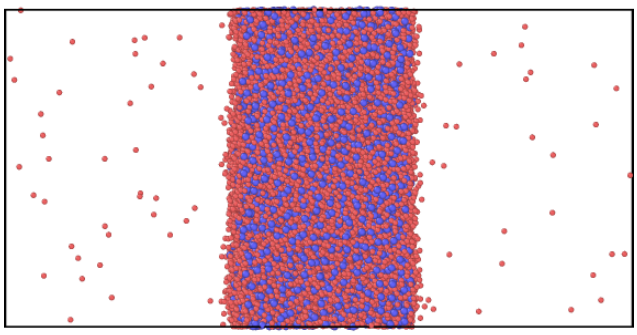

Figure 4. 1 Snapshot of a two-component system in the x-z plane with $T^* = 0.7$. The mole fraction of solvent particles is 0.75. The red particles represent the solvent and the blue particles the solute. For this simulation, the ε_{22} was set to 2, ε_{12} was 1.4 and the α_{12} was set to 1.5. This corresponds to simulation case F. All other Lennard-Jones/spline parameters were set to 1.

Figure 4.1 depicts that the surface mostly contained solvent particles. For this simulation case, the ε_{22} was equal to 2, ε_{12} was 1.4 and the α_{12} was equal to 1.5 Because of the increased solvent-solute and solute-solute attraction, a solute particle would want to be surrounded by solvent and other solute particles. In general, a particle on a vapor-liquid interface has much fewer neighbors than a particle in bulk liquids. For the solute to be surrounded by other particles, it is best to avoid the surface. Therefore, a thin film of solvent particles was formed.

For high concentrations of solute particles, for example a 50/50 solvent-solute mixture, it was challenging to achieve a separation effect because the solute particles were dominating in the mixture. A 75/25 solvent-solute mixture was considered as a threshold. If a separation effect was observed at this mixing ratio, this would also give a separation effect for more realistic mixing ratios. The mole fraction of solute component in a 75/25 solvent-solute mixture was plotted against position along the x-direction for all simulated cases, see figure 4.2. This was done to investigate which simulation cases achieved a separation effect. If the solute mole fraction in the vapor phase was greater than zero, then a separation effect had not been achieved.

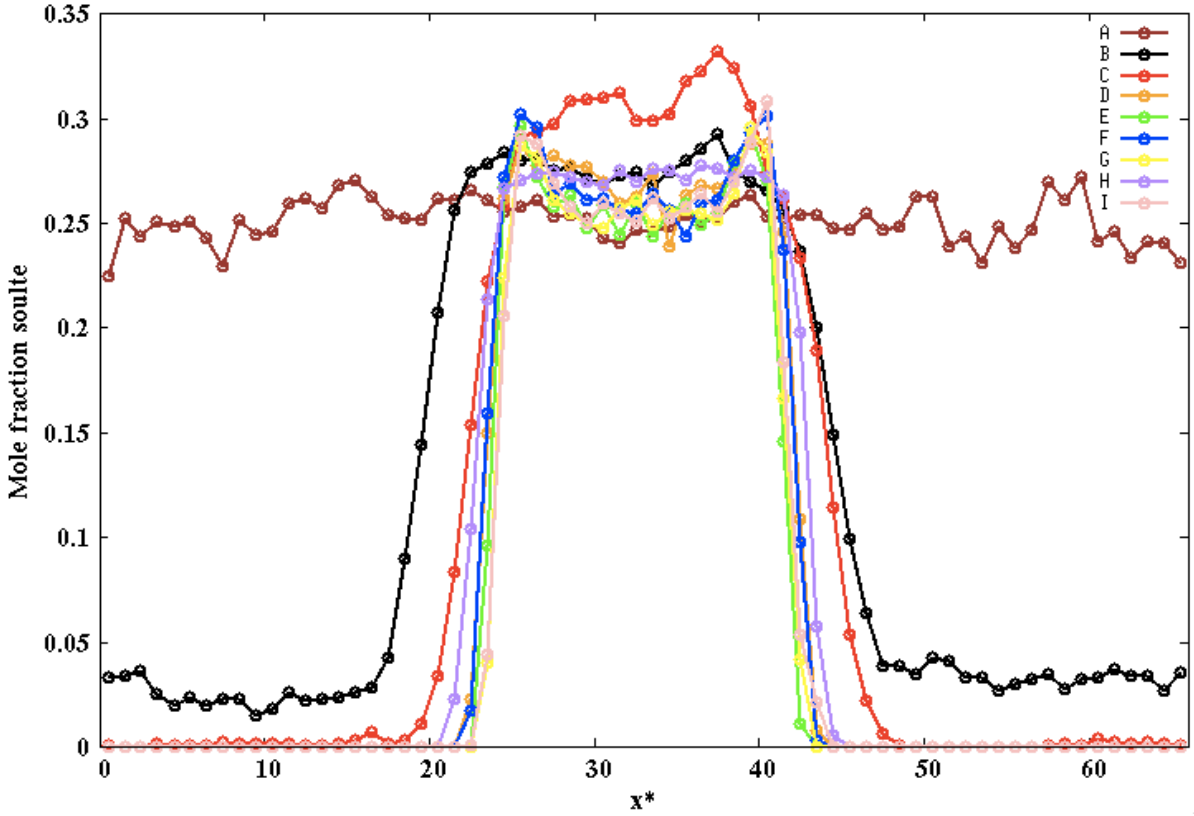

Figure 4. 2 Plot of mole fraction of solute particle along the x-axis with $T^* = 0.7$. The lines represent different simulation cases, explained in section 3.3.6. The initial mole fraction of solute particles was 0.25. All values are in reduced units.

Figure 4.2 depicts that the epsilon and alpha parameter were of great importance when it came to the presence of solute particles in the vapor phase. For simulation case A, B and C, the vapor phase was contaminated with solute particles. Additionally, the liquid in simulation case C had a significantly higher solute mole fraction than the initially 0.25. This was because the number of solvent particles in the vapor phase was quite high for this simulation case. This led to a smaller excess of solvent particles in the liquid phase.

The conditions under simulation case A, B and C were not ideal to obtain a separation effect. For these simulation cases α_{12} was equal to 1. This implies that an $\alpha_{12} > 1$ is important for the separation effect. For further studies, simulation case A, B and C were not included.

4.1.1 Epsilon and alphas effect on the vapor pressure

When changing the values of Lennard-Jones/spline parameters it is important to know what impact these changes will have on the system. As mentioned earlier, intermolecular forces between particles have an effect on the pressure. To understand how the Lennard-Jones/spline parameters affects the vapor pressure, the total pressure was plotted against the solvent mole fraction, see figure 4.3.

The total pressure was found as an average over the pressure in the vapor phase over the last 500,000 timesteps. Since the interface between the vapor and liquid was planar, the pressure was constant through the system, but fluctuated more in the liquid phase. Therefore, the pressure was found from the vapor phase. Since an average was used, the plots contain error bars. The pressure along the x-direction was approximately constant within the vapor phase, so the error bars were small, and for some data points, not visible.

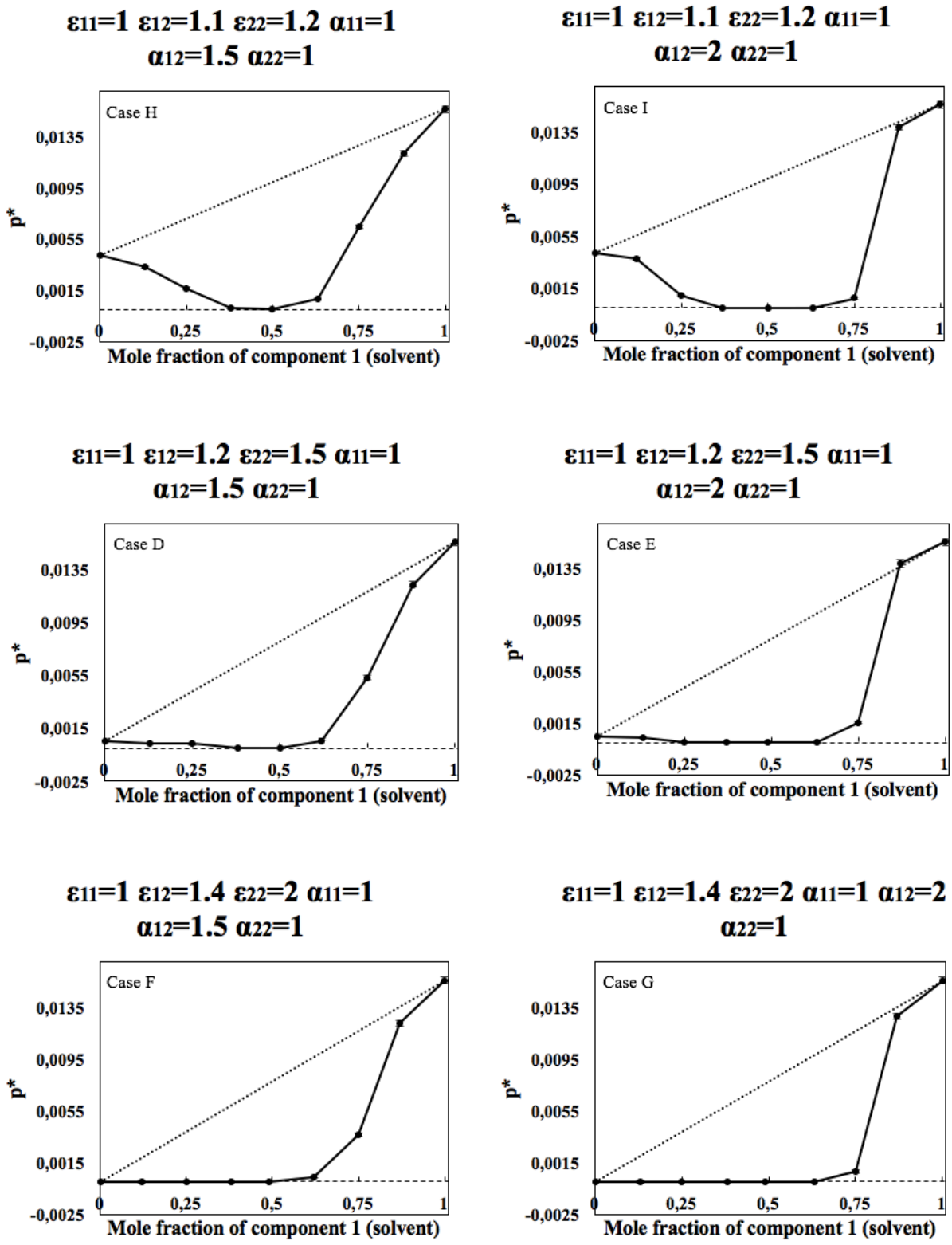

Figure 4. 3 Plot of total pressure, p^*, against mole fraction of solvent component for different combinations of ε_{22} and α_{12} with $T^* = 0.7$. Particle type 1 and 2 are solvent and solute particle, respectively. The dotted line represents Raoult's law. The error bars are calculated using standard deviation of mean, see equation (3.22), and represent $\pm 1\sigma_{SD,m}$. All values are in reduced units.

Figure 4.3 depicts a negative deviation from Raoult's law. A negative deviation means the intermolecular forces between solvent and solute particles are stronger than the forces between particles of same type.

As ε_{22} increased, the vapor pressure for low compositions of solvent particles approached zero. A vapor pressure equal to zero means that no particles were present in the vapor phase. Increasing ε_{22} means an increase in the interaction forces between a pair of solute particles. When the composition of solute particles was high and ε_{22}=2, solute particles would much rather stay close together, than diffuse into a vapor phase.

A vapor pressure equal to zero is not very realistic, but neither is a solvent mole fraction less than 0.5. For the pressure plots to be useful, one should investigate the areas where the mole fraction of solvent is high. So, for further investigation, only areas with a high concentration of solvent was considered. For a solvent mole fraction equal to 1, meaning a pure solvent, the pressure was equal for all values of ε_{22} and α_{12}. This was of course because there was only one type of particle present in the fluid, which made the ε_{22} and α_{12} parameters irrelevant for this mole fraction.

An increase in α_{12} means an increase in the attractive forces between solvent and solute particles. This means that the solvent and solute particles that are adjacent to each other would rather stay close, than diffuse into the vapor phase. The solvent particles that are not adjacent to a solute particle will be able to form a vapor phase. From figure 4.3 it was seen that increasing α_{12} lead to a decreasing vapor pressure for solvent mole fraction equal to 0.63 and 0.75. This was expected because increasing α_{12} means that fewer solvent particle will form a vapor phase because the strong attractive forces between solvent and solute. For a solvent mole fraction equal to 0.88, the pressure increased as the attraction force between the different particles increased. This could be because there was a large excess of solvent particles, hence only a few solvent particles were adjacent to a solute particle. The movement of the adjacent solvent and solute in the mixture could be inhibited by the strong, attractive forces between them, causing the particles to become locked in their position. This would allow the solvent particles not adjacent to a solute particle to enter the vapor phase more easily, as they were prevented from approaching solute particles. This could be a possible explanation for the trend observed for solvent mole fraction equal to 0.88.

4.1.2 Simulation case H

From the previous section, and figure 4.3, it was seen that ε_{22}=1.5 and ε_{22}=2 caused mixtures with high solute mole fractions to obtain an extremely low vapor pressure. This implies that these values were too extreme for the ε parameter. Simulation case H, with ε_{22}=1.2 and α_{12}=1.5, was chosen to use in further simulations as it provided a separation effect while the vapor pressure of pure solute was not equal to zero. α_{12}=2 gave a vapor pressure almost equal to zero for the threshold concentration, which was a 75/25 solvent-solute mixture. Therefore, this value was not chosen.

In simulation case H, the ε_{12} was equal to 1.1 due to the Berthelot rule, see equation (3.25). All other Lennard-Jones/spline parameters were set to 1. An ε_{22} of 1.2 created a desired vapor pressure difference between pure solvent and pure solute, and an α_{12} equal to 1.5 caused the mixture to behave miscible.

For simulation case H, the achievement of a two-phase system was confirmed by the number density profile, see figure 4.4. When the liquid and vapor was in equilibrium, the number density and temperature of the system were found as an average over time. The solvent mole fraction was equal to 0.75 for all presented data of simulation case H.

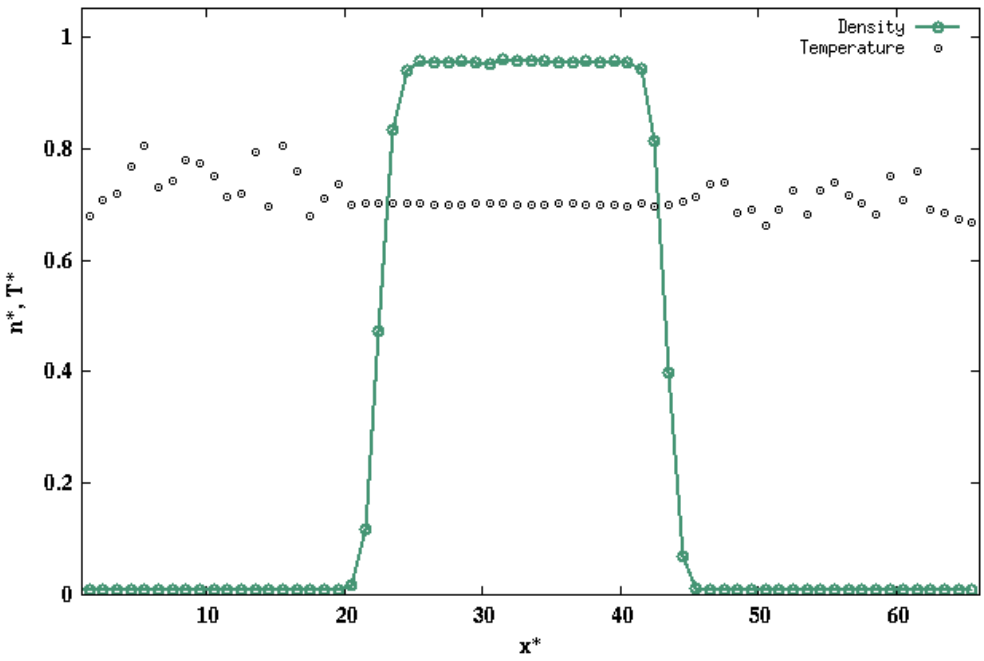

Figure 4. 4 Plot of the temperature and number density profile with $T^* = 0.7$. The mole fraction of solvent particles is 0.75. The line represents the number density and the dots represents the temperature. For this simulation, the ε_{22} was set to 1.2, ε_{12} was 1.1 and the α_{12} was set to 1.5. All other Lennard-Jones/spline parameters were set to 1. All values are in reduced units.

Figure 4.4 depicts that the density of the liquid was much higher that the density of the vapor. This significant difference in density confirms the achievement of a two-phase system. The initial density of the liquid was set to 0.8, but figure 4.4 depicts that the density in the liquid was higher. To create this two-phase system a large number of liquid particles were deleted. It was expected that the liquid density would decrease when the simulation started because some of the particles in the liquid phase would diffuse into the void and create a vapor phase. The density found in the mixture relative to the initial density indicates that the increased attractive forces between solvent and solute causes the mixture to be denser. The total density of the system was 0.31.

Figure 4.4 also depicts an approximately constant temperature in the liquid phase, but in the vapor phase it was fluctuating. That was because the vapor phase contained very few particles and the temperature was calculated based on a group of particles, see section 3.2.3. Since the temperature is dependent on the number of particles, regions with very low particle density, as for the vapor phase, would experience a fluctuation in the temperature profile.

A Lennard-Jones/spline phase diagram for simulation case H was constructed to obtain information regarding the vapor-liquid phase boundary, see figure 4.5. This was done by performing simulations the same way as described in section 3.3.1, but at several different temperatures. The temperature was plotted against the density. The density of the different phases was calculated according to the description in section 3.2.4. The phase diagram presents the different combinations of liquid, vapor and solid that can coexist.

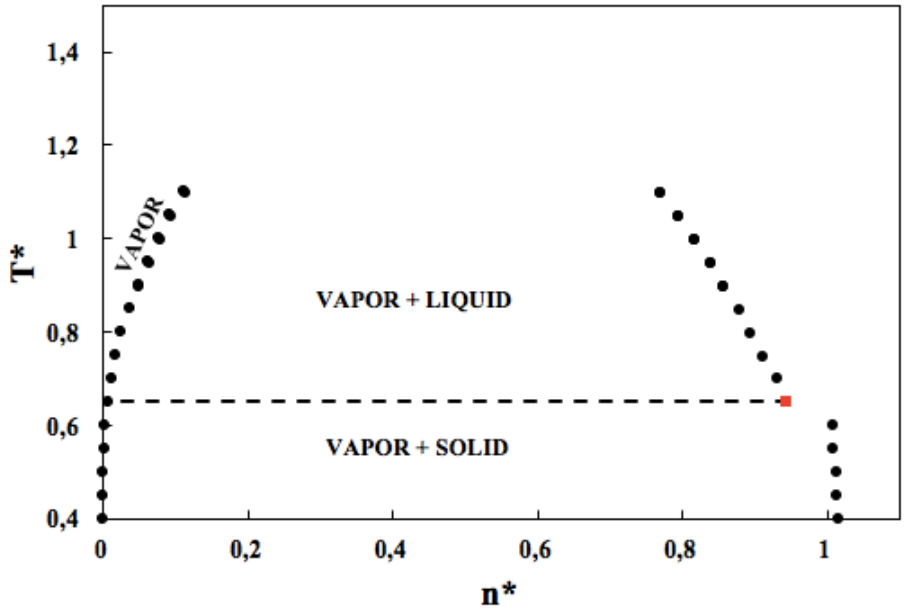

Figure 4. 5 Phase diagram for a two-component mixture of Lennard-Jones/spline particles. T^* is the temperature and n^* is the number density. The mole fraction of solvent particles is 0.75. For these simulations, the ε_{22} was set to 1.2, ε_{12} was set to 1.1 and α_{12} was set to 1.5. All other Lennard-Jones/spline parameters were set to 1. All values are in reduced units.

Figure 4.5 depicts the phase diagram created for a two-component mixture corresponding to simulation case H. The red square represents the data point that is, or is close to, the triple point. The triple point is the density and temperature where the three phases vapor, liquid and solid coexists in thermodynamic equilibrium [Clark, J. B. et al. (1994)]. The straight, dotted line was extracted from the red square, and marks the two-phase region of vapor and liquid. If the triple point was not equal to the data point represented by the red square, but had a lower value, the dotted line in figure 4.5 would be overestimated. Since the desire is to stay within the vapor-liquid region, the line would still be a good marker even with this overestimation. The region under the dotted line was the region where vapor and solid coexists.

The critical temperature is the temperature where the phase boundary between liquid and vapor does not exist [Clark, J. B. et al. (1994)]. This will be at the top of the phase equilibrium curve. There was no desire to run any simulations at the critical temperature, so this was not found. From figure 4.5 it is seen that the chosen temperature for the simulations of the separation effect, which was 0.7, was a good choice. This because the system lied within the vapor-liquid coexisting region.

Since some pore systems contain both a two-component mixture and a pure liquid, it was chosen to compare these fluids. A plot of the vapor pressure is presented in figure 4.6, where

the vapor pressure is plotted against various temperatures for simulation case A, pure fluid, and simulation case H, mixture. The plot shows the relation between pressure and temperature, and the relation between the pure liquid and the two-component mixture. The vapor pressure was found as an average over the pressure along the x-direction in the vapor phase, and the temperature was found as an average over the temperature in the liquid phase.

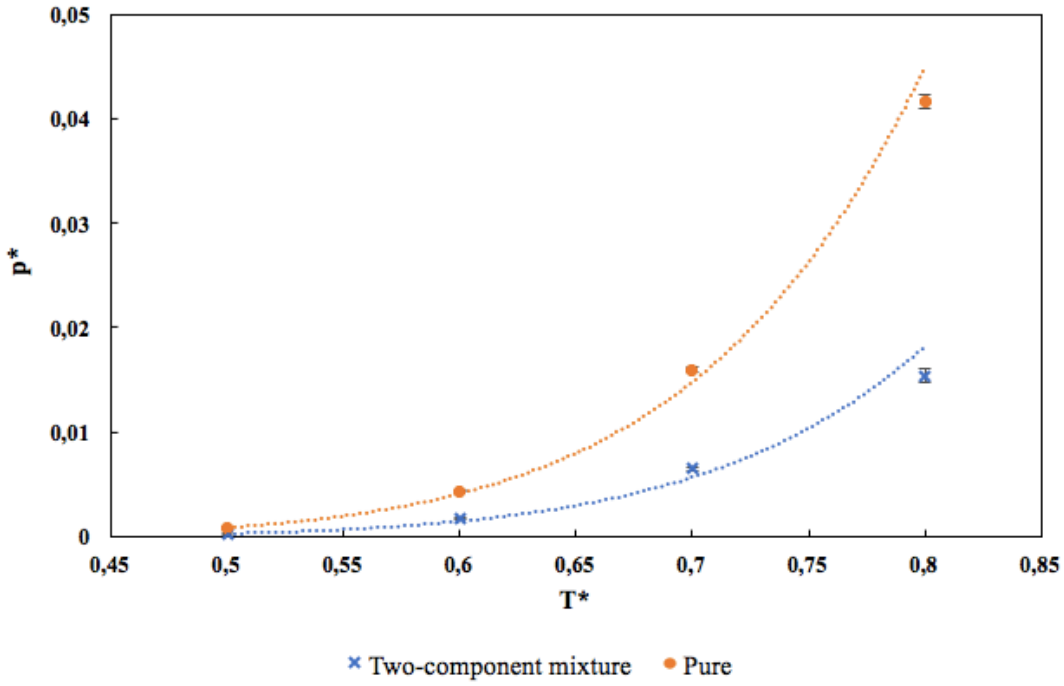

Figure 4. 6 Plot of vapor pressure, p^*, against temperature, T^*, for pure component, dots, and for a two-component mixture, crosses. The mole fraction of solvent particles is 0.75. For the mixture, ε_{22} was set to 1.2, ε_{12} was set to 1.1, α_{12} was set to 1.5 and all other Lennard-Jones/spline parameters were set to 1. For the pure fluid system, all Lennard-Jones/spline parameters were equal to 1. The error bars are calculated using standard deviation, see equation (3.22), and defined as $\pm 1\sigma_{SD,m}$. The dotted lines are power trend lines. All values are in reduced units.

The dotted lines seen in figure 4.6 are power trend lines, and shows the relations between temperature and pressure. The plot contains temperatures that from the phase diagram in figure 4.5 were known to be within the vapor-liquid coexisting region and the vapor-solid coexisting region.

The plot depicts that the pressure increased as the temperature increased. At higher temperatures, the particles obtain a greater kinetic energy, see equation (3.13). The liquid phase becomes more volatile when the temperature increases. This causes the particles to tear away from the liquid phase more easily, and diffuse into the vapor phase. A greater number of particles in the vapor phase causes a higher pressure. The vapor pressure of the one-component

fluid was higher than of the two-component mixture. This was expected because an increase of ε_{22} decreases the vapor pressure of the mixture.

For an open system consisting of both pure liquid and a two-component mixture separated by a hydrophobic pore, the direction of the mass transport can be indicated using figure 4.6. If the pure liquid had a significantly lower temperature than the mixture, such as a temperature difference equal to two, this would also imply that the pure liquid has a lower vapor pressure compared to the mixture. The theory states that mass transport would occur from the liquid with the highest vapor pressure, or from the liquid with the highest temperature. In this example, the two-component mixture would have both the highest temperature and vapor pressure, meaning mass transport would occur from the mixture towards the pure liquid.

If the pure liquid and mixture had the same temperature, then figure 4.6 depicts that the mass transport would be from pure liquid towards the two-component mixture, because the mixture had the lowest vapor pressure.

Vaporization enthalpy is the property of a liquid which states that a transformation from one phase to another is caused by the amount of heat introduced to the system [Helbæk, M., & Kjelstrup, S. (2006)]. Vaporization enthalpy per solvent particle was calculated as the difference between the enthalpy per solvent particle found in the vapor and liquid phase, $\Delta_{vap}H = H_{vapor} - H_{liquid}$. For this calculation, the chosen temperature was 0.7, but the vaporization enthalpy should be independent of temperature under small temperature ranges. Hence, other temperatures should give the same results. The values obtained are found in table 4.1. The reason why this property was found solely for solvent particles was because the vapor phase only contained solvent particles, while the liquid consisted of both solvent and solute. This means that the enthalpy found for the two different phases are not comparable as they do not have the same composition.

Table 4. 1 Table of vaporization enthalpy per particle of solvent component, $\Delta_{vap}H^*_{part,solvent}$. For these calculations $T^* = 0.7$ and the mole fraction of solvent particles was 0.75. The error bars are calculated using standard deviation, see equation (3.22), and defined as $\pm 1\sigma_{SD,m}$. All values are in reduced units.

System	$\Delta_{vap}H^*_{part,solvent}$
Pure	4.05 ± 0.01
Two-component mixture	6.49 ± 0.04

Table 4.1 reveals that the solvent vaporization enthalpy was higher for the two-component mixture than for the pure fluid. This means the amount of energy required to transform the mixture into vapor is greater than for the pure liquid. The mixture needs a higher temperature for solvent particles to diffuse into the vapor phase, which is consistent with the comparison of the different phase diagrams. The phase diagram of the mixture, figure 4.5, compared to the phase diagram of the pure liquid, appendix C, shows that the mixture needs a higher temperature for vapor and liquid to coexist. To check the data obtained for the vaporization enthalpy, the vaporization enthalpy was found by using Clausius equation and Clausius-Clapeyrons equation, see appendix D.

4.2 Calculations of resistivity coefficients

This section presents four different systems constructed to find the independent resistivity coefficients r_{qq}, $r_{\mu q}$ and $r_{\mu\mu}$. The resistivity coefficients are of interest in problems involving membrane distillation because they can provide accurate information regarding the mass flux.

The four systems constructed were; an equilibrium system made to determine how long the simulations must run before they reach stationary state, see section 4.2.1, a system containing two fluids in thermal equilibrium (system 1), see section 4.2.2, a one-component system under a temperature gradient (system 2), see section 4.2.3, and a system containing two fluids under a temperature gradient with a mass flux equal to zero (system 3), see section 4.2.4.

To calculate the resistivity coefficients, the mass flux and measurable heat flux are essential. These fluxes are therefore presented for system 1, 2 and 3. The properties of the different systems were found as averages over the last 500,000 timesteps. The calculated resistivity coefficients can be found in section 4.2.5.

4.2.1 Equilibrium system

An equilibrium system, meaning no driving forces, was created to obtain a time perspective and find the number of timesteps required for a system with driving forces to achieve stationary state. If the equilibrium system had a time average mass flux equal to zero at a given timestep, that would indicate that this number of timesteps was sufficient for this system to reach stationary state. A system with driving forces was expected to use longer time to reach

stationary state. The number of timesteps used in a non-equilibrium system was therefore set to twice the size as the number of timesteps found for the equilibrium system.

In the equilibrium system, the fluid only consisted of one type of Lennard-Jones/spline particle. There were no external forces, meaning the temperature was constant throughout the system. An illustration of the equilibrium system is presented in figure 4.7.

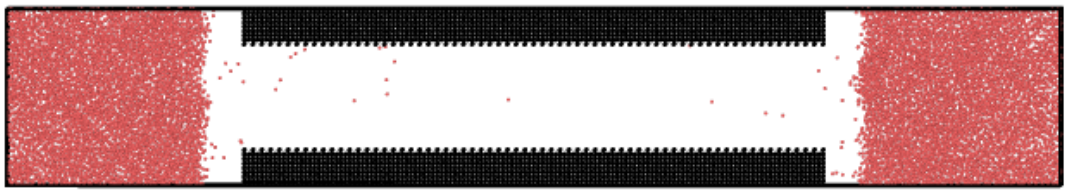

Figure 4. 7 Snapshot of a two-component system in the x-z plane with $T^* = 0.7$. The red particles represent the solvent and the black particles represent the pore wall. The pore diameter is $20\sigma_0$.

Figure 4.7 depicts a snapshot of the equilibrium system, showing vapor particles diffusing through the pore. To verify a constant temperature and that a two-phase system had been achieved, a temperature and density profile are presented in figure 4.8.

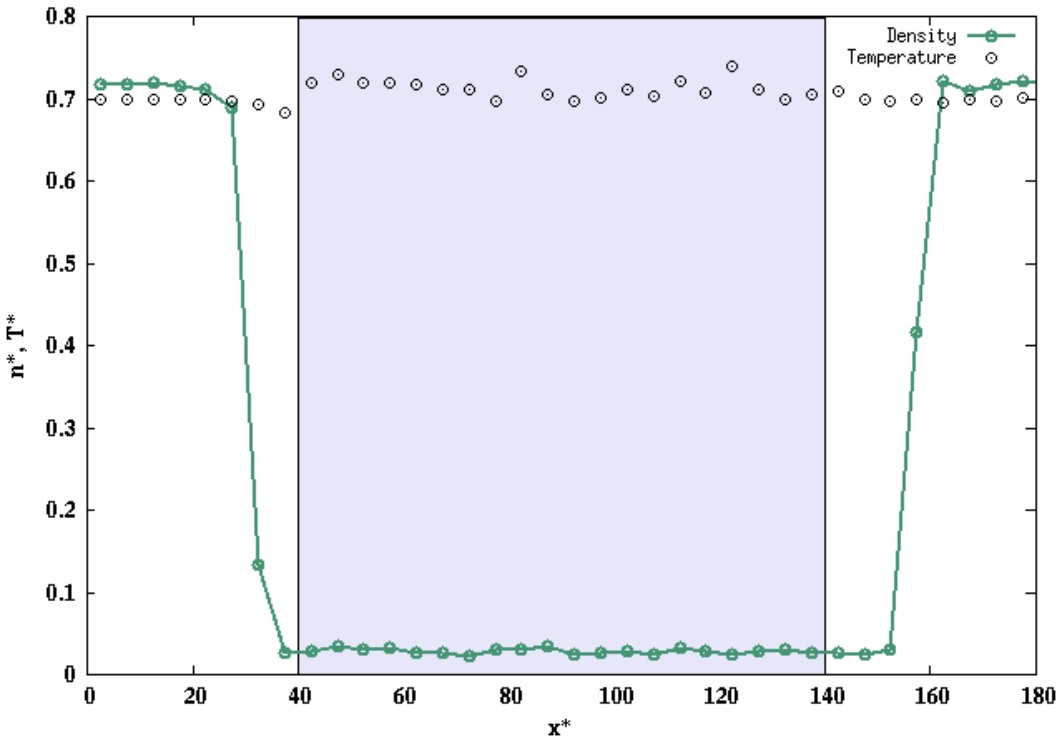

Figure 4. 8 Number density and temperature profile of the equilibrium pore system along the x-direction for $T^* = 0.7$. The colored area represents the pore. The line and the dots represent the number density and temperature, respectively. All values are in reduced units.

It is seen from figure 4.8 that the temperature fluctuated in the vapor phase, but was close to constant in the liquid phase. As discussed earlier, this was an expected behavior of the temperature. The density profile shows that the density dropped drastically when entering the vapor phase, as expected. The drop in density confirms that a two-phase system was achieved.

The mass flux was calculated using equation (3.10), and presented in figure 4.9 as an average over the last 500,000 timesteps. The pore is located from x^*=40 to x^*=140.

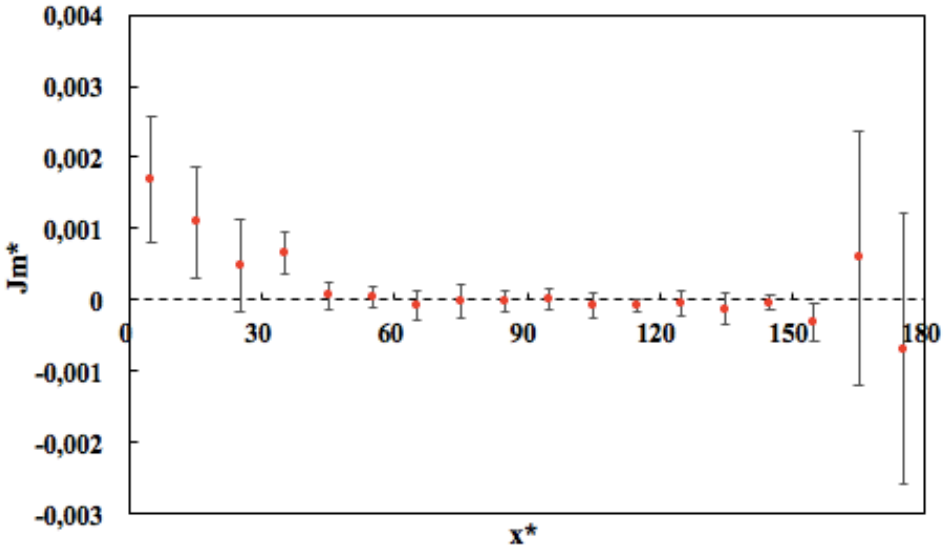

Figure 4. 9 Plot of the time average mass flux, J_m^*, against positon along the x-direction, x^*, for $T^* = 0.7$. The data points are found as an average from the 1.0 millionth timestep, to the 1.5 millionth. The error bars are calculated using standard deviation of mean, see equation (3.22), and represent $\pm 1\sigma_{SD,m}$. All values are in reduced units.

The data presented in figure 4.9 were obtained from a simulation ran for 1.5 million timesteps, where the mass flux was found as an average over that last 500,000 timesteps. Figure 4.9 depicts that the time average mass flux was not significantly different from zero. The error bars were large and overlapping with the x-axis. A two-sided t-test was conducted to confirm statistically whether the averages were significantly different from zero or not. All p-values obtained from this test are presented in Appendix A, see table A.1. The t-test confirmed that the mass flux was not significantly different from zero. Consequently, a number of timesteps equal to 1.5 million was sufficient for a system with no driving forces to achieve stationary state. It was expected that non-equilibrium systems would use a longer time to reach stationary state. A number of timesteps twice the size as for the equilibrium system was considered sufficient for non-equilibrium systems. Therefor the chosen number of timesteps was 3 million for systems exposed to driving forces.

4.2.2 System 1: Chemical potential gradient and thermal equilibrium

In order to calculate the resistivity coefficients, a system with a chemical potential driving force and a constant temperature was constructed. An illustration of such a system is presented in figure 4.10.

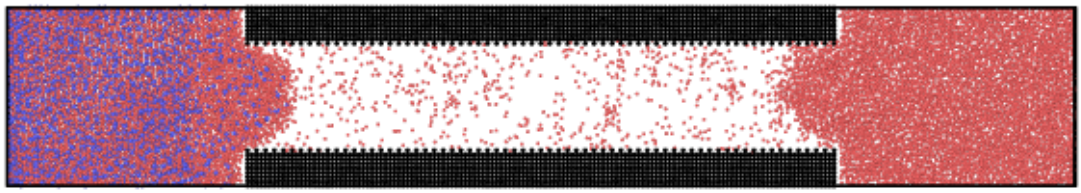

Figure 4. 10 Snapshot of a two-component system in the x-z plane with $T^* = 0.74$. The red particles represent the solvent and the blue particles the solute. The black particles represent the pore wall. The pore diameter is $20\sigma_0$.

Figure 4.10 depicts a snapshot of the system. Solvent particles, which were red, diffused through the pore in a vapor phase. A density profile is presented in figure 4.11 to verify that a two-phase system had been achieved.

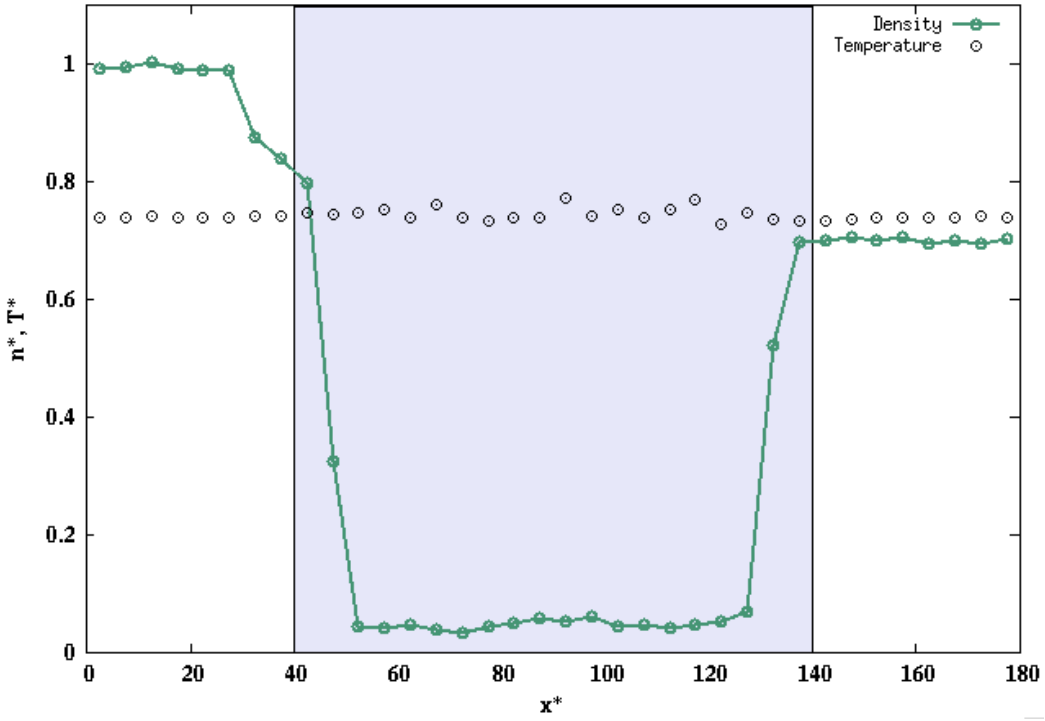

Figure 4. 11 Number density and temperature profile of system 1 along the x-direction for $T^* = 0.74$. The colored area represents the pore. The line and the dots represent the number density and temperature, respectively. All values are in reduced units.

Figure 4.11 depicts that the density in the mixture was greater than the density in the pure liquid. These densities were initially different, where the mixture had a higher density compared to the pure fluid. From figure 4.11 it was seen that the density of the mixture decreased near the pore. This was because there was an excess of solvent particles in this area, see figure 4.10. The attractive forces between solvent and solute particles were greater than between solvent and solvent. This means that regions in the mixture with high concentration of solvent particles will have a lower density.

The density in the pure liquid was lower than the initial density, which was 0.8. This was because some of the liquid particles formed a vapor phase and therefore reduced the number of liquid particles. A phase change was seen from the behavior of the density profile, where the density dropped drastically from liquid to vapor phase. The temperature was approximately constant throughout the system.

A plot of the mole fraction of both solvent and solute component are presented in figure 4.12, to verify that a separation effect had occurred.

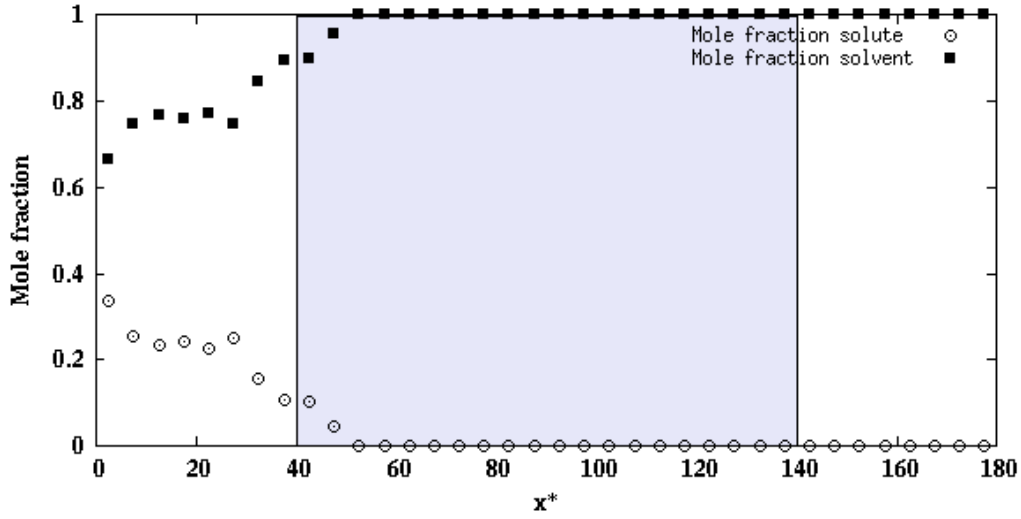

Figure 4. 12 Mole fraction of solvent, black squares, and solute, white dots, in system 1 along the x-direction for $T^* = 0.74$. The colored area represents the pore. All values are in reduced units.

It was seen from figure 4.12 that only solvent particles were transported through the pore. The mole fraction of solute particles decreased along the x-direction, as observed in figure 4.10. The mixture close to the pore opening contained a larger excess of solvent particles in contrast to what the initial composition was, which was a 75/25 solvent-solute mixture. In this system,

the mass transfer occurred from the pure liquid towards the mixture. This caused solvent particles to accumulate at the mixture-vapor interface and in regions close to the interface, as they condensed. As solvent particles moved away from the pore opening and further into the mixture, an approximately 75/25 solvent-solute mixture was achieved. At the start of the simulation box figure 4.12 depicts an increase of solute particles. This could be because a RPM membrane was positioned here (RPM membrane 1), and it only allowed solvent particles to cross from the mixture to pure liquid. This caused an excess of solute particles close to this RPM membrane.

A plot of the time average mass flux along the x-direction is presented in figure 4.13. This plot confirms the direction of the mass transport.

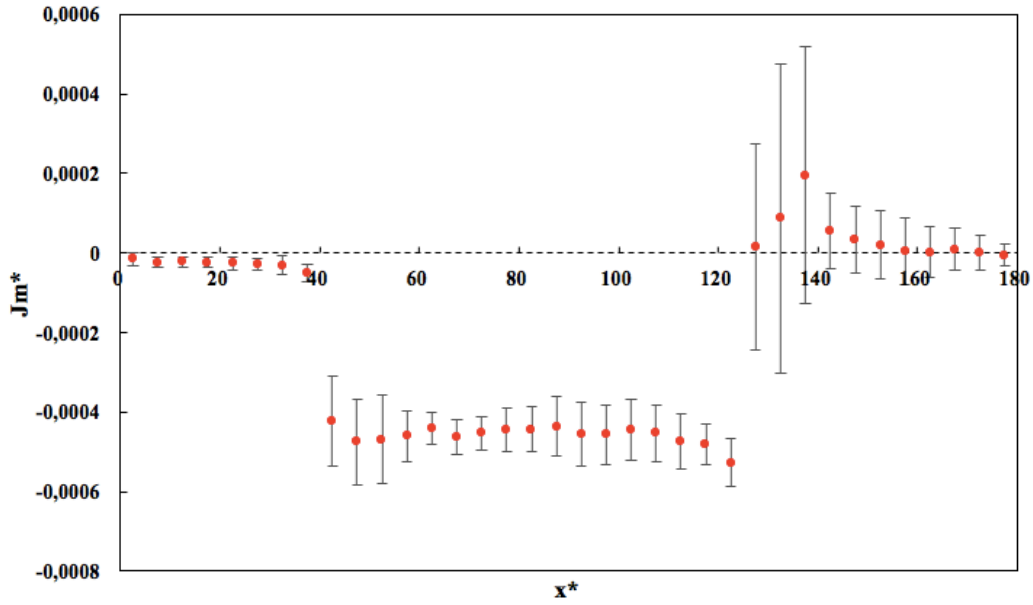

Figure 4. 13 Plot of the time average mass flux, J_m^*, against positon along the x-direction, x^*, for $T^* = 0.74$. The error bars are calculated using standard deviation of mean, see equation (3.22), and represent $\pm 1\sigma_{SD,m}$. The pore is located from x^*=40 to x^*=140. All values are in reduced units.

Figure 4.13 depicts a significantly negative mass flux inside the pore, confirmed by a t-test, see Appendix A table A.2. This means that the mass transport was from pure liquid towards the mixture. This is expected for a system under thermal equilibrium but with a chemical potential driving force. Outside the pore, the mass flux was not significantly different from zero. The mass flux was expected to be smaller in the liquid phases because mass flux is a function of the inverse flow area, and the flow area was much smaller inside the pore. Why the mass flux was not significantly different from zero in the liquid phases may be because the driving force in

the system was small. Under a higher gradient in chemical potential, the mass transport in both vapor and liquid phase would increase. This would have led to a liquid mass flux significantly different from zero, but still significantly smaller than the vapor mass flux.

The time average measurable heat flux is presented in figure 4.14 as a function of position along the x-direction.

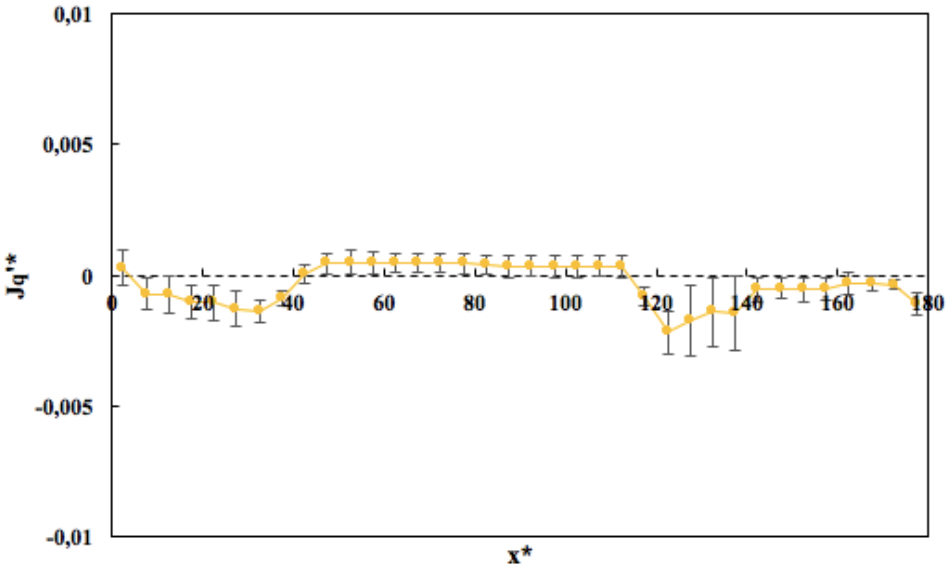

Figure 4. 14 Plot of the time average measurable heat flux, $J_q'^*$, against positon along the x-direction, x^*, for $T^* = 0.74$. The error bars are calculated using standard deviation of mean, see equation (3.22), and represent $\pm 1\sigma_{SD,m}$. The pore is located from x^*=40 to x^*=140. All values are in reduced units.

Figure 4.14 depicts that the measurable heat flux was not significantly different from zero. A measurable heat flux equal to zero was expected because the system was in thermal equilibrium. The graph showed some fluctuations but these were neglected because of the size of the error bars.

4.2.3 System 2: One-component fluid and temperature gradient

A system with a temperature gradient as its only driving force can be used to calculate the resistivity coefficients. An illustration of such a system is presented in figure 4.15.

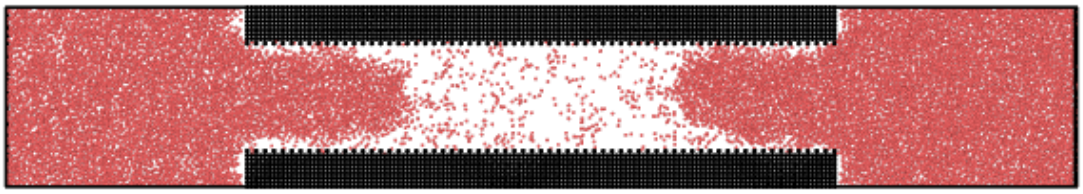

Figure 4. 15 Snapshot of a one-component system in the x-z plane with $T_h^* = 0.78$ and $T_c^* = 0.70$. The red particles represent the solvent and the black particles represent the pore wall. The pore diameter is $20\sigma_0$.

Figure 4.15 depicts that the liquid-vapor interface was defined well within the pore. The reason was the high temperature in the system. The fluids in the system only contains one component. The temperature used for the temperature gradient was primarily chosen so that another system, which had a two-component mixture, would achieve a mass flux equal to zero. This was explained in section 3.3.5. The selected temperatures were of such magnitude that the one-component liquids expanded and occupied a much larger area inside the pore than what they would do at significantly lower temperatures. A plot of the temperature and number density profile is presented in figure 4.16, to verify that a temperature gradient and a two-phase system were achieved.

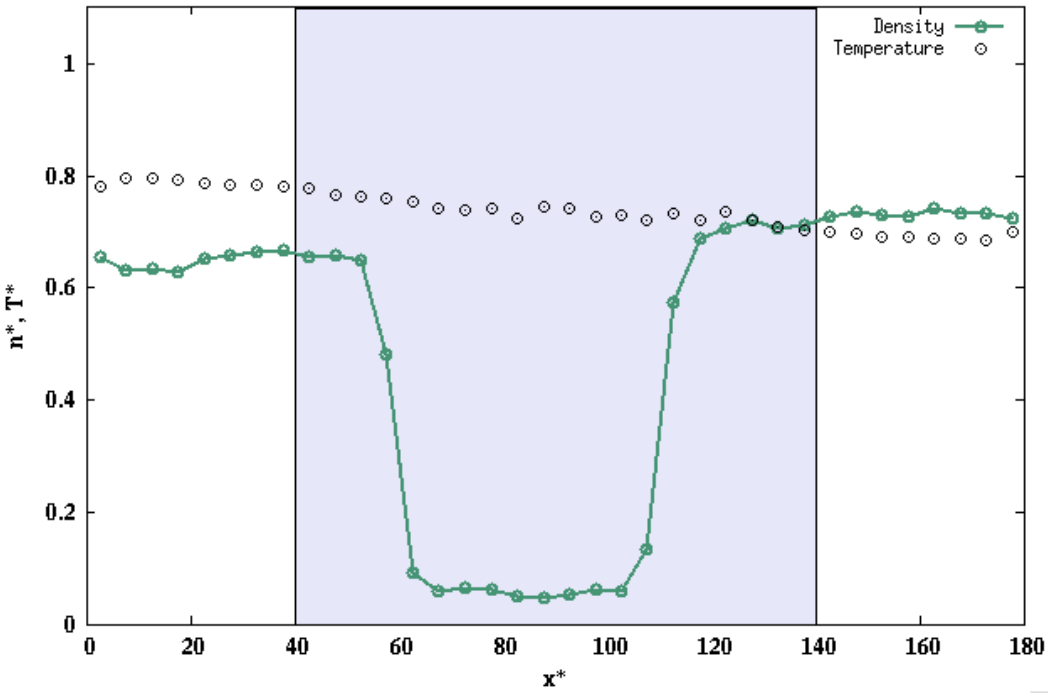

Figure 4. 16 Number density and temperature profile of system 2 along the x-direction for $T_h^* = 0.78$ and $T_c^* = 0.70$. The colored area represents the pore. The line and the dots represent the number density and temperature, respectively. All values are in reduced units.

Seen from figure 4.16, the hot thermostat was located at the start of the simulation box, and the cold at the end. The liquid density in the cold area of the system was higher than the liquid density in the hot area. This was because density is affected by temperature because an increase in temperature means an increase in kinetic energy. A higher kinetic energy means the particles are moving faster, which again reduces the density.

The temperature gradient was greatest in the vapor phase. This was because the heat conduction increases with increasing densities, which means that liquids have a higher conduction of heat than vapors. This results in smaller temperature gradients in liquids. Because the liquid close to the cold thermostat had a higher density, this liquid was expected to have a smaller temperature gradient than the liquid close to the hot thermostat. This was the case, but the difference between the temperature gradients was small.

It was also seen from figure 4.16 that the regions close to the hot thermostat had a higher temperature than the thermostatted value, and the regions close to the cold thermostat had a lower temperature. When the layers at the two ends of the simulation box were thermostatted, the temperature profile got affected by the fact that the hot and cold thermostat was right next to each other due to periodic boundary conditions. The placement of the thermostats means that there exist two heat fluxes from hot to cold thermostat. This is illustrated in figure 4.17.

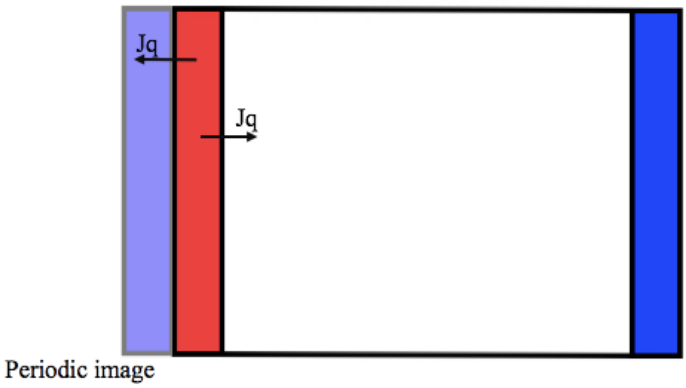

Figure 4. 17 Illustration of a thermostatted system with a periodic image. Hot thermostatted layer is represented in red, and the cold in blue. Jq is the heat flux.

Because the kinetic energy can be divided into x, y and z contributions, the temperature may also. Within the hot thermostatted layer, the temperature in y- and z-direction was greater than the temperature in x-direction because of the heat flux in x-direction. For the cold thermostatted

layer, the temperature in y- and z-direction was lower than the temperature in the x-direction. Although the total temperature in the thermostatted layers was equal to the desired value, the different temperature in the various dimensions created an error which spread to the areas near the thermostats. When calculating the temperature gradient, the thermostatted layers was neglected.

Even though the liquid-vapor interface was found to be far inside the pore, mass transport will continue to take place through the vapor phase. A plot of the time average mass flux as a function of position along x-direction is presented below in figure 4.18.

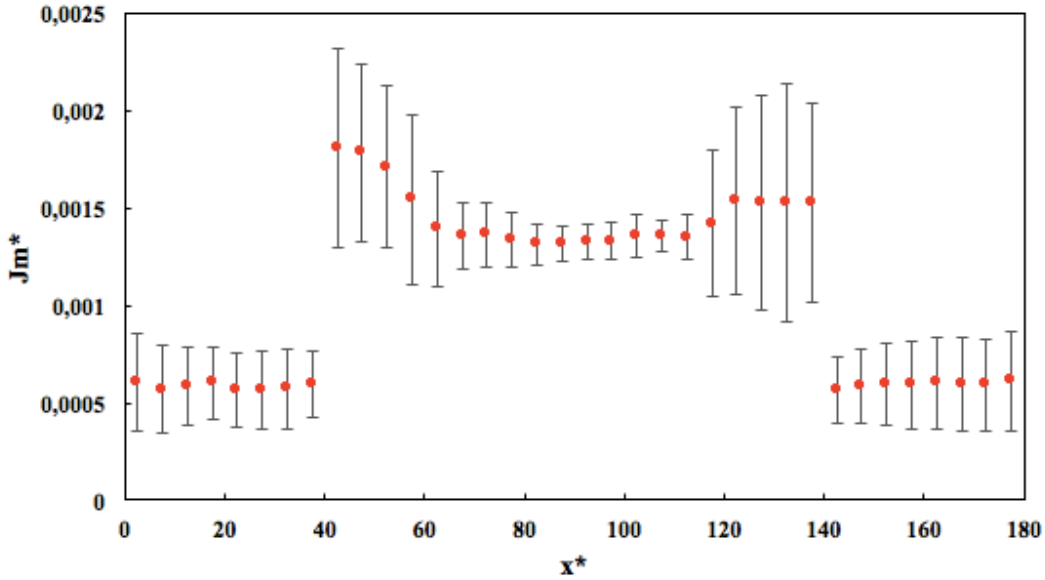

Figure 4. 18 Plot of the time average mass flux, J_m^*, against positon along the x-direction, x^*, for $T_h^* = 0.78$ and $T_c^* = 0.70$. The error bars are calculated using standard deviation of mean, see equation (3.22), and represent $\pm 1\sigma_{SD,m}$. The pore is located from x^*=40 to x^*=140. All values are in reduced units.

In figure 4.18, the data points with small error bars, in other words the data points that were significantly different from zero, correspond to the vapor phase. These points show that mass transport occurs from the hot area to the cold, which corresponds to the theory. The liquid phases had a mass flux that was not significantly different from zero. This was confirmed by a t-test, see appendix A table A.3. As for system 1, an increase in the thermal driving force would lead to a liquid mass flux significantly different from zero.

Inside the pore, a large mass flux was observed having large error bars. This corresponds to the liquid phase inside the pore, see figure 4.15. To calculate the mass flux, the liquid inside the pore was divided by a smaller flow area relative to the liquid outside the pore. This led to the

high values for the mass flux, but as the t-test indicated, these values were not significantly different from zero.

The time average measurable heat flux as a function of position along the x-direction is presented in figure 4.19.

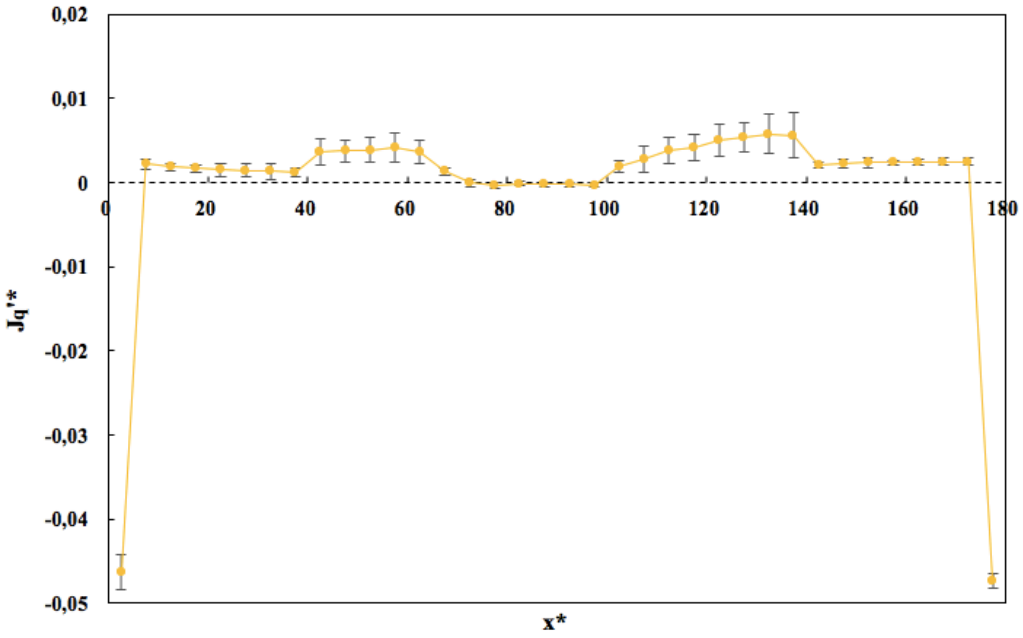

Figure 4. 19 Plot of the time average measurable heat flux, $J_q'^*$, against positon along the x-direction, x^*, for $T_h^* = 0.78$ and $T_c^* = 0.7$. The error bars are calculated using standard deviation of mean, see equation (3.22), and represent $\pm 1\sigma_{SD,m}$. The pore is located from x^*=40 to x^*=140. All values are in reduced units.

From figure 4.19 it was seen that the measurable heat flux had extreme values close to the two ends of the simulation box. This is related to the illustration shown in figure 4.17. Because of periodic boundary conditions, the hot thermostat was right next to the cold thermostat, and vice versa. This caused a large heat flux from hot to cold thermostat, as observed in the plot. For calculations regarding the bulk measurable heat flux, these extreme values were not included.

Figure 4.19 depicts a higher measurable heat flux in the liquid inside the pore, but the error bars show that the flux was not significantly different from what found outside the pore. In the vapor phase, which was located from approximately x^*=60 to x^*=100, the measurable heat flux was smaller than for the liquid phase. This is because liquid conducts heat better than vapor.

4.2.4 System 3: Gradient in chemical potential and temperature gradient with a mass flux equal to zero

A system with a temperature gradient, a gradient in chemical potential and a mass flux equal to zero is the last system needed to calculate all the resistivity coefficients. In this simulation case, the two driving forces, which are thermal and chemical potential, are balanced. As illustrated in figure 2.4, these two driving forces has the opposite effect on the direction of the mass flux, J_m. Balancing them means that they equalize each other, so that the mass flux becomes zero. To find the balance between the forces, the concentration of solute particles remained constant, while the temperature gradient was varied until the mass flux became zero. A too large temperature gradient created a positive mass flux, and a too small temperature gradient created a negative mass flux. Since mass transport was equal to zero for this system, the RPM membranes was set to not let any particles pass through. An illustration of the system is presented in figure 4.20.

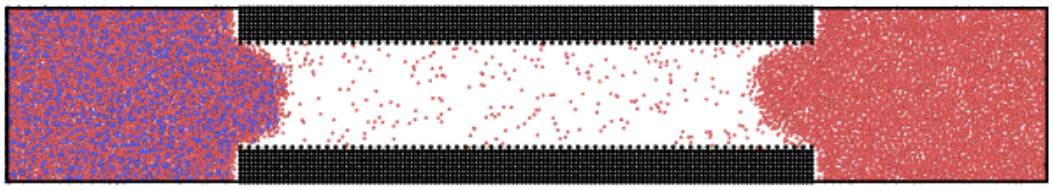

Figure 4. 20 Snapshot of a two-component system in the x-z plane with $T_h^* = 0.78$ and $T_c^* = 0.7$. The red particles represent the solvent and the blue particles the solute. The black particles represent the pore wall. The pore diameter is $20\sigma_0$.

Figure 4.20 alone is not enough to state that a two-phase system was achieved. For that a density profile is needed. A plot of the density and temperature profile is presented in figure 4.21.

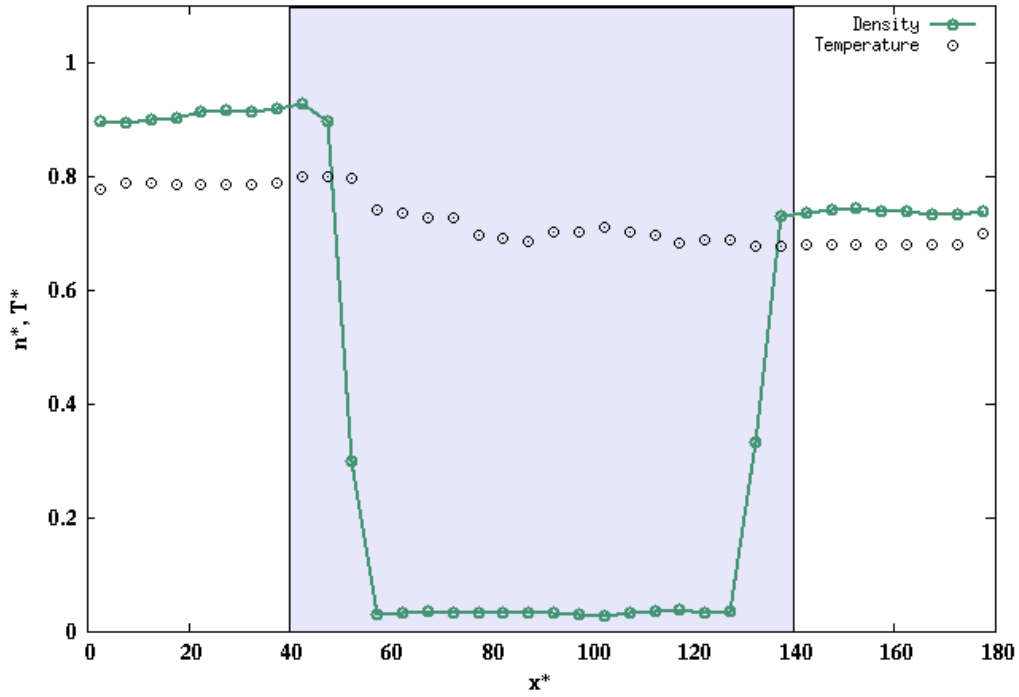

Figure 4. 21 Number density and temperature profile of system 3 along the x-direction for $T_h^* = 0.78$ and $T_c^* = 0.7$. The colored area represents the pore. The line and the dots represent the number density and temperature, respectively. All values are in reduced units.

Figure 4.21 depicts that the mixture had a higher density than the pure liquid. Initially, the density of the mixture and pure liquid was set to 1.0 and 0.8, respectively. Both liquids experienced a decrease in density from their initial value. This was because parts of the liquid phases formed a meniscus and vapor phase. The mixture experienced a large reduction because of the higher temperature, which contributed to reducing the density.

As for system 2, the regions close to the thermostatted layers were affected by the difference in the temperatures in the x, y and z dimension. The thermostatted layers were therefore neglected when calculating the temperature gradient. The temperature gradient was larger in the vapor phase compared to the liquid phase. As discussed earlier, this was expected. Since the mixture had a higher density compared to the pure liquid, it also had a smaller temperature gradient. The difference between the temperature gradients found in the mixture and pure liquid was so small that it was not visible in the temperature profile.

A plot of the mole fraction of both solvent and solute component are presented in figure 4.22, to verify that a separation effect has occurred.

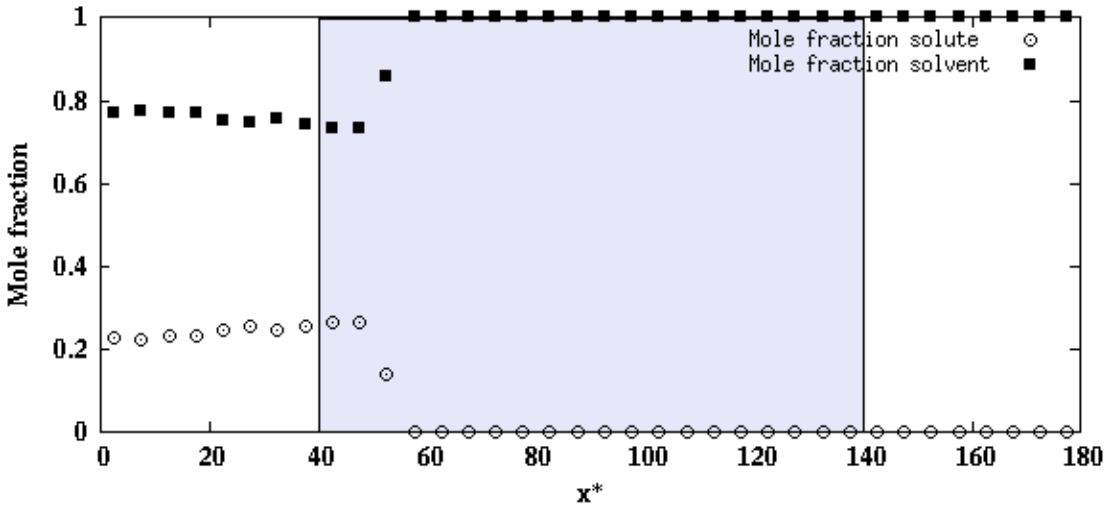

Figure 4. 22 Mole fraction of solvent, black squares, and solute, white dots, in system 3 along the x-direction for $T_h^* = 0.78$ and $T_c^* = 0.7$. The colored area represents the pore. All values are in reduced units.

Figure 4.22 depicts that only solvent particles were transported through the pore since the solute mole fraction in the vapor was equal to zero. In this system, the mole fraction of solute particles increase slightly along the x-direction until the surface was reached. This was due to evaporation. Since only solvent particles evaporate there will be a small excess of solute particles at the surface, and in the liquid close to the surface, as observed in figure 4.22.

System 3 relies on having a mass flux through the pore equal to zero. A plot of the time average mass flux along the x-direction is presented in figure 4.23.

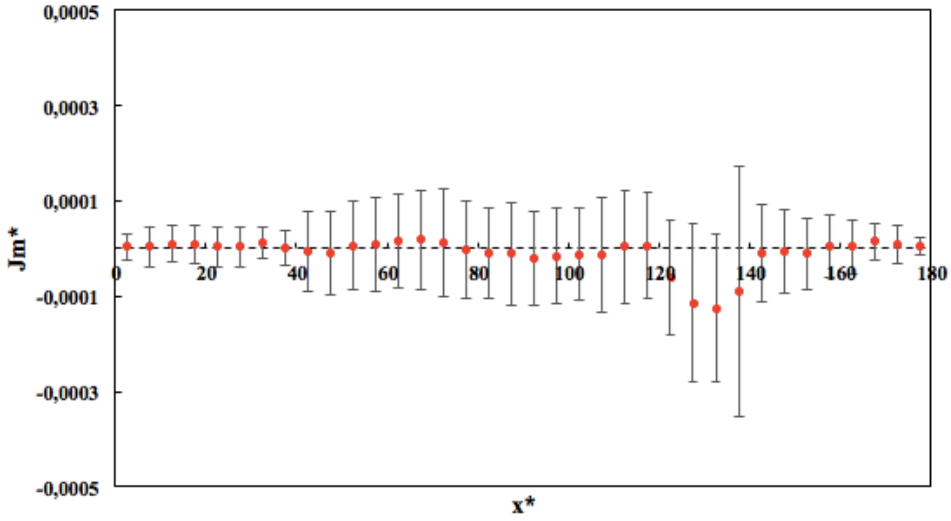

Figure 4. 23 Plot of the time average mass flux, J_m^*, against positon along the x-direction, x^*, for $T_h^* = 0.78$ and $T_c^* = 0.7$. The error bars are calculated using standard deviation of mean, see equation (3.22), and represent $\pm 1\sigma_{SD,m}$. The pore is located from x^*=40 to x^*=140. All values are in reduced units.

From figure 4.23 it was seen that the error bars were of such magnitude, and overlapped with the x-axis, that the mass flux was not significantly different from zero. This was confirmed with a t-test, see table A.4 in appendix A. A mass flux equal to zero means that the chemical potential driving force was canceled out by the thermal driving force.

The time average measurable heat flux was plotted against position along the x-direction and presented in figure 4.24.

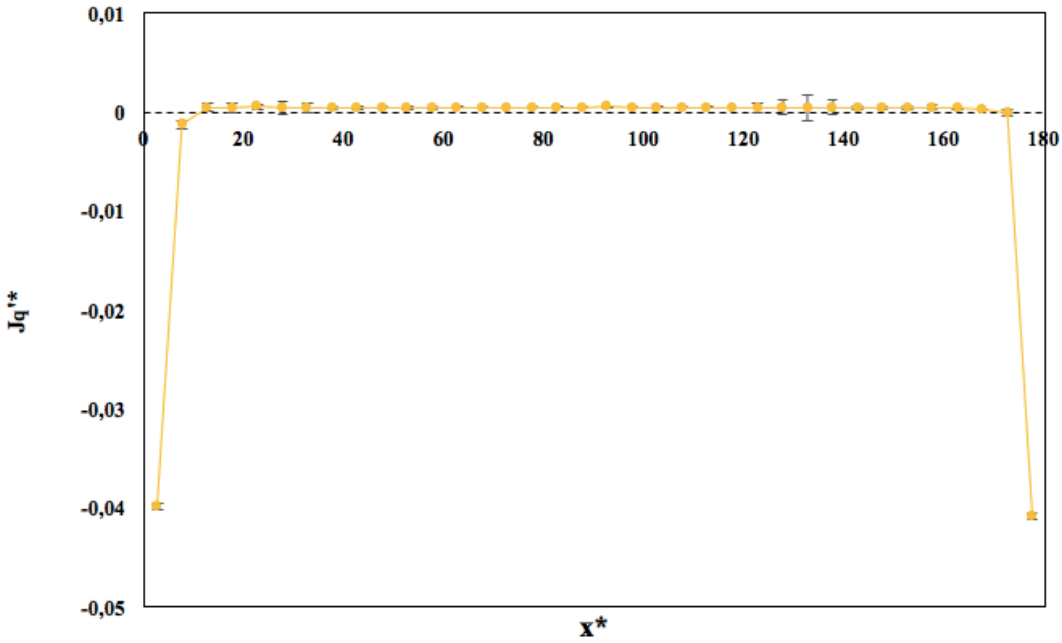

Figure 4. 24 Plot of the time average measurable heat flux, $J_q'^*$, against positon along the x-direction, x^*, for $T_h^* = 0.78$ and $T_c^* = 0.7$. The error bars are calculated using standard deviation of mean, see equation (3.22), and represent $\pm 1\sigma_{SD,m}$. The pore is located from x^*=40 to x^*=140. All values are in reduced units.

Figure 4.24 depicts that the measurable heat flux was very small except for the regions were the thermostats were defined. The error bars states that the measurable heat flux in the liquid was not significantly different from the flux in the vapor. The measurable heat flux is dependent on the velocity of the particles and the mass flux, see section 3.2.2. This system had a mass flux equal to zero, which means that the particle velocities were small. Small velocities and a mass flux equal to zero caused the measurable heat flux to be very small and close to zero.

4.2.5 Resistivity coefficients

The calculated resistivity coefficients are presented in this section. For these calculations, the results presented in section 4.2.2-4.2.4 were used. Resistivity coefficients can provide accurate information regarding the mass flux and are therefore of interest in problems involving purification and membrane distillation.

In this study, the total resistivity coefficients were calculated using equation (2.26), (2.27) and (2.28). Since the total resistivity coefficients also can be found using the local resistivity coefficients at the surfaces and in the vapor phase, these will also be presented in this section.

The resistivity coefficients corresponding to the bulk vapor and liquid phase were found using equation (2.7), (2.8) and (2.9). The bulk phases were considered as homogeneous systems and continuous values were used. The surface resistivity coefficients $r_{q\mu}$ and $r_{\mu\mu}$ were found using equation (2.17), (2.18) and (2.19) for the surface located between the vapor and mixture, and equation (2.20), (2.21) and (2.22) for the surface located between the vapor and pure liquid. Different equations were chosen for the two different surfaces so that the flux used in the equations would represent the same phase. For the surface between the vapor and mixture, outgoing flux means the flux in the vapor phase, while for the surface between vapor and pure liquid, it means the flux in the liquid phase. The same phase must be used for finding $r_{q\mu}$ and $r_{\mu\mu}$ for the two surfaces, and this phase was chosen to be liquid. This means that the surface between the vapor and mixture was defined using variables on the left side of the surface, while the surface between vapor and pure liquid was defined using variables on the right side of the surface. See figure 2.3 for a visual representation.

The surface resistivity coefficient $r_{qq}$was found using equation (2.23). This equation describes the entire surface, in contrast to $r_{q\mu}$ and $r_{\mu\mu}$, which were only defined using one of the fluxes (in or out), but still apply for the whole surface. For the surfaces and the total system, which was a heterogeneous system, discrete values were used.

The resistivity coefficients as functions of position along the x-direction are time averages over the last 500,000 timesteps, and presented in figure 4.25, 4.26 and 4.27. Some resistivity coefficients were dependent on other resistivity coefficients. For those cases, an average of the coefficient found in the respective phases was used.

All coefficients are presented on the same dimensional form. Since a temperature gradient was used for the homogeneous phases, the total resistivity coefficients were divided on the membrane thickness, which was the length of the pore. The surface resistivity coefficients were divided on the surface thickness found using the density profiles. The density profiles were found using planar chunks, meaning the chunks did not have the same geometry as the surfaces. This could have created an error in the calculations of the surface thickness. Despite knowledge about this possible error, the surface thickness found from the density profiles was used.

The resistivity coefficient for transport of heat is presented in figure 4.25 as a function of position along the x-direction.

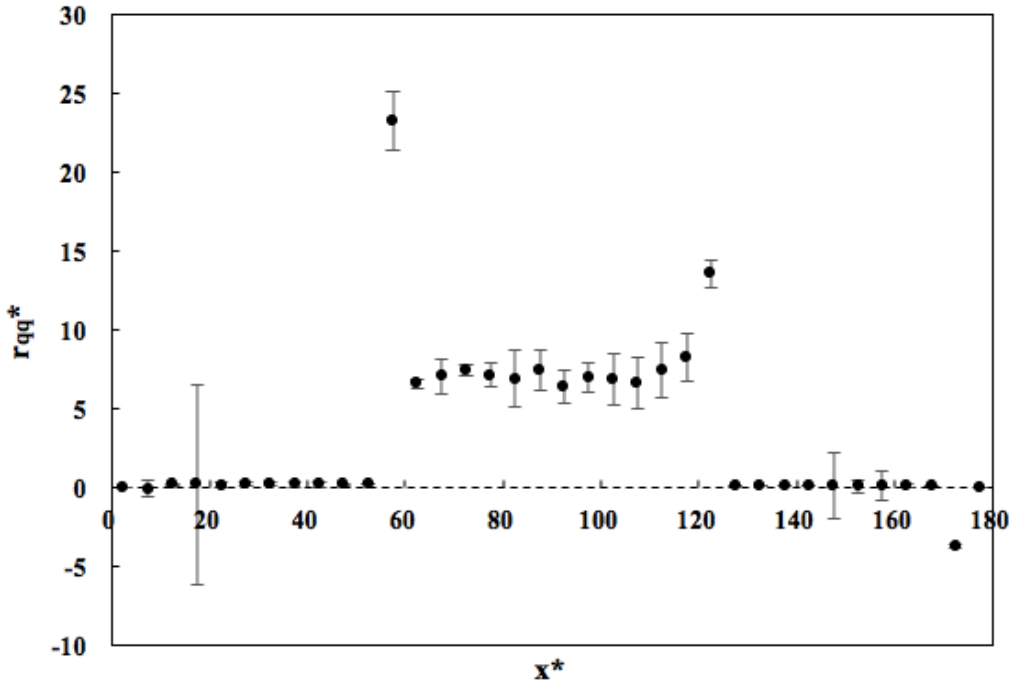

Figure 4. 25 Plot of resistivity coefficient r_{qq}^* against position along the x-direction, x^*. The error bars are calculated using standard deviation of mean, see equation (3.22), and represent $\pm 1\sigma_{SD,m}$. The pore is located from x^*=40 to x^*=140. All values are in reduced units.

In this plot, the mixture was located from x^*=0 to approximately x^*=40, and the pure liquid from x^*=140 to x^*=180. Between the liquid phases was the vapor phase. The coefficient r_{qq}^* was not significantly different from zero in the liquid phases, $r_{qq}^{mixture*}$= 0.2±0.8 and r_{qq}^{pure*}= 0.1±0.5. A resistivity coefficient equal to zero means heat was transported without hindrance. This corresponds to the small temperature gradients found in the liquid phases, see figure 4.21. The vapor phase had a positive resistivity coefficient significantly different from zero, see table

4.2. A positive r_{qq}^{*} means there was a hindrance present in the vapor when it came to transport of heat. This means that heat was not transported to the same extent as in the liquid phases. The resistivity coefficient in the vapor increased slightly from left to right, but the error bars indicated that the coefficients were not significantly different from each other.

Figure 4.25 depicts two points that differ from the trend in the vapor and liquid phase. These points corresponded to the surface resistivity coefficients. The surface between the mixture and vapor phase had a greater r_{qq}^{*} compared to the surface between vapor and pure liquid, see table 4.2. This was because the surface between vapor and pure liquid experienced a smaller jump in inverse temperature than the surface between the mixture and vapor. The jump was calculated from the difference between the inverse temperature found in liquid and vapor phase near the surface. The temperature found in the vapor was affected by the small number of particles in this phase. As a result, the temperature profile in the vapor phase showed a fluctuation in temperature and the calculation of the inverse temperature jump may have been affected by this. If the temperature difference over the surface had been the same for both surfaces, then the inverse temperature jump would be greatest for the surface with the lowest temperatures. This means the surface between the vapor and pure liquid would have been greatest due to a lower temperature in pure liquid. Since the other resistivity coefficients depend on r_{qq}^{*}, the fluctuation in the vapor temperature will also affect them.

The resistivity coefficient for coupling between heat and mass transport is presented in figure 4.26 as a function of position along x-direction.

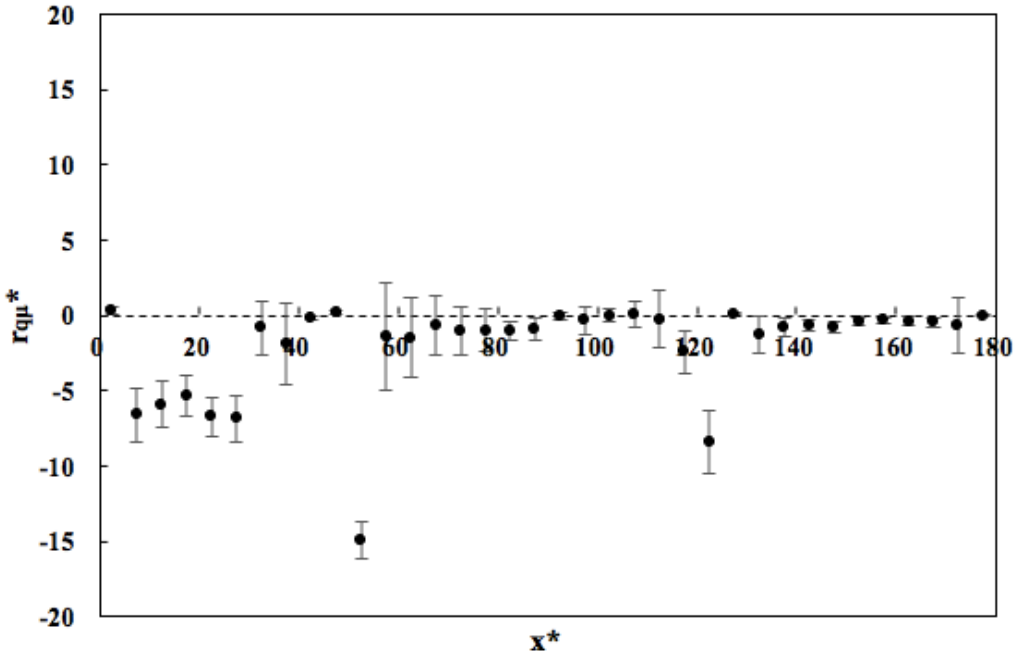

Figure 4. 26 Plot of resistivity coefficient $r_{q\mu}^{*}$ against position along the x-direction, x^{*}. The error bars are calculated using standard deviation of mean, see equation (3.22), and represent $\pm 1\sigma_{SD,m}$. The pore is located from x^{*}=40 to x^{*}=140. All values are in reduced units.

The mixture was located from x^{*}=0 to x^{*}=40, and the pure liquid from x^{*}=140 to x^{*}=180. Figure 4.26 depicts that both bulk liquids had a negative resistivity coefficient, but only the mixture was significantly different from zero, $r_{q\mu}^{mixture*}$= -6$\pm$2 and $r_{q\mu}^{pure*}$= -0.4$\pm$0.3. The coefficients at the start of the simulation box and close to the pore opening (from x^{*} ≈30 to x^{*} ≈50) did not follow the trend of the corresponding fluid. Some of these points belong to the meniscus and they were not considered as a part of the bulk mixture. The resistivity coefficient found in the vapor was not significantly different from zero, see table 4.2.

The surface resistivity coefficients were found to be negative. They were observed between the small coefficients in the meniscus and vapor phase. The surface between the mixture and vapor had a more negative coefficient than the surface between the vapor and pure liquid. The surface resistivity coefficient between the vapor and pure liquid was not significantly different from the coefficient obtained for the bulk mixture as they did not separate by two standard deviations. A negative surface coupling coefficient indicates that uphill transport of solvent could occur.

The resistivity coefficient for transport of mass is presented in figure 4.27 as a function of position along the x-direction.

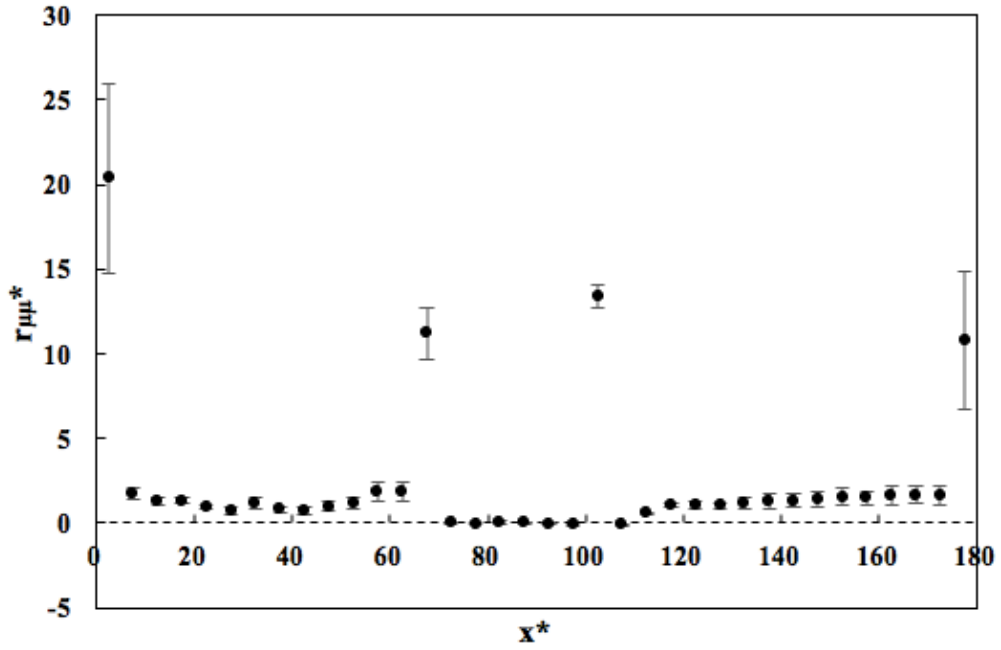

Figure 4. 27 Plot of resistivity coefficient $r^*_{\mu\mu}$ against position along the x-direction, x^*. The error bars are calculated using standard deviation of mean, see equation (3.22), and represent $\pm 1\sigma_{SD,m}$. The pore is located from x^*=40 to x^*=140. All values are in reduced units.

Figure 4.27 corresponds to the resistivity coefficient for mass transport of pure liquid only. The mixture was not accounted for because the coefficient was found for a system without gradient in chemical potential, which in this study corresponds to a system consisting of pure liquid. The resistivity coefficient found in the liquid phase was positive and significantly different from zero, $r_{\mu\mu}^{pure,left*}$= 1.0$\pm$0.2 and $r_{\mu\mu}^{pure,right*}$= 1.3$\pm$0.3. The two liquid resistivity coefficients were not significantly different from each other. This was because they were found for the same type of liquid. The coefficients found at the two ends of the simulation box did not follow the trend of the corresponding fluids. These data points were affected by the extreme heat flux observed in the figure 4.19 and were not defined as a part of the bulk liquid.

The resistivity coefficient in the vapor phase was not significantly different from zero, see table 4.2. A mass transport resistance coefficient equal to zero in the vapor phase agrees with mass mainly being transported in the vapor phase. In the liquid phases, the mass transport will be much smaller than in the vapor phase. This fits well with the higher resistivity coefficient found in liquid phase. The surface resistivity coefficients were positive but not significantly different from each other. Both surfaces were located between vapor and pure liquid, which could explain why they were not significantly different.

In this study, the total resistivity coefficients were calculated using equation (2.26), (2.27) and (2.28), but they could also be calculated using local resistivity coefficients. The total resistivity coefficients will arise from the surface between the mixture and vapor, the vapor inside the pore and the surface between the vapor and pure liquid. Table 4.2 contains all resistivity coefficients useful for calculating the total resistivity coefficients, and the calculated total resistivity coefficients. For the vapor phase the coefficients were found as averages over the position-dependent coefficients in each phase. As mentioned earlier, the surface resistivity coefficient $r_{qq}$was found using an equation that describes the entire surface. This was not possible for $r_{q\mu}$ and $r_{\mu\mu}$, so they were only defined using either the incoming or outgoing fluxes. They will regardless apply for the whole surface.

It is important to keep in mind that the total resistivity coefficients are not equal to the sum of the local resistivity coefficients, except for r_{qq}^{tot}. They are only functions of them. Also, the surface resistivity coefficients were divided by the surface thickness and the total resistivity coefficients by the pore length. This means that you cannot directly see a connection between the local and the calculated total resistivity coefficients from the values presented in table 4.2.

Table 4. 2 A table consisting of the values obtained for the different resistivity coefficients. r^{tot} corresponds to the total resistivity, $r^{s,l}$ to the interface between vapor and the mixture (except for $r_{\mu\mu}$ where it represented the first surface between pure liquid and vapor), $r^{s,r}$ to the interface between vapor and the pure liquid, and r^{vapor} to the vapor. The error bars are calculated using standard deviation of mean, see equation (3.22), and represent $\pm 1\sigma_{SD,m}$. All values are in reduced units.

Coefficient	r^{tot}	$r^{s,l}$	$r^{s,r}$	r^{vapor}
r_{qq}^{*}	13±3	23±2	13.6±0.8	7±1
$r_{q\mu}^{*}$	-20±2	-15±1	-8±2	-0.5±0.7
$r_{\mu\mu}^{*}$	35±2	11±2	13±1	0.05±0.04

The theory stated that $r_{qq}r_{\mu\mu} - r_{q\mu}^2$ had to be positive, or equal to zero, for the second law of thermodynamics to be fulfilled. Since table 4.2 contains error bars, a plot was constructed to show all combinations regarding the errors within each resistivity coefficient. This plot can be found in appendix E, figure E.1. It was seen that $r_{qq}r_{\mu\mu} - r_{q\mu}^2$ was positive for all coefficients. This means that the second law of thermodynamics was fulfilled for this system.

From table 4.2 it was seen that the surfaces had resistivity coefficients that were significantly different from the bulk vapor. This means that surfaces are important when it comes to mass

transport in heterogeneous systems, and they should be accounted for in all models regarding transport in a two-phase system.

The total coupling coefficient, $r_{q\mu}^{tot}$, was negative. This means that heat was transported in the same direction as the mass. The two total main resistivity coefficients were positive, which corresponds with the theory. r_{qq}^{tot} is defined as the sum of the local resistivity coefficients for transport of heat. This relation is possible to check using the calculated values in table 4.2. This was done by multiplying the surface coefficients with the surface thickness, the vapor coefficient with the extent of the vapor in the x-direction and the total coefficient with pore length. The result is presented in table 4.3.

Table 4. 3 A table consisting of values obtained for r_{qq}^{tot} found by using equation (2.26) and summation of the local resistivity coefficients for transport of heat. r^{tot} corresponds to the total resistivity, $r^{s,l}$ to the interface between vapor and the mixture, $r^{s,r}$ to the interface between vapor and the pure liquid, and r^{vapor} to the vapor. The error bars are calculated using standard deviation of mean, see equation (3.22), and represent $\pm 1\sigma_{SD,m}$. All values are in reduced values.

r_{qq}^{tot*}	$r_{qq}^{s,l*} + r_{qq}^{s,r*} + r_{qq}^{vapor*}$
1310±339	903±106

Table 4.3 shows that the two methods for finding r_{qq}^{tot} provided results that were not significantly different from each other. This boosts the credibility of the model, as it seemed to yield comparable results regardless of calculation method. The overlap between the values was thus small. The method used to determine the surface thickness could be a reason for this. An improved method for finding the surface thickness could possibly improve the model. Another way to improve the statistics could have been to increase the number of timesteps in the simulation, and increase the number of timesteps that the properties were calculated over.

4.3 System 4: Mass flux dependency

System 4 consisted of a gradient in both chemical potential and temperature. It was constructed to investigate how the mass flux varied with variation in the temperature and pore diameter. These variables were chosen because one of them, the temperature, indicates how changes in the external forces can affect the mass flux while the other, the pore diameter, says something about the membrane itself.

Section 4.3.1 provides information regarding the temperature dependency of the mass flux. As mentioned earlier, for a mass flux to occur from the mixture towards the pure liquid, the effect of the thermal driving force must be greater than that of the chemical potential driving force. By investigating how the mass flux changes with a change in temperature gradient, the minimum temperature gradient required to achieve the desired direction of mass transport can be found. The different temperatures examined are presented in table 3.2. The chosen pore diameter to run these simulations with was $20\sigma_0$.

Section 4.3.2 contains information about the mass flux dependency of the pore diameter. The different pore diameters were chosen to be $20\sigma_0$, which was the diameter used in the simulations in section 4.2, $15\sigma_0$, and $10\sigma_0$. The temperatures for the cold and hot thermostats were under these simulations chosen to be T_c^*=0.66 and T_h^*=0.82, which was the median of all temperature gradients studied. In section 4.3.3 the mass flux and correlation between the temperature and pore diameter was investigated.

4.3.1 Effect of temperature gradient

To understand how the temperature gradient affects the mass flux, system 4 was run with different temperatures for the hot and cold thermostat. An illustration of the system is presented in figure 4.28.

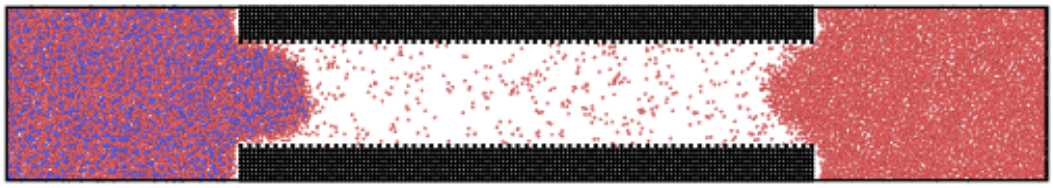

Figure 4. 28 Snapshot of a two-component system in the x-z plane with $T_h^* = 0.78$ and $T_c^* = 0.7$. The red particles represent the solvent and the blue particles the solute. The black particles represent the pore wall. The pore diameter is $20\sigma_0$.

A plot of the mass flux as a function of temperature gradient is presented in figure 4.29. The data points represent the average vapor mass flux found inside the pore at different temperature gradients found in the vapor phase. A list of the temperatures used in the simulations can be found in table 3.2. The temperature gradient was found for the vapor phase using equation (3.24). The mass flux and vapor temperature gradient were found as averages over the last 500,000 timesteps.

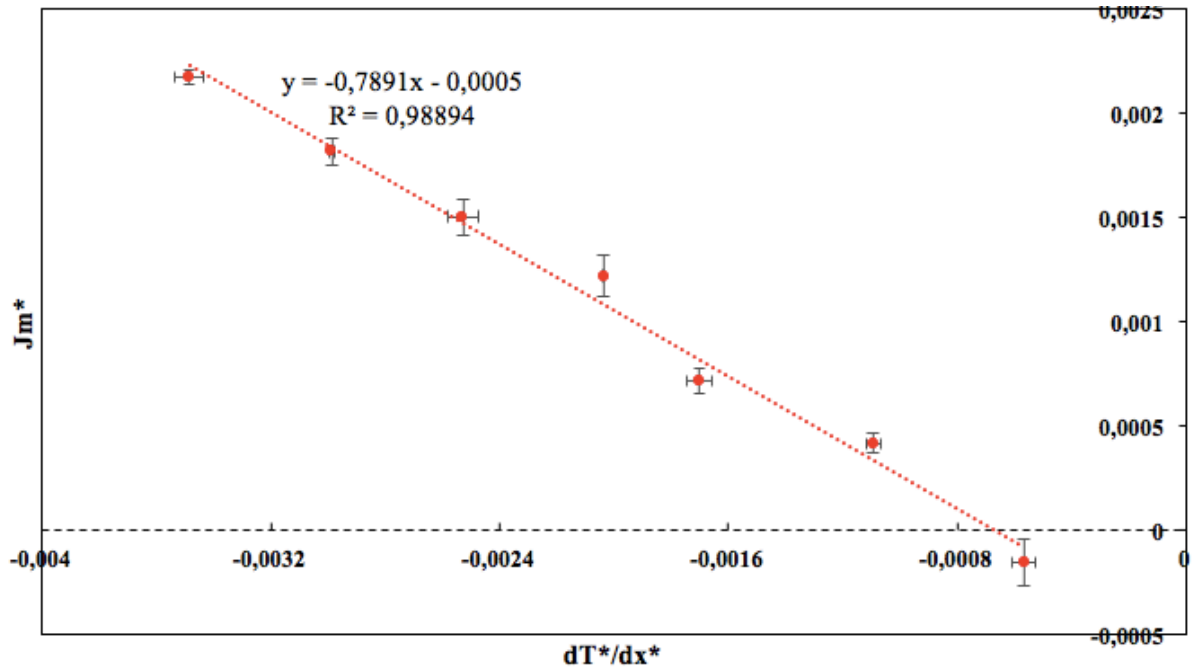

Figure 4. 29 Plot of the time average vapor mass flux, J_m^*, against temperature gradient, dT^*/dx^*, in the vapor phase. The dotted line is a linear trend line which is explained by the function of y. The y and x represent J_m^* and dT^*/dx^* , respectively. The error bars are calculated using standard deviation of mean, see equation (3.22), and represent $\pm 1\sigma_{SD,m}$. R^2 represents a measure of how well the variation in the data is explained by the linear trend line. All values are in reduced units.

A greater difference between T_c and T_h means a more negative temperature gradient, in other words a larger gradient. Figure 4.29 depicts that the mass flux increased with increasing temperature gradient. This was expected because a greater thermal driving force will to a greater extent cancel out the chemical potential driving force. This indicate that increasing the size of the temperature gradient will lead to an increased mass transport from the mixture to the pure liquid.

The dotted line in figure 4.29 represents a linear trend line, and was used to find a correlation between the mass flux and temperature gradient. The R^2 value shows a statistical measure of how well the linear trend line fits the data points. In this plot R^2=0.98894, which confirms that there was a linear correlation between the mass flux and temperature gradient. This linear correlation can be used to calculate the amount of heat needed to obtain a desired mass flux.

The smallest temperature gradient, which was T_c^*=0.72 and T_h^*=0.76, did not give a mass flux significantly different from zero. Although a large temperature gradient resulted in a large mass flux, some pollution was observed in the pure liquid at the two largest temperature gradients (T_h^*=0.86 and T_c^*=0.62, and T_h^*=0.88 and T_c^*=0.6). Figure 4.30 depicts the mole fraction of

solvent and solute for the two largest temperature gradients. Black arrows are included in the figure to show where the pollution was observed.

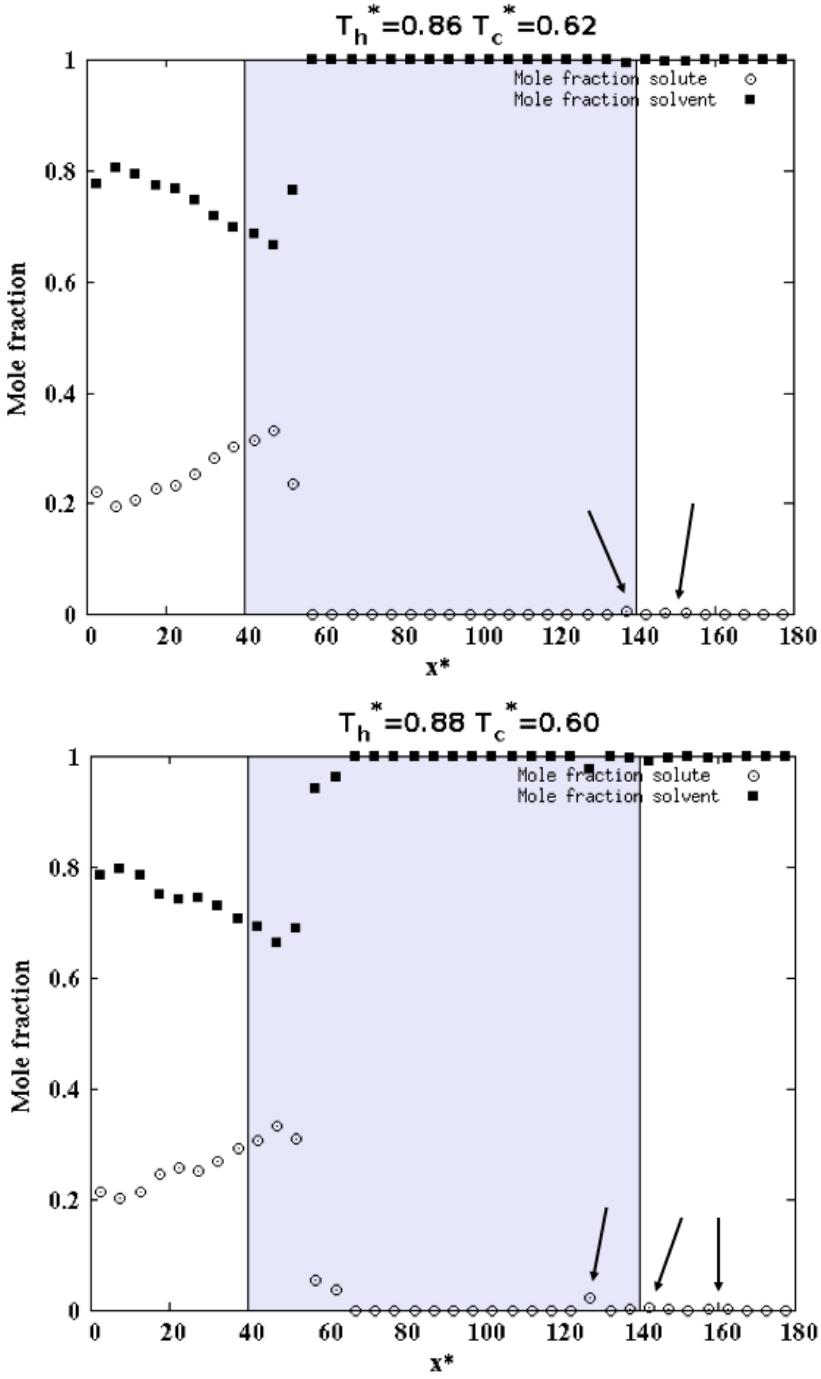

Figure 4. 30 Mole fraction of solvent, black squares, and solute, white dots, along the x-direction for $T_h^* = 0.86$ and $T_c^* = 0.62$, upper figure, and $T_h^* = 0.88$ and $T_c^* = 0.60$, lower figure. The colored area represents the pore. The black arrows show where the solute mole fraction is different from zero. All values are in reduced units.

From figure 4.30 it was seen that the pollution was very small. Solute particles accounted for less than 0.2% of the pure phase after completed simulation time. The composition used in

these systems had an unrealistic high concentration of solute (initially a 75/25 solvent-solute mixture). This means that for more realistic mixing ratios, the pollution is expected to be much smaller than 0.2%. For larger temperature gradients, the pollution would most likely be greater.

Figure 4.30 also depict a drastic increase of solute particles along the x-direction. Almost only solvent particles evaporated from the mixture, which created an excess of solute particles close to the interface between the mixture and the vapor. At the start of the simulation box, there was an excess of solvent particles. The RPM membranes in the system made sure that only solvent particles moved from the pure liquid to the mixture through the periodic boundaries, which explains this excess.

Since the degree of contamination was very low in relation to the high solute concentration used in this study, it was neglected in terms of evaluating the optimal conditions for mass transport. Based on figure 4.29, the temperature interval T_h^*=0.88 and T_c^*=0.60 was considered to give the greatest mass transport out of the gradients investigated in this study. The result from this study suggest that significantly increasing the temperature gradient from this level may yield unacceptable levels of solvent pollution in the pure liquid phase.

4.3.2 Effect of pore geometry

Since a membrane is an essential part of membrane distillation, it may be interesting to see how the pore geometry affects the mass transport. To find this effect, system 4 was run with different values for the pore diameter; $20\sigma_0$, $15\sigma_0$ and $10\sigma_0$, see figure 4.31.

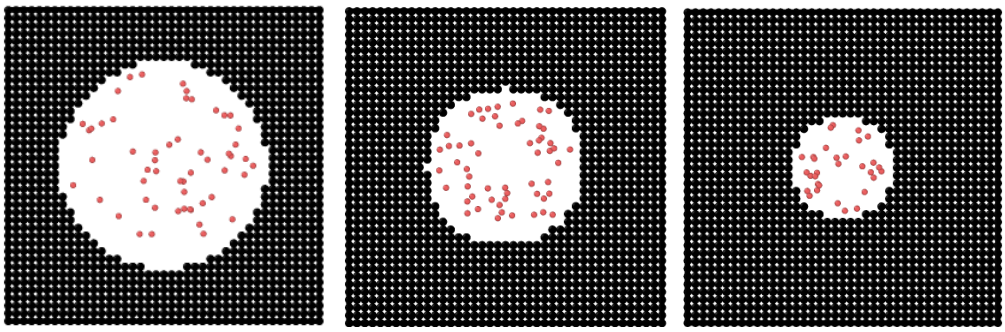

Figure 4. 31 Illustration of the different pore sizes. The pore diameter was $20\sigma_0$, $15\sigma_0$ and $10\sigma_0$ from left to right. The black particles represent the pore wall particles, and the red the solvent particles. All pores have the same length.

Figure 4.31 shows the different pore sizes and figure 4.32 presents a plot showing how the time average mass flux was affected by the change in pore diameter. Since mass was transported through the pore, only the mass flux in the vapor phase was presented. The mass flux was found as averages over the last 500,000 timesteps.

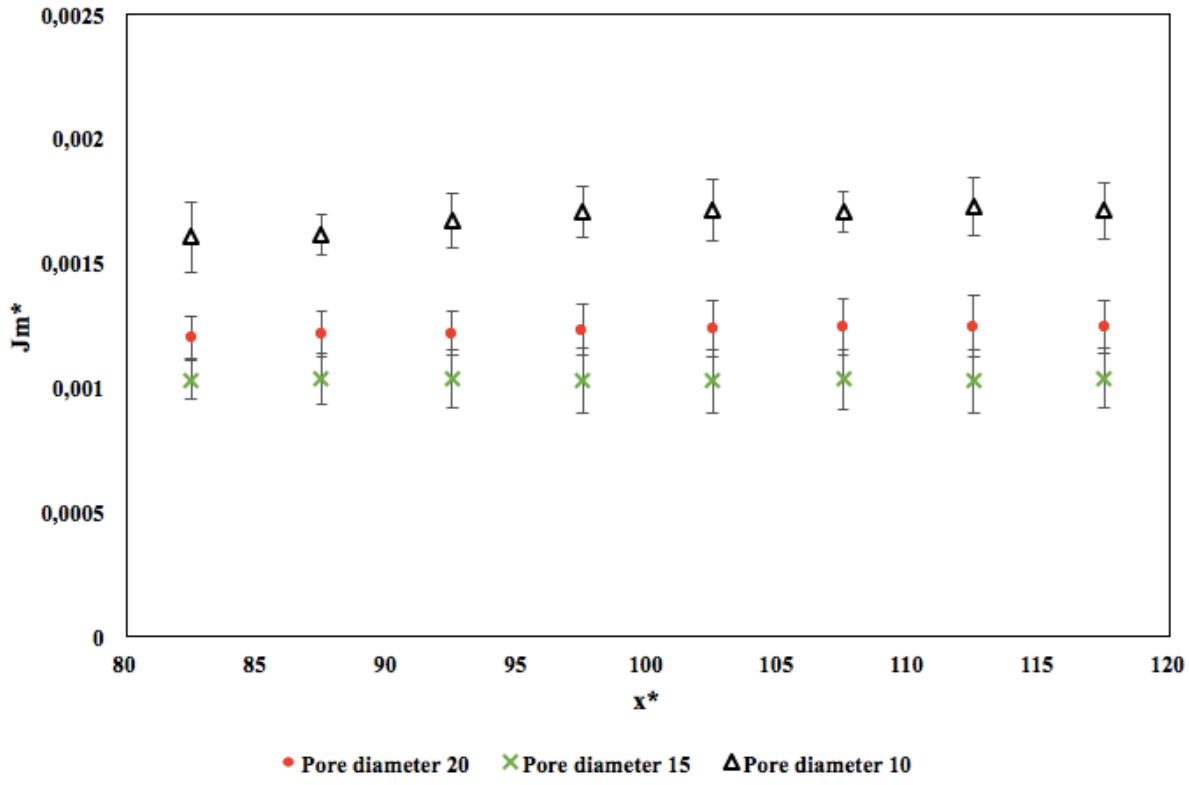

Figure 4. 32 Plot of the time average vapor mass flux, J_m^*, against position in vapor phase, x^*, for pore diameter equal to $20\sigma_0$, circle, $15\sigma_0$, cross, and $10\sigma_0$, triangle, for $T_h^* = 0.82$ and $T_c^* = 0.66$. The error bars are calculated using standard deviation of mean, see equation (3.22), and represent $\pm 1\sigma_{SD,m}$. All values are in reduced units.

From figure 4.32 it was seen that the vapor mass flux varied with the pore diameter. This implies that the mechanism for mass transport changes with pore geometry. The variation was found to be unsystematic, meaning there was no trend between mass flux and increasing pore diameter.

Figure 4.32 depicts that the greatest mass flux was obtained with a pore diameter equal to $10\sigma_0$. A pore diameter equal to $15\sigma_0$ gave a mass flux that was not significantly different from what was obtained with a pore diameter equal to $20\sigma_0$. The mass flux is dependent on both the inverse flow area and the number of particles flowing through the area. If all other variables are constant, a decrease in pore diameter means that the flow area and number of particles crossing the area will decrease. When the diameter was reduced to $10\sigma_0$, the decrease in flow area was greater than the decrease in number of particles flowing through the area, which resulted a high

mass flux. The result obtained in this section implies that a membrane with more pores with diameter $10\sigma_0$ will provide a greater mass transport compared to a membrane with fewer, larger pores for this temperature gradient. This was an unexpected result that may only apply to this particular temperature interval. The results obtained in section 4.3.3 can confirm whether this trend applies to all temperature gradients used in this study.

4.3.3 Correlation between temperature gradient and pore geometry

From section 4.3.1 and 4.3.2 it was seen that both the temperature and pore diameter influenced the mass flux. In this section, the correlation between these two variables was investigated. The different temperature gradients in section 4.3.1 were run with the different pore diameters in section 4.3.2. The vapor mass flux was found as averages over the last 500,000 timesteps.

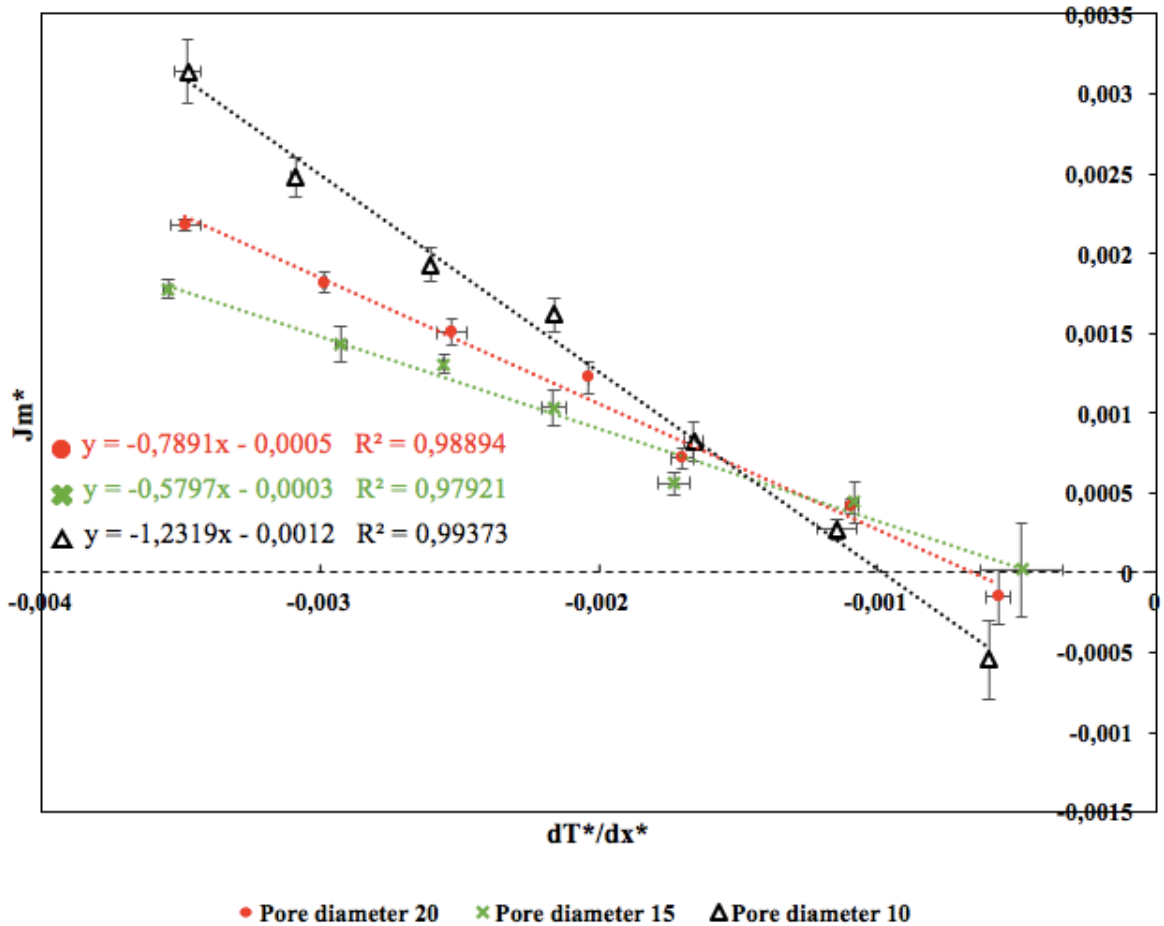

Figure 4. 33 Plot of the time average vapor mass flux, J_m^*, against temperature gradient, dT^*/dx^*, in vapor phase for three different pore diameters $20\sigma_0$, circle, $15\sigma_0$, cross, and $10\sigma_0$, triangle. The dotted lines are linear trend lines which are explained by the functions of y. The y and x represent J_m^* and dT^*/dx^*, respectively. The error bars are calculated using standard deviation of mean, see equation (3.22), and represent $\pm 1\sigma_{SD,m}$. R^2 represents a measure of how well the variation in the data is explained by the linear trend line. All values are in reduced units.

Figure 4.33 depicts that the smallest pore, with a diameter equal to $10\sigma_0$, gave the greatest mass flux for the four largest temperature gradients. These temperature intervals can be found in table 3.2. The pore diameter that gave the smallest mass flux was $15\sigma_0$. It was expected to find a clear trend between increasing pore diameter and mass flux, and not an unsystematic behavior as these result indicates. To check the model's credibility, the mass flux was multiplied by the flow area. The outcome of this is a particle flow, which is to be greatest for the largest pore diameter as there is room for more particles in a large pore versus a small one. The particle flow was greatest for the pore with a diameter of $20\sigma_0$, and smallest for the pore with a diameter of $10\sigma_0$, which was expected. This suggests that the unsystematic trend was not a result of model inadequacies, but rather a very interesting result. This means that to achieve a high mass flux, the pore diameter must be either small, $10\sigma_0$, or large, $20\sigma_0$, but not $15\sigma_0$.

For the three smallest gradients, the mass flux obtained for the different pore diameters was not significantly different. This implies that for small temperature gradients the pore size does not have a significant impact on the mass flux. However, the pore diameter has an effect when large gradients are used. All three R^2 values confirm that there was a linear correlation between the mass flux and temperature gradient, regardless of the pore diameter.

In section 4.3.1 it was discovered some pollution in the pure liquid at the two highest temperature gradients. This was also observed for the two smaller pores, $15\sigma_0$ and $10\sigma_0$. The pollutions in the smaller pores were of the same order of magnitude as in section 4.3.1, though slightly smaller. Since the mixture in this study had an unrealistic high concentration of solute, the level of pollution was considered very small, and therefore also neglected when evaluating optimal condition for mass transport.

Using figure 4.33, the largest temperature gradient (T_h^*=0.88 and T_c^*=0.60) and a pore diameter equal to $10\,\sigma_0$ were considered as optimal for purification of a two-component mixture consisting of Lennard-Jones/spline particles. Some pollution was present, but the amount was so small it was neglected. For more realistic mixing ratios between solvent and solute, this pollution would be significantly smaller.

It was observed that the mechanism for mass transport changed with pore geometry. We encourage others to further investigate the impact of pore geometry on the mass flux. It may be

interesting to run more simulations between pore diameters $20\sigma_0$ and $10\sigma_0$ to better map the unsystematic trend. The linear relationship between temperature gradient and mass flux holds strong for all three pore diameters studied in this thesis. A greater temperature gradient will yield a greater driving force for solvent migration over the membrane. However, the relation between induced temperature gradients and mass flux may not be linear for temperature intervals greater than the ones investigated in this study. Moreover, a greater temperature gradient may yield unacceptable levels of pollution in the pure solvent phase. In order to optimize processing conditions, it would be highly interesting to investigate the effects of increasing temperature gradients beyond what was done in this study.

5 Conclusion

Non-equilibrium thermodynamics and molecular dynamics simulations were used to describe membrane distillation of solvent against a chemical potential gradient. First a simple two-component mixture was created to understand how to obtain a separation effect. This was done changing some of the Lennard-Jones/spline parameters. It was found using trial and error that a separation would occur when the solute particles had ε_{22}=1.2, ε_{12}=1.1 and α_{12}=1.5, while the other parameters were equal to 1. The solvent particles had all Lennard-Jones/spline parameters equal to 1.

The system to be studied was a two-phase system containing Lennard-Jones/spline fluids, separated by a hydrophobic pore. Four different systems were constructed to find the independent resistivity coefficients r_{qq}, $r_{\mu q}$ and $r_{\mu\mu}$. These coefficients are important in membrane distillation because they can provide accurate information about the mass transport. The four systems were

- An equilibrium system made to determine how long the simulations must run before they reach stationary state.
- A system containing two liquids in thermal equilibrium (system 1).
- A one-component system under a temperature gradient (system 2).
- A system containing two liquids under a temperature gradient, with a mass flux equal to zero (system 3).

The resistivity coefficients were calculated for the total system, but local resistivity coefficients, such as surface and vapor resistivity coefficients, were also found. This was because the total resistivity coefficients can be found using these. In this study, the total resistivity coefficients were calculated without using the local coefficients, and found to be r_{qq}^{tot}= 13±3, $r_{q\mu}^{tot}$= -20±2 and $r_{\mu\mu}^{tot}$= 35±2. The resistivity coefficients for the surface between the mixture and vapor was $r_{qq}^{s,l}$= 23±2, $r_{q\mu}^{s,l}$= -15±1 and $r_{\mu\mu}^{s,l}$= 11±2. For the surface between the vapor and pure liquid they were $r_{qq}^{s,r}$= 13.6±0.8, $r_{q\mu}^{s,r}$= -8±2 and $r_{\mu\mu}^{s,r}$= 13±1. The resistivity coefficients in the vapor phase were found to be r_{qq}^{vapor}= 7±1, $r_{q\mu}^{vapor}$= -0.5±0.7 and $r_{\mu\mu}^{vapor}$= 0.05±0.04.

It was confirmed that the second law of thermodynamics was fulfilled for the systems, something that was considered extremely important for the credibility of the model. The total

coupling coefficient, $r_{q\mu}^{tot}$, was negative, meaning that heat was transported in the same direction as mass. The two other total resistivity coefficients were positive. It was also seen that the surfaces had resistivity coefficients that were significantly different from the bulk coefficients. This confirms that the surface plays a central role when it comes to transport in heterogeneous systems.

The mass flux dependence on the size of the temperature gradient and pore diameter was also evaluated. The mass flux over the membrane changed with a change in both temperature gradient and pore diameter. It was observed that the mass flux increased linearly with increasing temperature gradient. Some pollution was observed at the two greatest temperature gradients, solute particles accounted for less than 0.2% of the pure phase after completed simulation time. This was considered a very low degree of pollution since the solute concentration in the mixture was unrealistically high. The presence of the pollution was therefore disregarded. The temperature interval T_h^*=0.88 and T_c^*=0.60 was considered to give the greatest mass transport relative to the other gradients investigated in this study.

The greatest mass flux was obtained with a pore diameter equal to $10\sigma_0$, which was the smallest pore studied. This implied that a membrane consisting of pores with diameter $10\sigma_0$ would provide a greater mass transport compared to a membrane with fewer, larger pores. A change in mass flux with changing pore geometry means the mechanism for mass transport also changes with pore geometry. The variation was found to be unsystematic, which suggests that one needs to further study this mechanism to gain a better understanding of the underlying mechanics.

Modeling of more realistic systems, for example water, would be an interesting next step. This allows the simulation system to be more comparable to real life conditions for water rinsing, which may give a greater understanding of water transport across a nanometer pore.

6 References

Allen, M. P., & Tildesley, D. J. (1987). “Computer simulation of liquids”. Oxford university press.

Allen, M. P. (2004). “Introduction to molecular dynamics simulation”. Computational soft matter: from synthetic polymers to proteins, 23, 1-28.

Caro, M., Béland, L. K., Samolyuk, G. D., Stoller, R. E., & Caro, A. (2015). Lattice thermal conductivity of multi-component alloys. Journal of Alloys and Compounds, 648, 408-413.

Clark, J. B., Hastie, J. W., Kihlborg, L. H. E., Metselaar, R., & Thackeray, M. M. (1994). “Definitions of terms relating to phase transitions of the solid state”. Pure Appl Chem, 66, 577-594.

Delhommelle, J., & Millié, P. (2001). “Inadequacy of the Lorentz-Berthelot combining rules for accurate predictions of equilibrium properties by molecular simulation”. Molecular Physics, 99(8), 619-625.

Frenkel, D., & Smit, B. (2001). “Understanding molecular simulation: from algorithms to applications” (Vol. 1). Elsevier.

Guggenheim, E. A. (1937). “The theoretical basis of Raoult's law”. Transactions of the Faraday Society, 33, 151-156.

Hafskjold, B., Ikeshoji, T., & Ratkje, S. K. (1993). On the molecular mechanism of thermal diffusion in liquids. Molecular Physics, 80(6), 1389-1412.

Hafskjold, B. (2002). “Computer simulations of thermal diffusion in binary fluid mixtures”. In Thermal Nonequilibrium Phenomena in Fluid Mixtures (Vol. 584, p. 3). Springer Berlin Heidelberg.

Hafskjold, B. (2017). “Non-equilibrium molecular dynamics simulations of the transient Ludwig-Soret effect in a binary Lennard-Jones/spline mixture”. The European Physical Journal E, 40(1), 4.

Hafskjold, B., & Travis, K. “Phase diagram and Joule-Thomson coefficients for the 3D Lennard-Jones/spline model” (to be published).

Hale, W. R., Dohrer, K. K., Tant, M. R., & Sand, I. D. (2001). “A diffusion model for water vapor transmission through microporous polyethylene/CaCo 3 films”. Colloids and Surfaces A: Physicochemical and Engineering Aspects, 187, 483-491.

He, W., Lv, W., & Dickerson, J. H. (2014). “Gas diffusion mechanisms and models”. In Gas Transport in Solid Oxide Fuel Cells (pp. 9-17). Springer, Cham.

Helbæk, M., & Kjelstrup, S. (2006). ”Fysikalsk kjemi” 2nd edition. Fagbokforl.

Hiemenz, P. C., & Rajagopalan, R. (1997). “Principles of Colloid and Surface Chemistry, revised and expanded” (Vol. 14). CRC press.

Holian, B. L., & Evans, D. J. (1983). Shear viscosities away from the melting line: A comparison of equilibrium and nonequilibrium molecular dynamics. The Journal of chemical physics, 78(8), 5147-5150.

Hoover, W. G. (1985). "Canonical dynamics: equilibrium phase-space distributions." Physical review A 31(3): 1695.

Jansen, A. E., Assink, J. W., Hanemaaijer, J. H., Van Medevoort, J., & Van Sonsbeek, E. (2013). “Development and pilot testing of full-scale membrane distillation modules for deployment of waste heat”. Desalination, 323, 55-65.

Khayet, M. (2011). “Membranes and theoretical modeling of membrane distillation: a review”. Advances in colloid and interface science, 164(1-2), 56-88.

Kjelstrup, S., & Bedeaux, D. (2008). “Non-equilibrium thermodynamics of heterogeneous systems”, Volume 16, World Scientific Publishing Company.

Keulen, L., van der Ham, L. V., Kuipers, N. J. M., Hanemaaijer, J. H., Vlugt, T. J. H., & Kjelstrup, S. (2017). “Membrane distillation against a pressure difference”. Journal of Membrane Science, 524, 151-162.

Lawson, K. W., & Lloyd, D. R. (1997). “Membrane distillation”. Journal of membrane Science, 124(1), 1-25.

Lebon, G., Jou, D., & Casas-Vázquez, J. (2008). “Understanding non-equilibrium thermodynamics” (Vol. 295). Berlin: Springer.

Li, J., Liao, D., & Yip, S. (1998). ”Coupling continuum to molecular-dynamics simulation: Reflecting particle method and the field estimator”. Physical Review E, 57(6), 7259.

Plimpton, S. (1995). “Fast Parallel Algorithms for Short-Range Molecular Dynamics”, J Comp Phys, 117, 1-19. http://lammps.sandia.gov

Rice B.M., & Sewell T.D. (2009). “Equilibrium Molecular Dynamics Simulations”. In: Peiris S.M., Piermarini G.J. (eds) Static Compression of Energetic Materials. Shock Wave and High Pressure Phenomena. Springer, Berlin, Heidelberg.

Roger W. Kugel (1998). “Raoult's Law: Binary Liquid-Vapor Phase Diagrams: A Simple Physical Chemistry Experiment”. Journal of Chemical Education 1998 75 (9), 1125.

Ross, S. M. (2014). “Introduction to probability and statistics for engineers and scientists”. Academic Press.

Taylor, J. R. (1997). “An Introduction to Error Analysis”, 2nd edition, Sausalito, CA.

Vörösmarty, C. J., Green, P., Salisbury, J., & Lammers, R. B. (2000). “Global water resources: vulnerability from climate change and population growth”. science, 289(5477), 284-288.

Wold, I., & Hafskjold, B. (1999). “Nonequilibrium molecular dynamics simulations of coupled heat and mass transport in binary fluid mixtures in pores”. International journal of thermophysics, 20(3), 847-856.

Xie, Charles. "Molecular Dynamics Simulations Beyond the Lennard-Jones Particles".

Ã–zisik, M. N. (1993). “Heat conduction”. 2nd edition, John Wiley & Sons.

Appendix A

This section provides tables with information about the p-value in the test statistic. The p-value was used to decide from a statistical view if the mass fluxes were significantly different from zero.

Table A. 1 P-value obtained from a student t-test for the mass flux in the equilibrium system in section 4.2.1. For this t-test, the null hypothesis was that the mass flux at a given position was equal to zero. The significance level was chosen to be 0.05, so a p-value equal or less than 0.05 means that the null hypothesis is rejected. The pore has position $x^* = \{40, 140\}$.

x^*	P-value
5	0.15
15	0.26
25	0.53
35	0.10
45	0.76
55	0.83
65	0.71
75	0.97
85	0.94
95	0.96
105	0.69
115	0.46
125	0.78
135	0.63
145	0.74
155	0.35
165	0.77
175	0.75

Table A. 2 P-value obtained from a student t-test for system 1, see section 4.2.2. For this t-test, the null hypothesis was that the mass flux at a given position was equal to zero. The significance level was chosen to be 0.05, so a p-value equal or less than 0.05 means that the null hypothesis is rejected. The pore has position $x^* = \{40, 140\}$.

x^*	P-value
2.5	0.63
7.5	0.30
12.5	0.38
17.5	0.32
22.5	0.40
27.5	0.27
32.5	0.45
37.5	0.20
42.5	0.08
47.5	0.05
52.5	0.05
57.5	0.01
62.5	0.00
67.5	0.00
72.5	0.00
77.5	0.00
82.5	0.01
87.5	0.02
92.5	0.02
97.5	0.02
102.5	0.02
107.5	0.01
112.5	0.01
117.5	0.00
122.5	0.54
127.5	0.98
132.5	0.90
137.5	0.73
142.5	0.74
147.5	0.82

152.5	0.89
157.5	0.97
162.5	0.99
167.5	0.92
172.5	0.98
177.5	0.90

Table A. 3 P-value obtained from a student t-test for system 2, see section 4.2.3. For this t-test, the null hypothesis was that the mass flux at a given position was equal to zero. The significance level was chosen to be 0.05, so a p-value equal or less than 0.05 means that the null hypothesis is rejected. The pore has position $x^* = \{40, 140\}$.

x^*	P-value
2.5	0.21
7.5	0.19
12.5	0.14
17.5	0.11
22.5	0.14
27.5	0.15
32.5	0.15
37.5	0.10
42.5	0.09
47.5	0.07
52.5	0.06
57.5	0.09
62.5	0.04
67.5	0.01
72.5	0.00
77.5	0.00
82.5	0.00
87.5	0.00
92.5	0.00
97.5	0.00
102.5	0.00

107.5	0.00
112.5	0.00
117.5	0.07
122.5	0.11
127.5	0.16
132.5	0.20
137.5	0.13
142.5	0.11
147.5	0.12
152.5	0.15
157.5	0.18
162.5	0.19
167.5	0.20
172.5	0.19
177.5	0.22

Table A. 4 P-value obtained from a student t-test for system 3, see section 4.2.4. For this t-test, the null hypothesis was that the mass flux at a given position was equal to zero. The significance level was chosen to be 0.05, so a p-value equal or less than 0.05 means that the null hypothesis is rejected. The pore has position $x^* = \{40, 140\}$.

x^*	P-value
2.5	0.93
7.5	0.96
12.5	0.89
17.5	0.89
22.5	0.96
27.5	0.96
32.5	0.84
37.5	0.99
42.5	0.97
47.5	0.95
52.5	0.97
57.5	0.96
62.5	0.93

67.5	0.92
72.5	0.95
77.5	0.99
82.5	0.95
87.5	0.95
92.5	0.90
97.5	0.93
102.5	0.95
107.5	0.95
112.5	0.99
117.5	0.97
122.5	0.77
127.5	0.70
132.5	0.65
137.5	0.85
142.5	0.96
147.5	0.97
152.5	0.93
157.5	0.97
162.5	0.97
167.5	0.82
172.5	0.91
177.5	0.87

Appendix B

This section contains the input scripts used in LAMMPS, version August 2017 [Plimpton, S. (1995)]. The scripts used in LAMMPS have been run with variations in temperature, mole fractions of solvent and pore diameters.

B.1 Simple two-component system

```
units           lj
atom_style      atomic

variable        L equal 66

region          box block 0 $L 0 $L 0 $L units box
region          init block 0.2 $L 0.2 $L 0.2 $L units box

create_box      2 box

lattice         fcc 0.2 origin 0.0 0.0 0.0
create_atoms    1 region init

lattice         fcc 0.2 origin 0.25 0.25 0.25
create_atoms    1 region init

lattice         fcc 0.2 origin 0.5 0.5 0.5
create_atoms    2 region init

lattice         fcc 0.2 origin 0.75 0.75 0.75
create_atoms    1 region init


group           atoms type 1 2
mass            * 1.0

pair_style      lj/spline
pair_coeff      1 1 1 1 1 0
pair_coeff      1 2 1.1 1 1.5 0
pair_coeff      2 2 1.2 1 1 0

neighbor        0.3 bin
neigh_modify    every 20 delay 0 check yes

velocity        atoms create 10 87287
```

```
fix             1 atoms nvt temp 10 10 0.02
thermo          1000
timestep        0.002
run             200000

unfix           1

region          gas block 20 46 0 $L 0 $L units box
delete_atoms    region gas

group           water type 1
group           salt type 2
group           fluid type 1 2

velocity        all scale 0.7
dump            dump all custom 50000 dump.out id type x y z
fix             2 all nvt temp 0.7 0.7 0.02
run             500000


compute         chunk_cv fluid chunk/atom bin/1d &
                x lower 1 units box

compute         atom_number1 water property/chunk chunk_cv count
compute         atom_number2 salt property/chunk chunk_cv count

fix             dens_profile2 salt ave/time 1000 100 100000 &
                c_atom_number2 file density2.out mode vector

fix             dens_profile1 water ave/time 1000 100 100000 &
                c_atom_number1 file density1.out mode vector

fix             temp_profile fluid ave/chunk 1000 100 100000 &
                chunk_cv temp file temp.out

compute         pressure1 water stress/atom NULL

fix             dump_p1 water ave/chunk 1000 100 100000 &
                chunk_cv c_pressure1[*] file dump_pmix.out

compute         kin water ke/atom
compute         pot water pe/atom

fix             energy water ave/chunk 1000 100 100000 &
                chunk_cv c_pot c_kin file energymix.out
```

```
thermo_style    custom step pe

run             2000000
```

B.2 Equilibrium system

```
#MELTING PURE LIQUID

units           lj
atom_style      atomic

#Defining variables
variable        L equal 180
variable        W equal v_L/6.0
variable        X1 equal v_L/4.5
variable        X2 equal 3.5*v_L/4.5
variable        T equal 10.0
variable        N equal 87287
variable        Tn equal 0.7
variable        D1 equal ${X1}-1.0
variable        D2 equal ${X2}+1.0


#Defining the simulation box
region          box block 0 $L 0 $W 0 $W units box
region          init1 block 10.0 ${D1} 0.1 $W 0.1 $W units box
region          init2 block ${D2} 170.0 0.1 $W 0.1 $W units box
region          impure union 2 init1 init2

region          R1 block ${X1} ${X2} 0 $W 0 $W units box

create_box      2 box

lattice         fcc 0.8
create_atoms    1 region impure

lattice         fcc 1.189
create_atoms    2 region R1

group           fluid type 1
group           pore_atoms type 2
mass            * 1.0


pair_style      lj/spline
pair_coeff      1 1 1 1 1 0
pair_coeff      1 2 1 1 0.25 0
pair_coeff      2 2 1 1 1 0

neighbor        0.3 bin
neigh_modify    every 20 delay 0 check no
```

```
neigh_modify    exclude type 2 2


velocity        fluid create $T $N

fix             1 fluid nvt temp $T $T 0.02
dump            dump1 all custom 1000 dump.out id type x y z
thermo          1000
timestep        0.002
run             500000

write_data      melt.out




#CREATING A CONSTANT TEMPERATURE THROUGH THE SYSTEM
units           lj
atom_style      atomic

pair_style      lj/spline
read_data       melt.out
pair_coeff      1 1 1 1 1 0
pair_coeff      1 2 1 1 0.25 0
pair_coeff      2 2 1 1 1 0

group           fluid type 1

mass            * 1.0


#Keeping the temperature constant
variable        T equal 0.7

velocity        fluid scale ${T}

fix             NVT_fix fluid nvt temp ${T} ${T} 0.02
thermo          1000
run             500000
write_data      temperature.out



#CALCULATIONS OF MASS FLUX, PRESSURE, DENSITY AND TEMPERATURE

units           lj
atom_style      atomic
```

```
pair_style      lj/spline
read_data       temperature.out
pair_coeff      1 1 1 1 1 0
pair_coeff      1 2 1 1 0.25 0
pair_coeff      2 2 1 1 1 0

group           fluid type 1

mass            * 1.0

#Defining variables
variable        L equal 180
variable        W equal v_L/6.0
variable        X1 equal v_L/4.5
variable        X2 equal 3.5*v_L/4.5
variable        W2 equal v_W/2.0
variable        R equal 10.0


#creating the pore
region          pore cylinder x ${W2} ${W2} $R ${X1} ${X2} units box
delete_atoms    region pore


#Keeping the temperature constant
variable        T equal 0.7

fix             NVT_fix fluid nvt temp ${T} ${T} 0.02


#Calculations

compute         chunk_cv all chunk/atom bin/1d &
                x lower 10 units box

compute         pressure1 fluid stress/atom NULL

fix             dump_p1 fluid ave/chunk 1000 10 50000 &
                chunk_cv c_pressure1[*] file dump_p.out norm none

fix             velo1 fluid ave/chunk 1000 10 50000 &
                chunk_cv vx vy vz file velocity.out norm none

compute         atom_number fluid property/chunk chunk_cv count

fix             dens_profile1 fluid ave/time 1000 10 10000 &
```

```
                c_atom_number1 file density.out mode vector


fix             temp_profile fluid ave/chunk 1000 10 500000 &
                chunk_cv temp file temp.out


run             1500000
```

B.3 System 1

```
#melting 75/25 mixture
units           lj
atom_style      atomic

variable        L equal 180
variable        W equal v_L/6.0
variable        X1 equal v_L/4.5
variable        X2 equal 3.5*v_L/4.5

variable        T equal 10.0
variable        N equal 87287
variable        D1 equal ${X1}-1.0
variable        D2 equal ${X2}+1.0

#Defining the simulation box
region          box block 0 $L 0 $W 0 $W units box
region          impure block 0.2 ${D1} 0.1 $W 0.1 $W units box
region          init2 block ${D2} 179.8 0.1 $W 0.1 $W units box

region          R1 block ${X1} ${X2} 0 $W 0 $W units box

create_box      3 box

lattice         fcc 0.25 origin 0 0 0
create_atoms    1 region impure

lattice         fcc 0.25 origin 0.25 0.25 0.25
create_atoms    1 region impure

lattice         fcc 0.25 origin 0.5 0.5 0.5
create_atoms    2 region impure
```

```
lattice         fcc 0.25 origin 0.75 0.75 0.75
create_atoms    1 region impure

lattice         fcc 1.189
create_atoms    3 region R1

lattice         fcc 0.8
create_atoms    1 region init2

group           fluid type 1 2
group           water type 1
group           salt type 2
group           pore_atoms type 3
mass            * 1.0

pair_style      lj/spline
pair_coeff      1 1 1 1 1 0
pair_coeff      1 2 1.1 1 1.5 0
pair_coeff      2 2 1.2 1 1 0
pair_coeff      3 3 1 1 1 0
pair_coeff      1 3 1 1 0.25 0
pair_coeff      2 3 1 1 0.25 0

neighbor        0.3 bin
neigh_modify    every 20 delay 0 check no
neigh_modify    exclude type 3 3

velocity        fluid create $T $N

fix             1 fluid nvt temp $T $T 0.02
fix             reflect fluid wall/rpm xlo EDGE 1 units box
fix             reflect2 fluid wall/rpm xhi EDGE 1 units box

dump            dump1 all custom 10000 dump1.out id type x y z
thermo          1000
timestep        0.002
run             500000
unfix           1


#Gradient
variable        T1 equal v_L/36.0
variable        T2 equal 35.0*${L}/36.0

region          hot block 0 ${T1} 0 $W 0 $W units box
region          cold block ${T2} ${L} 0 $W 0 $W units box
```

```
compute         hot_temp fluid temp/region hot
compute         cold_temp water temp/region cold

fix             hot_rescale fluid temp/rescale 10 0.74 0.74 0.001 1.0
fix_modify      hot_rescale temp hot_temp

fix             cold_rescale water temp/rescale 10 0.74 0.74 0.001 1.0
fix_modify      cold_rescale temp cold_temp

fix             fix_nve fluid nve
timestep        0.002
run             500000

write_data      temperature.out


#CALCULATIONS OF MASS FLUX, PRESSURE, DENSITY, TEMPERATURE AND MEASURABLE HEAT FLUX
units           lj
atom_style      atomic

pair_style      lj/spline
read_data       temperature.out
pair_coeff      1 1 1 1 1 0
pair_coeff      1 2 1.1 1 1.5 0
pair_coeff      2 3 1 1 0.25 0
pair_coeff      2 2 1.2 1 1 0
pair_coeff      3 3 1 1 1 0
pair_coeff      1 3 1 1 0.25 0

group           water type 1
mass            * 1.0

#Defining the pore

variable        L equal 180
variable        W equal v_L/6.0
variable        X1 equal v_L/4.5
variable        X2 equal 3.5*v_L/4.5
variable        W2 equal 15
variable        R equal 10.0

group           water type 1
group           fluid type 1 2
group           salt type 2
group           pore_atoms type 3

# Temperature gradient
```

```
variable        T1 equal v_L/36.0
variable        T2 equal 35.0*${L}/36.0

region          hot block 0 ${T1} 0 $W 0 $W units box
region          cold block ${T2} ${L} 0 $W 0 $W units box

compute         hot_temp fluid temp/region hot
compute         cold_temp water temp/region cold

fix             hot_rescale fluid temp/rescale 10 0.74 0.74 0.0001 1.0
fix_modify      hot_rescale temp hot_temp

fix             cold_rescale water temp/rescale 10 0.74 0.74 0.0001 1.0
fix_modify      cold_rescale temp cold_temp

region          pore1 cylinder x ${W2} ${W2} $R ${X1} ${X2} units box

fix             fix_nve fluid nve

delete_atoms    region pore1

fix             reflect1 salt wall/rpm xlo EDGE 1 units box
fix             reflect2 water wall/rpm xhi EDGE 0.9 units box
fix             reflect3 water wall/rpm xlo EDGE 0.45 units box

#Computations

compute         chunk_cv fluid chunk/atom bin/3d &
                x lower 5 y 10 10 z 10 10 bound y 10 20 bound z 10 20 units box

compute         atom_number1 water property/chunk chunk_cv count
compute         atom_number2 salt property/chunk chunk_cv count

fix             dens_profile1 water ave/time 1000 10 10000 &
                c_atom_number1 file density1.out mode vector

fix             dens_profile2 salt ave/time 1000 10 10000 &
                c_atom_number2 file density2.out mode vector

compute         chunk_cv2 fluid chunk/atom bin/1d &
                x lower 5 units box

compute         pressure1 fluid stress/atom NULL
compute         pressure water stress/atom NULL
```

```
fix             dump_p1 fluid ave/chunk 10 10000 100000 &
                chunk_cv2 c_pressure1[*] file dump_p.out norm none

fix             velo1 water ave/chunk 10 10000 100000 &
                chunk_cv2 vx vy vz file velocity.out norm none

compute         kin fluid ke/atom
compute         pot fluid pe/atom

compute         kinw water ke/atom
compute         potw water pe/atom

compute         STRESS fluid stress/atom NULL virial

variable        kevx atom c_kin*vx
variable        pevx atom c_pot*vx
variable        SVX atom (c_STRESS[1]*vx+c_STRESS[4]*vy+c_STRESS[5]*vz)

fix             dump_stress fluid ave/chunk 10 10000 100000 &
                chunk_cv2 v_kevx v_pevx v_SVX file heatflux.out norm none

fix             dump_stress2 water ave/chunk 10 10000 100000 &
                chunk_cv2 c_potw c_kinw c_pressure[*] file enthalpy.out

fix             energy fluid ave/chunk 10 10000 3000000 &
                chunk_cv2 c_pot c_kin file energy.out

fix             temp_profile fluid ave/chunk 10 10000 3000000 &
                chunk_cv2 temp file temp.out

dump            dump1 all custom 10000 dumptot.out id type x y z

thermo_style    custom step pe

thermo          1000
run             3000000
```

B.4 System 2

```
#melting 75/25 mixture
units           lj
atom_style      atomic

variable        L equal 180
variable        W equal v_L/6.0
```

```
variable        X1 equal v_L/4.5
variable        X2 equal 3.5*v_L/4.5

variable        T equal 10.0
variable        N equal 87287
variable        D1 equal ${X1}-1.0
variable        D2 equal ${X2}+1.0


#Defining the simulation box
region          box block 0 $L 0 $W 0 $W units box
region          impure block 0.2 ${D1} 0.1 $W 0.1 $W units box
region          init2 block ${D2} 179.8 0.1 $W 0.1 $W units box

region          R1 block ${X1} ${X2} 0 $W 0 $W units box

create_box      2 box

lattice         fcc 0.8
create_atoms    1 region impure

lattice         fcc 1.189
create_atoms    2 region R1

lattice         fcc 0.8
create_atoms    1 region init2

group           fluid type 1
group           pore_atoms type 2
mass            * 1.0

pair_style      lj/spline
pair_coeff      1 1 1 1 1 0
pair_coeff      1 2 1 1 0.25 0
pair_coeff      2 2 1 1 1 0


neighbor        0.3 bin
neigh_modify    every 20 delay 0 check no
neigh_modify    exclude type 2 2


velocity        fluid create $T $N
fix             1 fluid nvt temp $T $T 0.02

fix             reflect fluid wall/rpm xlo EDGE 1 units box
fix             reflect2 fluid wall/rpm xhi EDGE 1 units box
```

```
dump            dump1 all custom 10000 dump1.out id type x y z
thermo          1000
timestep        0.002
run             500000
unfix           1

#Gradient
variable        T1 equal v_L/36.0
variable        T2 equal 35.0*${L}/36.0

region          hot block 0 ${T1} 0 $W 0 $W units box

region          cold block ${T2} ${L} 0 $W 0 $W units box

compute         hot_temp fluid temp/region hot
compute         cold_temp fluid temp/region cold

fix             hot_rescale fluid temp/rescale 10 0.78 0.78 0.001 1.0
fix_modify      hot_rescale temp hot_temp

fix             cold_rescale fluid temp/rescale 10 0.7 0.7 0.001 1.0
fix_modify      cold_rescale temp cold_temp

fix             fix_nve fluid nve

timestep        0.002
run             500000

write_data      temperature.out



#CALCULATIONS OF MASS FLUX, PRESSURE, DENSITY, TEMPERATURE AND MEASURABLE HEAT FLUX
units           lj
atom_style      atomic

pair_style      lj/spline
read_data       temperature.out
pair_coeff      1 1 1 1 1 0
pair_coeff      1 2 1 1 0.25 0
pair_coeff      2 2 1 1 1 0
mass            * 1.0

# Defining the pore

variable        L equal 180
variable        W equal v_L/6.0
variable        X1 equal v_L/4.5
```

```
variable        X2 equal 3.5*v_L/4.5
variable        W2 equal 15
variable        R equal 10.0


group           fluid type 1
group           pore_atoms type 2

# Temperature gradient

variable        T1 equal v_L/36.0
variable        T2 equal 35.0*${L}/36.0

region          hot block 0 ${T1} 0 $W 0 $W units box

region          cold block ${T2} ${L} 0 $W 0 $W units box

compute         hot_temp fluid temp/region hot
compute         cold_temp fluid temp/region cold

fix             hot_rescale fluid temp/rescale 10 0.78 0.78 0.001 1.0
fix_modify      hot_rescale temp hot_temp

fix             cold_rescale fluid temp/rescale 10 0.7 0.7 0.001 1.0
fix_modify      cold_rescale temp cold_temp

region          pore1 cylinder x ${W2} ${W2} $R ${X1} ${X2} units box

fix             fix_nve fluid nve

delete_atoms    region pore1


fix             reflect2 fluid wall/rpm xhi EDGE 0.009 units box


#Computation

compute         chunk_cv fluid chunk/atom bin/3d &
                x lower 5 y 10 10 z 10 10 bound y 10 20 bound z 10 20 units box


compute         atom_number1 fluid property/chunk chunk_cv count



fix             dens_profile1 fluid ave/time 1000 10 10000 &
```

```
                c_atom_number1 file density1.out mode vector


compute         chunk_cv2 fluid chunk/atom bin/1d &
                x lower 5 units box

compute         pressure1 fluid stress/atom NULL

compute         pressure fluid stress/atom NULL

fix             dump_p1 fluid ave/chunk 10 10000 100000 &
                chunk_cv2 c_pressure1[*] file dump_p.out norm none

fix             velo1 fluid ave/chunk 10 10000 100000 &
                chunk_cv2 vx vy vz file velocity.out norm none

compute         kin fluid ke/atom
compute         pot fluid pe/atom

compute         kinw fluid ke/atom
compute         potw fluid pe/atom

compute         STRESS fluid stress/atom NULL virial

variable        kevx atom c_kin*vx
variable        pevx atom c_pot*vx
variable        SVX atom (c_STRESS[1]*vx+c_STRESS[4]*vy+c_STRESS[5]*vz)

fix             dump_stress fluid ave/chunk 10 10000 100000 &
                chunk_cv2 v_kevx v_pevx v_SVX file heatflux.out norm none

fix             dump_stress2 fluid ave/chunk 10 10000 100000 &
                chunk_cv2 c_potw c_kinw c_pressure[*] file enthalpy.out

fix             energy fluid ave/chunk 10 10000 3000000 &
                chunk_cv2 c_pot c_kin file energy.out

fix             temp_profile fluid ave/chunk 10 10000 3000000 &
                chunk_cv2 temp file temp.out

dump            dump1 all custom 5000 dumptot.out id type x y z

thermo_style    custom step pe

thermo          1000
run             3000000
```

B.5 System 3

```
#melting 75/25 mixture

units           lj
atom_style      atomic

variable        L equal 180
variable        W equal v_L/6.0
variable        X1 equal v_L/4.5
variable        X2 equal 3.5*v_L/4.5

variable        T equal 10.0
variable        N equal 87287
variable        D1 equal ${X1}-1.0
variable        D2 equal ${X2}+1.0


#Defining the simulation box
region          box block 0 $L 0 $W 0 $W units box
region          impure block 0.2 ${D1} 0.1 $W 0.1 $W units box
region          init2 block ${D2} 179.8 0.1 $W 0.1 $W units box

region          R1 block ${X1} ${X2} 0 $W 0 $W units box

create_box      3 box

lattice         fcc 0.25 origin 0 0 0
create_atoms    1 region impure

lattice         fcc 0.25 origin 0.25 0.25 0.25
create_atoms    1 region impure

lattice         fcc 0.25 origin 0.5 0.5 0.5
create_atoms    2 region impure

lattice         fcc 0.25 origin 0.75 0.75 0.75
create_atoms    1 region impure

lattice         fcc 1.189
create_atoms    3 region R1

lattice         fcc 0.8
create_atoms    1 region init2
```

```
group           fluid type 1 2
group           water type 1
group           salt type 2
group           pore_atoms type 3
mass            * 1.0

pair_style      lj/spline
pair_coeff      1 1 1 1 1 0
pair_coeff      1 2 1.1 1 1.5 0
pair_coeff      2 2 1.2 1 1 0
pair_coeff      3 3 1 1 1 0
pair_coeff      1 3 1 1 0.25 0
pair_coeff      2 3 1 1 0.25 0

group           fluid type 1 2
neighbor        0.3 bin
neigh_modify    every 20 delay 0 check no
neigh_modify    exclude type 3 3


velocity        fluid create $T $N

fix             1 fluid nvt temp $T $T 0.02

fix             reflect fluid wall/rpm xlo EDGE 1 units box
fix             reflect2 fluid wall/rpm xhi EDGE 1 units box

dump            dump1 all custom 10000 dump1.out id type x y z
thermo          1000
timestep        0.002
run             500000
unfix           1

#Gradient
variable        T1 equal v_L/36.0
variable        T2 equal 35.0*${L}/36.0

region          hot block 0 ${T1} 0 $W 0 $W units box

region          cold block ${T2} ${L} 0 $W 0 $W units box

compute         hot_temp fluid temp/region hot
compute         cold_temp water temp/region cold

fix             hot_rescale fluid temp/rescale 10 0.78 0.78 0.001 1.0
fix_modify      hot_rescale temp hot_temp
```

```
fix             cold_rescale water temp/rescale 10 0.7 0.7 0.001 1.0
fix_modify      cold_rescale temp cold_temp

fix             fix_nve fluid nve

timestep        0.002
run             500000

write_data      temperature.out



#CALCULATIONS OF MASS FLUX, PRESSURE, DENSITY, TEMPERATURE AND MEASURABLE HEAT FLUX
units           lj
atom_style      atomic

pair_style      lj/spline
read_data       temperature.out
pair_coeff      1 1 1 1 1 0
pair_coeff      1 2 1.1 1 1.5 0
pair_coeff      2 3 1 1 0.25 0
pair_coeff      2 2 1.2 1 1 0
pair_coeff      3 3 1 1 1 0
pair_coeff      1 3 1 1 0.25 0

group           water type 1
mass            * 1.0

#Defining pore

variable        L equal 180
variable        W equal v_L/6.0
variable        X1 equal v_L/4.5
variable        X2 equal 3.5*v_L/4.5
variable        W2 equal 15
variable        R equal 10.0

group           water type 1
group           fluid type 1 2
group           salt type 2
group           pore_atoms type 3


#Gradient

variable        T1 equal v_L/36.0
variable        T2 equal 35.0*${L}/36.0
```

```
region          hot block 0 ${T1} 0 $W 0 $W units box

region          cold block ${T2} ${L} 0 $W 0 $W units box

compute         hot_temp fluid temp/region hot
compute         cold_temp water temp/region cold

fix             hot_rescale fluid temp/rescale 10 0.78 0.78 0.001 1.0
fix_modify      hot_rescale temp hot_temp

fix             cold_rescale water temp/rescale 10 0.7 0.7 0.001 1.0
fix_modify      cold_rescale temp cold_temp

region          pore1 cylinder x ${W2} ${W2} $R ${X1} ${X2} units box

fix             fix_nve fluid nve

delete_atoms    region pore1

fix             reflect1 fluid wall/rpm xhi EDGE 1 units box
fix             reflect2 fluid wall/rpm xlo EDGE 1 units box

#Computations

compute         chunk_cv fluid chunk/atom bin/3d &
                x lower 5 y 10 10 z 10 10 bound y 10 20 bound z 10 20 units box


compute         atom_number1 water property/chunk chunk_cv count
compute         atom_number2 salt property/chunk chunk_cv count


fix             dens_profile1 water ave/time 1000 10 10000 &
                c_atom_number1 file density1.out mode vector

fix             dens_profile2 salt ave/time 1000 10 10000 &
                c_atom_number2 file density2.out mode vector


compute         chunk_cv2 fluid chunk/atom bin/1d &
                x lower 5 units box

compute         pressure1 fluid stress/atom NULL
compute         pressure water stress/atom NULL

fix             dump_p1 fluid ave/chunk 10 10000 100000 &
                chunk_cv2 c_pressure1[*] file dump_p.out norm none
```

```
fix             velo1 water ave/chunk 10 10000 100000 &
                chunk_cv2 vx vy vz file velocity.out norm none

compute         kin fluid ke/atom
compute         pot fluid pe/atom

compute         kinw water ke/atom
compute         potw water pe/atom

compute         STRESS fluid stress/atom NULL virial

variable        kevx atom c_kin*vx
variable        pevx atom c_pot*vx
variable        SVX atom (c_STRESS[1]*vx)

fix             dump_stress fluid ave/chunk 10 10000 100000 &
                chunk_cv2 v_kevx v_pevx v_SVX  file heatflux.out norm none

fix             dump_stress2 fluid ave/chunk 10 10000 100000 &
                chunk_cv2 c_potw c_kinw c_pressure[*] file enthalpy.out

fix             energy fluid ave/chunk 10 10000 3000000 &
                chunk_cv2 c_pot c_kin file energy.out



fix             temp_profile fluid ave/chunk 10 10000 3000000 &
                chunk_cv2 temp file temp.out

dump            dump1 all custom 5000 dumptot.out id type x y z

thermo_style    custom step pe

thermo          1000
run             3000000
```

B.6 System 4

```
#melting 75/25 mixture
units           lj
atom_style      atomic

variable        L equal 180
```

```
variable        W equal v_L/6.0
variable        X1 equal v_L/4.5
variable        X2 equal 3.5*v_L/4.5

variable        T equal 10.0
variable        N equal 87287
variable        D1 equal ${X1}-1.0
variable        D2 equal ${X2}+1.0

#Defining the simulation box
region          box block 0 $L 0 $W 0 $W units box
region          mixbox block 0.2 ${D1} 0.5 $W 0.5 $W units box
region          purebox block ${D2} 179.8 0.5 $W 0.5 $W units box

region          R1 block ${X1} ${X2} 0 $W 0 $W units box

create_box      3 box

lattice         fcc 0.25 origin 0 0 0
create_atoms    1 region mixbox

lattice         fcc 0.25 origin 0.25 0.25 0.25
create_atoms    1 region mixbox

lattice         fcc 0.25 origin 0.5 0.5 0.5
create_atoms    2 region mixbox

lattice         fcc 0.25 origin 0.75 0.75 0.75
create_atoms    1 region mixbox

lattice         fcc 1.189
create_atoms    3 region R1

lattice         fcc 0.8
create_atoms    1 region purebox

group           fluid type 1 2
group           water type 1
group           salt type 2
group           pore_atoms type 3
mass            * 1.0

pair_style      lj/spline
pair_coeff      1 1 1 1 1 0
pair_coeff      1 2 1.1 1 1.5 0
pair_coeff      2 2 1.2 1 1 0
pair_coeff      3 3 1 1 1 0
```

```
pair_coeff      1 3 1 1 0.25 0
pair_coeff      2 3 1 1 0.25 0

group           fluid type 1 2
neighbor        0.3 bin
neigh_modify    every 20 delay 0 check no
neigh_modify    exclude type 3 3

velocity        fluid create $T $N

fix             1 fluid nvt temp $T $T 0.02

fix             reflect1 fluid wall/rpm xlo EDGE 1 units box
fix             reflect2 fluid wall/rpm xhi EDGE 1 units box

dump            dump1 all custom 1000 dump1.out id type x y z
thermo          1000
timestep        0.002
run             500000


unfix           1

#Gradient

variable        T1 equal v_L/12.0
variable        T2 equal 11.0*${L}/12.0

variable        Th equal 0.8
variable        Tc equal 0.7

region          H block 0 ${T1} 0 $W 0 $W units box
region          C block ${T2} $L 0 $W 0 $W units box

compute         hot_temp fluid temp/region H
compute         cold_temp water temp/region C

fix             hot_rescale fluid temp/rescale 10 0.78 0.78 0.001 1.0
fix_modify      hot_rescale temp hot_temp

fix             cold_rescale water temp/rescale 10 0.7 0.7 0.001 1.0
fix_modify      cold_rescale temp cold_temp

fix             fix_nve fluid nve

run             500000
write_data      temperature.out
```

```
#CALCULATIONS OF MASS FLUX, PRESSURE, DENSITY, TEMPERATURE AND MEASURABLE HEAT FLUX
units           lj
atom_style      atomic

pair_style      lj/spline
read_data       temperature.out
pair_coeff      1 1 1 1 1 0
pair_coeff      1 2 1.1 1 1.5 0
pair_coeff      2 3 1 1 0.25 0
pair_coeff      2 2 1.2 1 1 0
pair_coeff      3 3 1 1 1 0
pair_coeff      1 3 1 1 0.25 0

group           water type 1
group           fluid type 1 2
group           salt type 2
mass            * 1.0

variable        L equal 180
variable        W equal v_L/6
variable        W2 equal v_W/2.0
variable        R equal 10.0
variable        X1 equal v_L/4.5
variable        X2 equal 3.5*${L}/4.5
variable        T1 equal v_L/36.0
variable        T2 equal 35.0*${L}/36.0

region          H block 0 ${T1} 0 $W 0 $W units box
region          C block ${T2} $L 0 $W 0 $W units box

compute         hot_temp fluid temp/region H
compute         cold_temp water temp/region C

fix             hot_rescale fluid temp/rescale 10 0.78 0.78 0.001 1.0
fix_modify      hot_rescale temp hot_temp

fix             cold_rescale water temp/rescale 10 0.7 0.7 0.001 1.0
fix_modify      cold_rescale temp cold_temp

region          pore1 cylinder x ${W2} ${W2} $R ${X1} ${X2} units box

fix             fix_nve fluid nve

delete_atoms    region pore1
```

```
fix             reflect1 water wall/rpm xhi EDGE 0.08 units box
fix             reflect2 salt wall/rpm xlo EDGE 1 units box

#CALCULATIONS
compute         chunk_cv fluid chunk/atom bin/3d &
                x lower 5 y 10 10 z 10 10 bound y 10 20 bound z 10 20 units box


compute         atom_number1 water property/chunk chunk_cv count
compute         atom_number2 salt property/chunk chunk_cv count

fix             dens_profile1 fluid ave/time 10 1000 10000 &
                c_atom_number1 file density1.out mode vector

fix             dens_profile2 fluid ave/time 10 1000 10000 &
                c_atom_number2 file density2.out mode vector


compute         chunk_cv2 fluid chunk/atom bin/1d &
                x lower 5 units box


compute         pressure1 fluid stress/atom NULL

fix             dump_p1 fluid ave/chunk 10 10000 100000 &
                chunk_cv2 c_pressure1[*] file dump_p.out norm none

fix             velo1 water ave/chunk 10 10000 100000 &
                chunk_cv2 vx vy vz file velocity.out norm none

fix             temp_profile fluid ave/chunk 10 10000 500000 &
                chunk_cv2 temp file temp1.out

dump            dump1 all custom 5000 dumppore.out id type x y z
thermo          1000
run             3000000
```

Appendix C

Figure C.1 depicts a phase diagram for a system consisting of one type of Lennard-Jones/spline particles, used to determine values for the density and temperature, so that a two-phase system could be obtained.

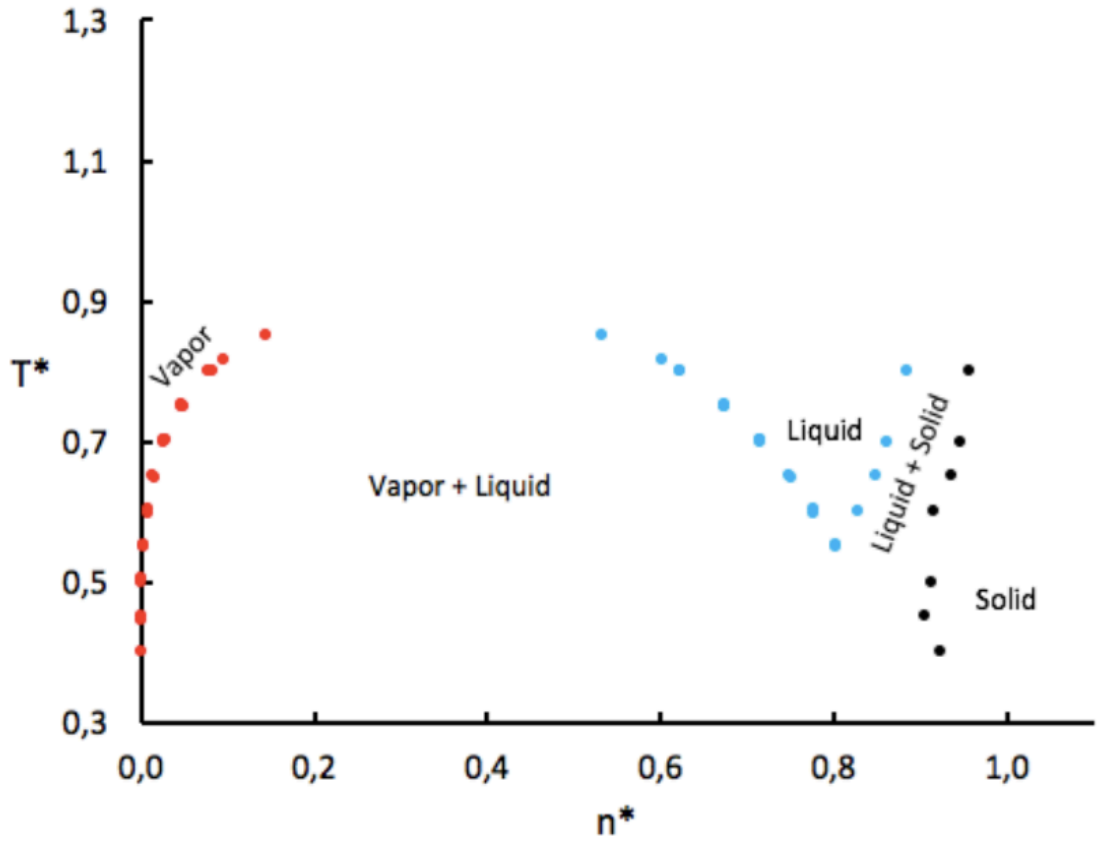

Figure C. 1 Phase diagram for Lennard-Jones/spline particles. T^* is the temperature and n^* is the number density [Hafskjold, B., & Travis, K]. All values are in reduced units.

Appendix D

D.1 Clapeyrons and Clausius Clapeyrons equation

Clapeyrons equation is a differential equation that provides a mathematical relationship between vapor pressure and temperature for a two-phase system in equilibrium [Helbæk, M., & Kjelstrup, S. (2006)]. When two phases are in equilibrium, a change in pressure or temperature will bring the system out of equilibrium.

For a system at equilibrium with two components in liquid phase and one component in vapor phase, equation (D.1) holds if the concentration in each phase is constant.

$$d\mu_i{}^l = d\mu_i{}^v \tag{D.1}$$

where μ_i is chemical potential of component i, l and v denotes liquid and vapor phase, respectively. It is known that

$$d\mu_i = -S_i dT + V_i dp + RTd \ln a_i \tag{D.2}$$

where S_i is entropy, T is temperature, p is pressure, V_i is volume, R is the gas constant and a_i is the activity for component i. Since the concentration is constant, the term consisting of the activity becomes zero. Inserting equation (D.2) in equation (D.1)

$$-S_i^l dT + V_i^l dp = -S_i^v dT + V_i^v dp \tag{D.3}$$

Clapeyrons equation is found for component i by rewriting equation (D.3), and inserting $\Delta S_m = \Delta H_m / T$

$$\frac{dp}{dT} = \frac{\Delta_{vap} H_{M,i}}{T \Delta_{vap} V_{M,i}} \tag{D.4}$$

where $\Delta_{vap} H_{M,i}$ is the enthalpy of vaporization per mole of component i and $\Delta_{vap} V_{M,i}$ is the difference between the molar volume of vapor and liquid phases. The enthalpy of vaporization

is defined as the amount of heat that is required to induce a phase change from liquid to vapor, and defined as

$$\Delta_{vap}H = H_{vapor} - H_{liquid} \tag{D.5}$$

where enthalpy is defined as

$$H = U + pV \tag{D.6}$$

where U is internal energy, p is pressure and V is volume.

Rewriting equation (D.4) gives another form of the Clapeyrons equation for component i.

$$\frac{dp}{d\ln T} = \frac{\Delta_{vap}H_{M,i}}{\Delta_{vap}V_{M,i}} \tag{D.7}$$

Clausius Clapeyrons equation is a modified version of Clapeyrons equation [Helbæk, M., & Kjelstrup, S. (2006)]. The Clausius Clapeyrons equation is valid for the two-phase systems vapor-liquid and vapor-solid, and can be used to find relations between temperature and pressure along phase boundaries.

The Clausius Clapeyrons equation comes with assumptions. The assumptions are that the molar volume of liquid is much smaller than the molar volume of vapor, vaporization enthalpy is independent of temperature and that the vapor is an ideal gas. If the vapor is ideal, it should follow the ideal gas law given by

$$pV = nRT \tag{D.8}$$

where p is the pressure, V is the volume, n is the number of moles, R is the gas constant and T is the temperature.

For the molar volume of liquid to be much smaller than the molar volume of vapor, the temperature must be considerably lower than the critical temperature. When the conditions approach the critical temperature, the density of the vapor phase becomes more similar to the

liquid phase, until these no longer can be separated and a distinct liquid and vapor phase do not exist. These assumptions make it possible to rewrite the change in molar volume, $\Delta_{vap}V_M$, from Clapeyrons equation, to

$$\Delta_{vap}V_M = V_{M,vapor} - V_{M,liquid} \approx V_{M,vapor} = \frac{RT}{p} \tag{D.9}$$

Inserting equation (D.9) in Clapeyrons equation gives Clausius Clapeyrons equation for a vapor-liquid system, with equilibrium between the two phases

$$\frac{dp}{pdT} = \frac{d\ln(p)}{dT} = \frac{\Delta_{vap}H_M}{RT^2} \tag{D.10}$$

where p is pressure, T is temperature, $\Delta_{vap}H_M$ is the enthalpy of vaporization per mole and R is the gas constant. For a mixture, the Clausius Clapeyrons equation for component i will become

$$\frac{dp}{p_i dT} = \frac{d\ln(p_i)}{dT} = \frac{\Delta_{vap}H_{M,i}}{RT^2} \tag{D.11}$$

where p_i is the equilibrium pressure of component i over the mixture and $\Delta_{vap}H_{M,i}$ is the enthalpy of vaporization of component i. Equation (D.11) can be solved by integrating the differential equation and assuming a constant change in enthalpy over the given temperature interval

$$\int d\ln(p) = \frac{\Delta_{vap}H_M}{R}\int \frac{dT}{T^2} \tag{D.12}$$

Equation (D.12) is an approximation because the vaporization enthalpy is a function of temperature. Solving the integral results in

$$\ln(p) = -\frac{\Delta_{vap}H_M}{R}\left(\frac{1}{T}\right) + constant \tag{D.13}$$

If the vaporization enthalpy is constant, then equation (D.13) states that plotting ln (p) against $1/T$ will give a straight line with slope $\frac{\Delta_{vap}H_M}{R}$.

In this study, it is more beneficial to look at a quantity per particle, compared to molar quantities. To go from molar quantities to quantities per particle, Avogadro's number is used. The gas constant relates to Avogadro's number through

$$R = k_B N_A \tag{D.14}$$

where N_A is Avogadro's number and k_B is Boltzmann constant.

D.2 Simulation case H and a pure liquid- Clapeyrons equation

Clapeyrons equation can be used to find the vaporization enthalpy per particles. This is done by plotting p^* against $\ln(T^*)$ and fitting a second order polynomial curve to the data points. The polynomial equation can be used to find the vaporization enthalpy per solvent particle. Such a plot for the solvent component is presented in figure D.1. Only temperature known to be within the vapor-liquid coexisting region was used. These temperatures were 0.7, 0.75 and 0.8.

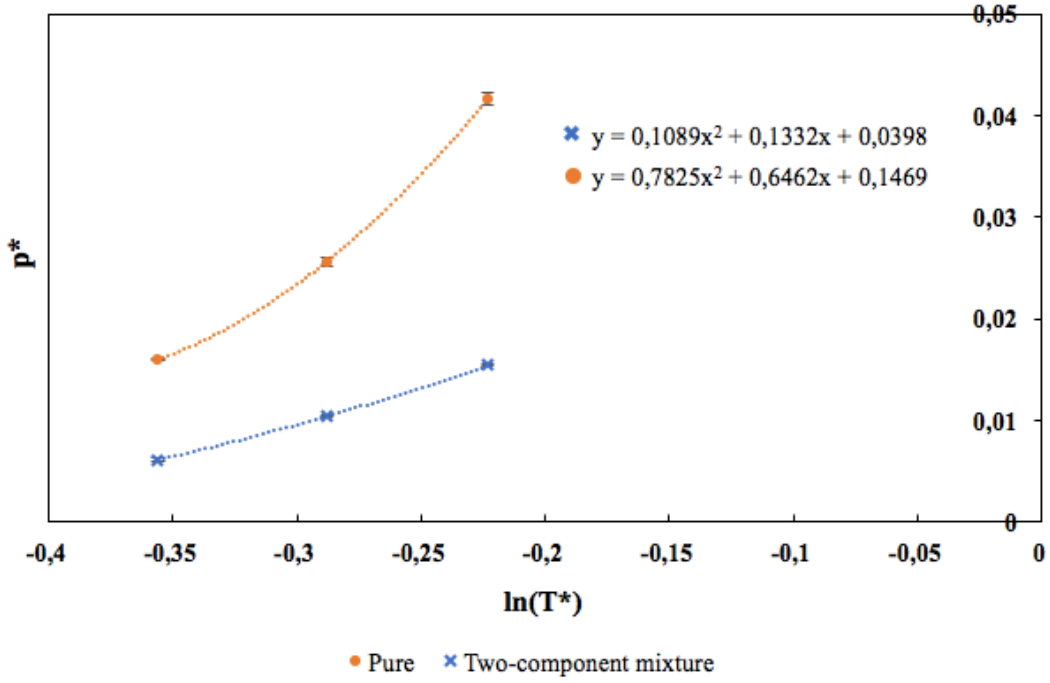

Figure D.1 Plot of the vapor pressure, p^*, against the natural logarithm of the temperature, $\ln(T^*)$, for pure liquid, dots, and two-component mixture, crosses. The dotted lines are second order polynomial fits which is explained by the different functions of y. The y and x represent p^* and $\ln(T^*)$, respectively. For the mixture, ε_{22} was set to 1.2, ε_{12} was set to 1.1, α_{12} was set to 1.5 and all other Lennard-Jones/spline parameters were set to 1. For the pure fluid, all Lennard-Jones/spline parameters were equal to 1. The error bars are calculated using standard deviation, see equation (3.22), and defined as $\pm 1\sigma_{SD,m}$. All values are in reduced units.

The slope of the second order polynomial curves will be $\frac{dp}{d\ln T}$, which according to the Clapeyrons equation, equation (D.7), is a function of the vaporization enthalpy. This slope is equal to the first derivative of the second-order equation defined for each curve, where x equals $\ln(T^*)$. The slope can be found for all three temperatures, but the vaporization enthalpy should be approximately constant for this temperature range. Any deviations from this will be observed using standard deviations. Equation (D.7) was used to find the vaporization enthalpy per solvent particle, and the results are presented in table D.1. The vaporization enthalpy was found as an average over the different slopes obtained from the different temperatures.

Table D.1 Table of vaporization enthalpy per particle of solvent component, $\Delta_{vap}H^*_{part,solvent}$, obtained by using equation (D.7). The error bars are calculated using standard deviation, see equation (3.22), and defined as $\pm 1\sigma_{SD,m}$. All values are in reduced units.

System	$\Delta_{vap}H^*_{part,solvent}$
Pure	3.5 ± 0.3
Two-component mixture	4.8 ± 0.5

Table D.1 reveals that the vaporization enthalpy of the solvent particle was higher for the two-component mixture than for the pure fluid. This means that the amount of energy required to transform a quantity of the mixture into vapor is greater than the amount required for the pure liquid. The standard deviations for the two vaporization enthalpies were large. This could mean that the assumption regarding the vaporization enthalpy being independent of temperature might not be valid. The vaporization enthalpy for the pure liquid and the mixture was not even significantly different within $2\sigma_{SD,m}$.

D.3 Simulation case H and a pure liquid- Clausius Clapeyrons equation

Clausius Clapeyrons equation is another equation that can be used to find the vaporization enthalpy of the solvent particle. For Clausius Clapeyron equation to apply for simulation case H and the pure liquid, and all other systems for that matter, the assumptions mentioned in section 2.6 must be fulfilled. The assumption that the molar volume of the vapor had to be much greater than the molar volume of the liquid was analyzed using table D.2. Table D.2 contains information regarding the volume per particle of the vapor and the liquid for both the two-component mixture and the pure fluid. The volume per particle is the inverse of the number

density, and found as an average over the respective phase. The temperatures investigated are chosen so that the systems are within the vapor-liquid coexisting region.

Table D.2 Table of volume, where $V_{part,v}$ is volume per solvent particle for vapor phase, and $V_{part,l}$ is volume per solvent particle for liquid phase. The error bars are calculated using standard deviation, see equation (3.22), and defined as $\pm 1\sigma_{SD,m}$. All units are in reduced units.

	Mixture		**Pure**	
Temperature	$V_{part,v}$	$V_{part,l}$	$V_{part,v}$	$V_{part,l}$
0.70	$107.9\pm5*10^{-1}$	$1.46\pm1*10^{-2}$	$36.7\pm5*10^{-1}$	$1.400\pm2*10^{-3}$
0.75	$67.4\pm2*10^{-1}$	$1.493\pm1*10^{-3}$	$21.6\pm2*10^{-1}$	$1,476\pm1*10^{-3}$
0.80	$47.1\pm2*10^{-1}$	$1.531\pm4*10^{-3}$	$13.40\pm8*10^{-2}$	$1.596\pm2*10^{-3}$

The assumption was that $V_{part,v} \gg V_{part,l}$. It was seen from table D.2 that the volume per particle in the vapor phase was greater than in the liquid phase. As the temperature increased, the deviation from the assumption also increased because the difference between the liquid and vapor volume became smaller. This was because when the temperature increases towards the critical temperature, the density of the liquid and vapor will become more and more similar. At the critical temperature, the density of liquid and vapor are equal. From the different phase-diagrams it was seen that the pure liquid had a lower critical temperature than the mixture. The deviation from the assumption was therefore greater for the pure liquid. This deviation could inhibit the result obtained from Clausius Clapeyrons equation.

The assumption regarding that the vapor must be ideal, or obey ideal gas law, was analyzed in table D.3. The pressure obtained in the simulations were compared with the pressure found using ideal gas law, see equation (D.8). Since temperature plays an important role in the ideal gas law, the temperature was presented more accurately and with uncertainties in this table. The temperature in the system was set to be constant, but the temperature fluctuated in the vapor phase due to few particles present. Therefore, the temperature was found as an average over the

temperature in the liquid phase. The vapor pressure was found as an average over the pressure in the vapor phase.

Table D.3 Table of the vapor pressure, p, of the two-component mixture and the pure fluid, found by ideal gas law and data obtained from simulations. T is temperature. The error bars are calculated using standard deviation, see equation (3.22), and defined as $\pm 1\sigma_{SD,m}$. All values are in reduced units.

		Ideal gas law		**Simulation data**	
$T^*_{mixture}$	T^*_{pure}	$p^*_{mixture}$	p^*_{pure}	$p^*_{mixture}$	p^*_{pure}
$0.7005 \pm 3*10^{-4}$	$0.7000 \pm 4*10^{-4}$	$0.0065 \pm 3*10^{-4}$	$0.0192 \pm 5*10^{-4}$	$0.0064 \pm 3*10^{-4}$	$0.0160 \pm 6*10^{-4}$
$0.7496 \pm 3*10^{-4}$	$0.7498 \pm 2*10^{-4}$	$0.0109 \pm 3*10^{-4}$	$0.0348 \pm 6*10^{-4}$	$0.0104 \pm 3*10^{-4}$	$0.0256 \pm 6*10^{-4}$
$0.8000 \pm 2*10^{-4}$	$0.8017 \pm 1*10^{-4}$	$0.0169 \pm 2*10^{-4}$	$0.0597 \pm 5*10^{-4}$	$0.0154 \pm 3*10^{-4}$	$0.0416 \pm 8*10^{-4}$

The data in table D.3 are presented with one standard deviation. In this study, it was assumed that if two numbers are separated by two standard deviations, they are significantly different from each other. For temperature 0.7 and 0.75, the pressure of the mixture found using ideal gas law was equal to what found by simulations. This was not the case for temperature 0.8, which was considered as a deviation from ideal gas law.

For the pure liquid, there was a significant difference between the pressures for all temperatures, and the difference increased with increasing temperature. The reason why the pure liquid had a greater deviation from ideal gas law compared to the two-component mixture, was because the pure liquid had an overall larger vapor pressure. A gas will behave more ideally when the vapor pressure is low.

Solving Clausius Clapeyrons equation and plotting $\ln(p^*)$ against $1/T^*$ will give the vaporization enthalpy for solvent component, see equation (D.13). Such a plot is presented in figure D.2.

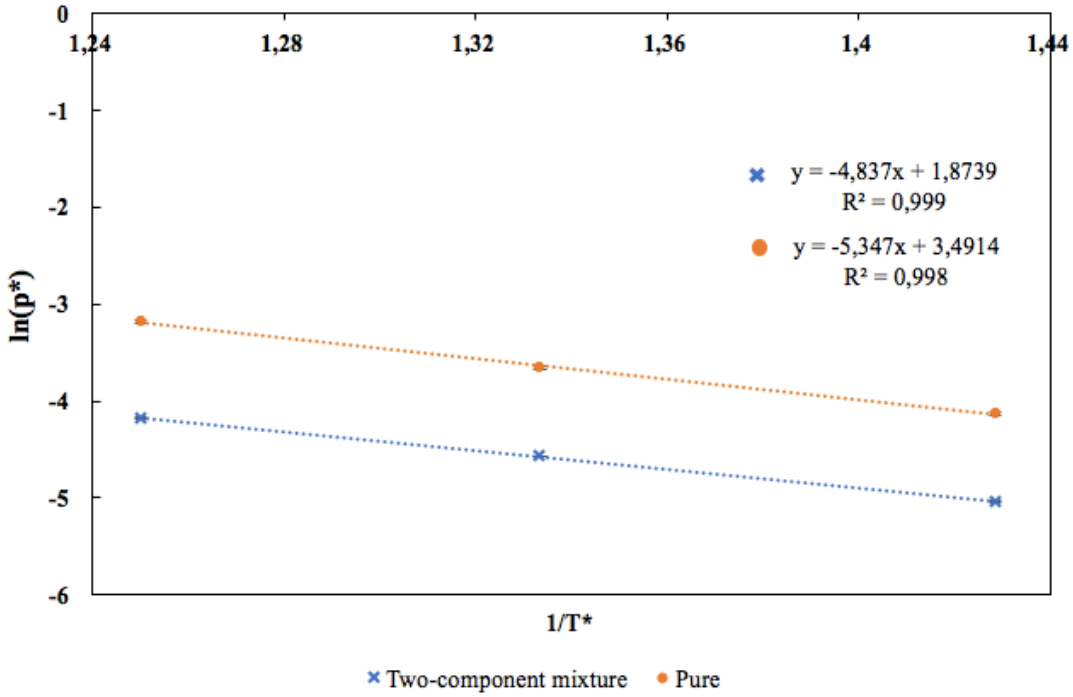

Figure D.2 Plot of the natural logarithm of the vapor pressure, $\ln(p^*)$, against the inverse temperature, $1/T^*$, for pure fluid, dots, and two-component mixture, crosses. The dotted lines are linear trend lines which are explained by the different functions of y. The y and x represent $\ln(p^*)$ and $1/T^*$, respectively. R^2 represents a measure of how well the variation in the data is explained by the linear trend lines. For the mixture, ε_{22} was set to 1.2, ε_{12} was set to 1.1, α_{12} was set to 1.5 and all other Lennard-Jones/spline parameters were set to 1. For the pure fluid system, all Lennard-Jones/spline parameters were equal to 1. The error bars are calculated using standard deviation, see equation (3.22), and defined as $\pm 1\sigma_{SD,m}$. All values are in reduced units.

Since the vapor only contains solvent particles, $\ln(p^*)$ is understood as the natural logarithm of the vapor pressure of solvent particles. This means that the slope only contains information regarding the solvent particles. Figure D.2 depicts that the linear relationship between $\ln(p^*)$ and $1/T^*$ holds well over the chosen range of temperatures since the R^2 values were so close to 1. This implies that the vaporization enthalpy was approximately constant for these temperatures, which was an assumption regarding the Clausius Clapeyrons equation. According to equation (D.13), the slope of the curves will be equal to $\frac{-\Delta_{vap}H_{M,solvent}}{R}$, which can be rewritten as vaporization enthalpy per particle. The values obtained from the slopes in figure D.2 are presented in table D.4.

Table D.4 Table of values for the slope found in figure D.2. The slope represents $-\Delta_{vap}H^*_{part,solvent}$, which is the vaporization enthalpy per particle. All values are in reduced units.

System	$\Delta_{vap}H^*_{part,solvent}$
Pure	5.347
Two-component mixture	4.837

Table D.4 reveals that the vaporization enthalpy of the solvent particle was higher for the pure fluid than for the two-component mixture. This was not expected when Clapeyrons equation gave the opposite result. The vaporization enthalpy found for the two-component mixture was the same as found using Clapeyrons equation. An explanation of why the vaporization enthalpy of the pure fluid had this unexpected result may be because this fluid experienced the most deviation from the assumptions made in Clausius Clapeyrons equation. This could mean that the results achieved in this section is not representative of the system.

D.4 Enthalpy of vaporization for simulation case H and pure fluid

Since the vaporization enthalpy should be independent of temperature under small temperature ranges, the different methods used in section 4.1.2, D.2 and D.3 can be compared.

The vaporization enthalpy per solvent particle was only equal for the mixture comparing Clapeyrons equation and Clausius Clapeyrons equation. All other values were different for the different methods. This could indicate that the enthalpy was not independent of temperature within the chosen temperature range. This was reflected in the great uncertainties found for the results using the Clapeyrons equation.

Both Clapeyrons equation and the method using the enthalpy calculated in the simulations, table D.2 and 4.1 respectively, showed that the enthalpy of vaporization of solvent particle was greatest for the two-component mixture. Based on this, the mixture would require a higher temperature, compared to the pure liquid, for solvent particles to diffuse into the vapor phase. This trend was confirmed from the phase diagrams of the two different fluids, where the pure liquid achieves a vapor-liquid coexisting system at lower temperatures than the mixture.

From Clausius Clapeyrons equation, table D.4, the outcome was opposite. Using this method, the enthalpy of vaporization was greatest for the pure phase. Using the method of Clausius

Clapeyrons, some assumptions were made. These were investigated in section D.2, and it was found that the assumption that $V_{part,v} \gg V_{part,l}$ did not hold for all temperatures. Also, for the pure fluid, the assumption regarding ideal gas did not hold. This could explain why the enthalpy trend was different using Clausius Clapeyrons compared to the two other methods.

The calculated vaporization enthalpy will not be used further in this study. If this value had been necessary for further use, a thorough investigation should have been carried out to get a deeper understanding of why the different methods did not provide the same results.

Appendix E

Figure E.1 depict a plot created to confirmed that the second law of thermodynamics was fulfilled. The resistivity coefficients presented in section 4.2.5 included uncertainties. Table 4.2 was used to solve $r_{qq}r_{\mu\mu} - r_{q\mu}^2$ for all combinations regarding the uncertainties presented in the table. This was done using percentage error. Percentage error is the percentage obtained by dividing the error by the quantity value and multiplying with 100. The percentages for all quantities are added to get the total percentage uncertainty in the final value.

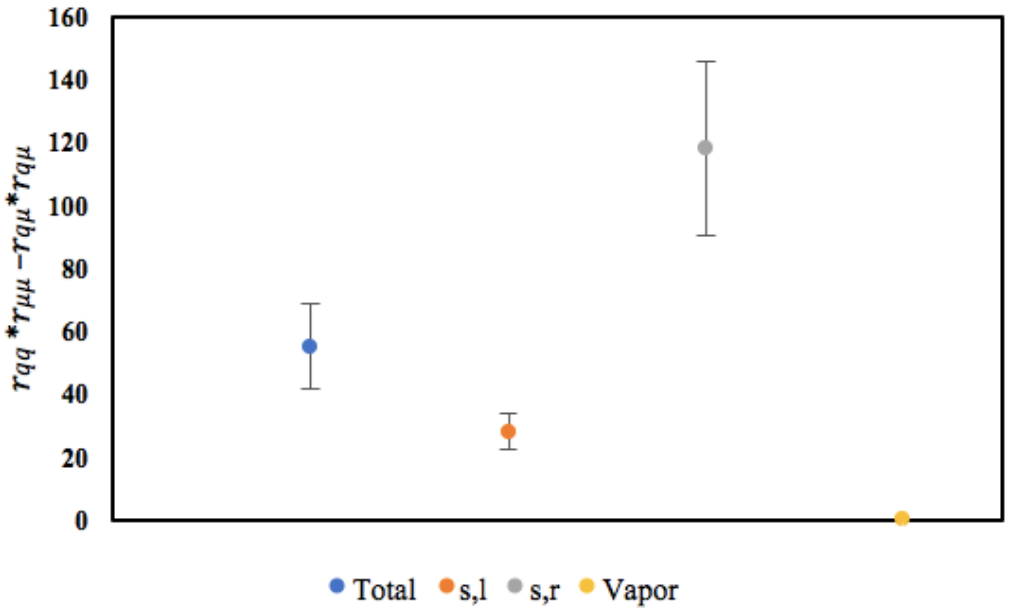

Figure E. 1 Plot of the combinations of $r_{qq}r_{\mu\mu} - r_{q\mu}^2$ from table 4.2. The uncertainties reflect all combinations based on the uncertainties given in table 4.2. Total, s,l, s,r and vapor represent the total system, the surface between the mixture and vapor, the surface between the vapor and pure phase part of the system. The error bars represent one standard deviation.

Figure E.1 was used to verify that $r_{qq}r_{\mu\mu} - r_{q\mu}^2 \geq 0$.